UNIVERSITY OF THESSALY
SCHOOL OF ENGINEERING
DEPARTMENT OF MECHANICAL ENGINEERING

ANALYSIS AND OPTIMIZATION OF FRICTION STIR WELDING

by

GEORGIOS MAVRIDIS

Submitted in partial fulfillment of the requirements for the degree of Diploma in Mechanical Engineering at the University of Thessaly

Volos, 2025

Institutional Repository - Library & Information Centre - University of Thessaly
04/09/2026 08:51:35 EEST - 216.73.216.250

UNIVERSITY OF THESSALY
SCHOOL OF ENGINEERING
DEPARTMENT OF MECHANICAL ENGINEERING

ANALYSIS AND OPTIMIZATION OF FRICTION STIR WELDING

by

GEORGIOS MAVRIDIS

Submitted in partial fulfillment of the requirements for the degree of Diploma in Mechanical Engineering at the University of Thessaly

Volos, 2025

Institutional Repository - Library & Information Centre - University of Thessaly
04/09/2026 08:51:35 EEST - 216.73.216.250

© 2024 Georgios Mavridis

All rights reserved. The approval of the present D Thesis by the Department of Mechanical Engineering, School of Engineering, University of Thessaly, does not imply acceptance of the views of the author (Law 5343/32 art. 202).

Institutional Repository - Library & Information Centre - University of Thessaly
04/09/2026 08:51:35 EEST - 216.73.216.250

Approved by the Committee on Final Examination:

Advisor Dr. Bouzakis Emmanouil,
Associate Professor, Department of Mechanical Engineering,
University of Thessaly

Member Dr. Zervaki D. Anna,
Assistant Professor, School of Naval Architecture and Marine Engineering, National Technical University of Athens

Member Dr. Haidemenopoulos Gregory,
Professor, Department of Mechanical Engineering,
University of Thessaly

Date Approved: [February, 2025]

Institutional Repository - Library & Information Centre - University of Thessaly
04/09/2026 08:51:35 EEST - 216.73.216.250

ANALYSIS AND OPTIMIZATION OF FRICTION STIR WELDING

Georgios Mavridis

Department of Mechanical Engineering, University of Thessaly

Supervisor: Dr Bouzakis Emmanouil

Associate Professor of Manufacturing Processes

Abstract

Friction-Stir-Welding (FSW) has developed as an innovative joining process conducted in “solid-state” materials and is recognized for its energy efficacy, versality and environmental friendliness. This process is particularly valuable for welding “high-strength aluminum alloys” engineered for aerospace applications, alongside other metallic alloys that pose challenges for conventional fusion welding methods. It stands as a breakthrough in metal joining, holding the distinction of being the most significant advancement in the field in the past two decades. This study critically examines the current state of the evolution of knowledge and practical application of Friction Stir Welding. Special attention is given to (a) elucidating the mechanisms responsible for weld formation and “microstructural refinement” and (b) investigating the effects of the process constraints on the resulting microstructure and ultimate mechanical properties. Though the primary focus is on aluminum alloys, noteworthy advancements have been made in extending the application of the process to other metals and alloys. However, despite the rapid diffusion of technology, there exists a notable gap between technological implementation and a comprehensive understanding of microstructural evolution and their influence on material behavior.

Institutional Repository - Library & Information Centre - University of Thessaly
04/09/2026 08:51:35 EEST - 216.73.216.250

The present study emphasizes the need for a deeper exploration of these fundamental aspects to bridge the existing knowledge gap. By doing so, there will be more informed decision-making in selecting parameters and optimizing conditions for a broad range of metallic materials. As Friction Stir Welding technology continues to advance, a more robust understanding of its underlying principles will be crucial for maximizing its potential across various industrial applications.

Key words:

- Friction Stir Welding (FSW)
- Process Parameters
- Optimization Techniques

Institutional Repository - Library & Information Centre - University of Thessaly
04/09/2026 08:51:35 EEST - 216.73.216.250

ΑΝΑΛΥΣΗ ΚΑΙ ΒΕΛΤΙΣΤΟΠΟΙΗΣΗ ΤΗΣ ΣΥΓΚΟΛΛΗΣΗΣ ΤΡΙΒΗΣ ΜΕ ΑΝΑΔΕΥΣΗ

ΓΕΩΡΓΙΟΣ ΜΑΥΡΙΔΗΣ

Τμήμα Μηχανολόγων Μηχανικών, Πανεπιστήμιο Θεσσαλίας, 2025

Επιβλέπων Καθηγητής: Δρ. Εμμανουήλ Μπουζάκης,

Αναπληρωτής Καθηγητής Κατεργασίες Μορφοποίησης Υλικών

Περίληψη

Η μέθοδος συγκόλλησης τριβής με ανάδευση (Friction Stir Welding - FSW) έχει αναδειχθεί ως μια καινοτόμος διαδικασία συγκόλλησης στερεάς κατάστασης, αναγνωρισμένη για την ενεργειακή της αποδοτικότητα, τη φιλικότητα προς το περιβάλλον και την πολυλειτουργικότητά της. Αυτή η τεχνική είναι ιδιαίτερα πολύτιμη για τη συγκόλληση κραμάτων αλουμινίου υψηλής αντοχής που χρησιμοποιούνται παραδείγματος χάριν στην αεροναυπηγική, καθώς και άλλων μεταλλικών κραμάτων, που ενέχουν σημαντικές προκλήσεις στην εφαρμογή παραδοσιακών διαδικασιών συγκόλλησης σύντηξης. Η συγκόλληση με ανάδευση συνιστά μια σημαντική πρόοδο στον τομέα της σύνδεσης μετάλλων, καθώς θεωρείται η πλέον σημαντική εξέλιξη στον τομέα την τελευταία εικοσαετία. Η παρούσα μελέτη εξετάζει κριτικά την τρέχουσα κατάσταση κατανόησης και ανάπτυξης της μεθόδου αυτής. Ιδιαίτερη έμφαση δίνεται: (α) στην αποσαφήνιση των μηχανισμών που ευθύνονται για τη διαμόρφωση της συγκόλλησης και τη βελτίωση της μικροδομής, και (β) στη διερεύνηση των επιδράσεων των παραμέτρων της διαδικασίας στη διαμορφούμενη μικροδομή και τις τελικές μηχανικές ιδιότητες. Παρόλο που το κύριο πεδίο εφαρμογής είναι τα κράματα αλουμινίου, έχουν σημειωθεί αξιοσημείωτες εξελίξεις στην επέκταση της χρήσης της μεθόδου και σε άλλα μέταλλα και κράματα. Ωστόσο, παρά τη ραγδαία διάδοση της τεχνολογίας, παραμένει ένα αξιοσημείωτο κενό ανάμεσα στην τεχνολογική εφαρμογή και τη συνολική κατανόηση της εξέλιξης της μικροδομής και της σχέσης μεταξύ μικροδομής και ιδιοτήτων.

Η παρούσα μελέτη υπογραμμίζει την ανάγκη βαθύτερης διερεύνησης αυτών των θεμελιωδών πτυχών με στόχο τη γεφύρωση του υφιστάμενου γνωστικού κενού. Με αυτόν τον τρόπο, θα καταστεί δυνατή η καλύτερη λήψη αποφάσεων για την επιλογή παραμέτρων

Institutional Repository - Library & Information Centre - University of Thessaly
04/09/2026 08:51:35 EEST - 216.73.216.250

και τη βελτιστοποίηση των συνθηκών για μια ευρεία γκάμα μεταλλικών υλικών. Καθώς η τεχνολογία συγκόλλησης τριβής με ανάδευση συνεχίζει να εξελίσσεται, η ενδελεχής κατανόηση των υποκείμενων αρχών της θα είναι κρίσιμη για την πλήρη αξιοποίηση του δυναμικού της σε ποικίλες βιομηχανικές εφαρμογές.

Λέξεις-κλειδιά:

- Συγκόλληση Τριβής με Ανάδευση
- Παράμετροι Διαδικασίας
- Τεχνικές Βελτιστοποίησης

Institutional Repository - Library & Information Centre - University of Thessaly
04/09/2026 08:51:35 EEST - 216.73.216.250

Contents

Institutional Repository - Library & Information Centre - University of Thessaly
04/09/2026 08:51:35 EEST - 216.73.216.250

Institutional Repository - Library & Information Centre - University of Thessaly
04/09/2026 08:51:35 EEST - 216.73.216.250

List Of Tables

Institutional Repository - Library & Information Centre - University of Thessaly
04/09/2026 08:51:35 EEST - 216.73.216.250

List of Figures

Institutional Repository - Library & Information Centre - University of Thessaly
04/09/2026 08:51:35 EEST - 216.73.216.250

Institutional Repository - Library & Information Centre - University of Thessaly
04/09/2026 08:51:35 EEST - 216.73.216.250

Institutional Repository - Library & Information Centre - University of Thessaly
04/09/2026 08:51:35 EEST - 216.73.216.250

Institutional Repository - Library & Information Centre - University of Thessaly
04/09/2026 08:51:35 EEST - 216.73.216.250

Chapter 1. Introduction

Industry confronts a formidable challenge in achieving welds of superior strength, fatigue resistance, and fracture resistance in aluminum alloys, particularly within the highly alloyed 2-thousand and 7-thousand series. The inherent difficulties stem from “solidification defects in microstructures, porosity in the fusion zone, and a substantial loss in mechanical properties compared to the base material.” These challenges have long categorized these alloys as non-weldable through conventional welding methods, casting doubt on the viability of welding for joining structures.

In response to these challenges, this welding process (FSW) emerges as a transformative “solid-state” joining technique, not melting but keeping the metal into the plastic zone. Initially deployed with a focus on aluminum alloys, FSW introduces a fundamentally straightforward concept. To join sheets or plates, a specialized rotating tool is employed. This tool, equipped with a unique pin and shoulder design, is inserted between the edges to be joined and moved along the joint line. This “solid-state” welding method circumvents the pitfalls inherent in traditional welding methods, promising a remedy to the difficulties posed by “poor solidification microstructures and porosity” in the welded area.

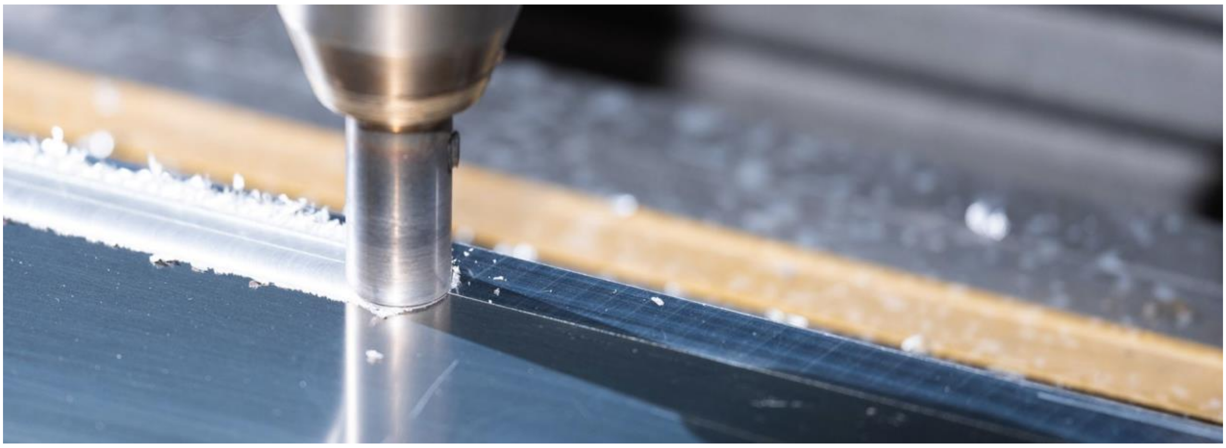

Figure 1 Close look to a FSW

Institutional Repository - Library & Information Centre - University of Thessaly
04/09/2026 08:51:35 EEST - 216.73.216.250

In this thesis, the focus will be on analyzing the fundamental principles and decisive process parameters of the process. Specifically, this work will explore the influence of key process variables as tool “rotational speed (RS), traverse speed(TS), and axial force” on the weld quality, microstructural characteristics, and mechanical properties of aluminum alloys. By synthesizing findings from existing literature and theoretical models, this thesis seeks to enhance the understanding of the interplay among these parameters and the performance of stir-welded joints. The insights gained will be particularly relevant for researchers and professionals working with aluminum alloy fabrication in industries where high-performance welding is essential.

The scope of this research is limited to a theoretical analysis, with no laboratory-based experimentation. As such, the study will rely on secondary data and previously established empirical models. While this approach precludes the validation of findings through experimental trials, it provides a comprehensive theoretical basis that can inform future experimental work and practical applications.

Institutional Repository - Library & Information Centre - University of Thessaly
04/09/2026 08:51:35 EEST - 216.73.216.250

Chapter 2. Literature Review and Fundamentals of Stir Welding

2.1 Fundamentals of Stir Welding

The concept firstly been known by Yu. Klimenko who initially patented friction stir welding in the Soviet Union in 1967. However, it wasn't until 1991 that The Welding Institute (TWI) in the UK experimentally validated and successfully commercialized this process. TWI subsequently obtained patents, with the initial patent providing the most detailed description, so the FSW the is accredited to Wayne Thomas and his team, describing the process as a solid-phase welding.

After initial laboratory trials, FSW saw its first practical applications in the aerospace with Boeing manufacturing parts for Delta II and Delta IV rockets, which required defect-free welds in aluminum-lithium alloys, such the fuel tanks, also NASA used FSW extensively in the construction of spacecraft and launch vehicles, for instance “the Orion Multi-Purpose Crew Vehicle and the Space Launch System” and in marine industry, manufacturing hulls and decks in high-speed ferries due to its ability to produce long, continuous welds in aluminum. These applications showcased the ability of this process to produce highly reliable welds in critical components.

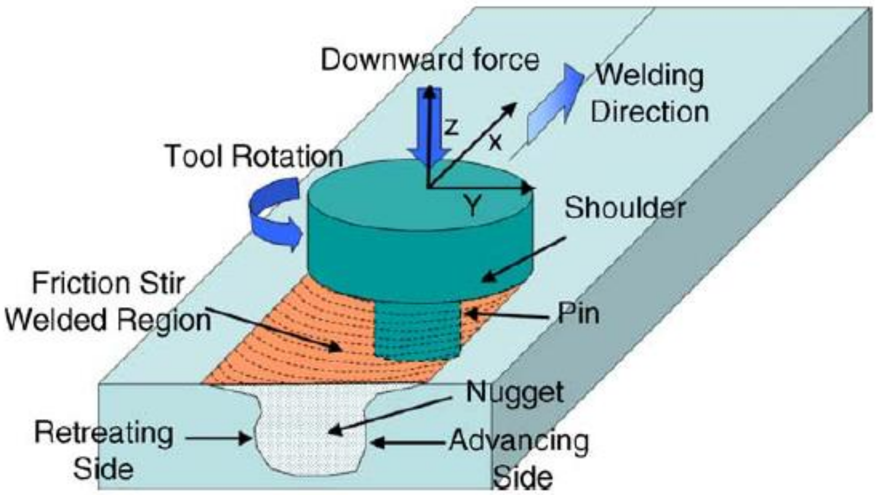

Figure 2 FSW schematic representation [1]

Institutional Repository - Library & Information Centre - University of Thessaly
04/09/2026 08:51:35 EEST - 216.73.216.250

The main idea of the process is the bonding of the workpieces without making it up to their melting points. The process exploits the thermal and mechanical effects of a specially designed tool to soften and stir the materials at the interface, enabling intermixing and consolidation under pressure.

This tool is the most significant part of the whole process. A non-consumable material, often wear-resistant, such as tool steel or tungsten carbide, with specific geometry that makes the material(s) of the pieces that been weld, to flow in the appropriate way around it. This tool consists of a "shoulder", which produces heat via friction and helps contain the plasticized material and a "pin" which penetrates the material and facilitates stirring at the joint interface. In some occasions a second shoulder can be applied at the end of the pin, this method is called **Bobbin tool** Friction-Stir-Welding (BTFSW) and will be discussed later on, as also the importance of the geometry of the pin. The materials that are joined are called **workpieces**. The system is complete with the presence of the clamping system which ensures that the workpieces remain securely fixed during the process to prevent distortion and misalignment and the machine, a rigid platform, often a CNC machine or a dedicated FSW system, able to resist the significant forces involved. The tool is characterized by two distinct sides: the "Advancing Side (AS) and the Retreating Side (RS)". The Advancing Side is the area where the vector representing welding speed aligns with Rotational Speed (RS) vector (though in opposite directions). "During the welding process, a non-consumable rotating pin is inserted into the faying surface of the sheets at an appropriate tilt angle and then moves along the welding line. Through the combined action of tool rotation and linear motion, the weld metal undergoes significant plastic deformation and intricate mixing around the axis of rotation". [2]

Three discrete zones — "the flow transition zone, the stir zone, and the torsion zone—are formed during the welding process as a result of the rotational, horizontal, and vertical movements of the plasticized metal. As illustrated in Figure 3, the threaded pin tool generates a unique plastic flow of metal around the rotation axis. Friction from the tool shoulder initially causes the metal beneath it to move toward the pin tool (motion 1), followed by a downward movement along the pin surface (motion 2). Upon reaching the pin tip, the metal is forced outward and then follows a helical rotational path back upward (motion 3), as depicted by the arrows in Figure 3. Repetition of these motions leads to the formation of onion ring structures in the stir zone".[3]

Institutional Repository - Library & Information Centre - University of Thessaly
04/09/2026 08:51:35 EEST - 216.73.216.250

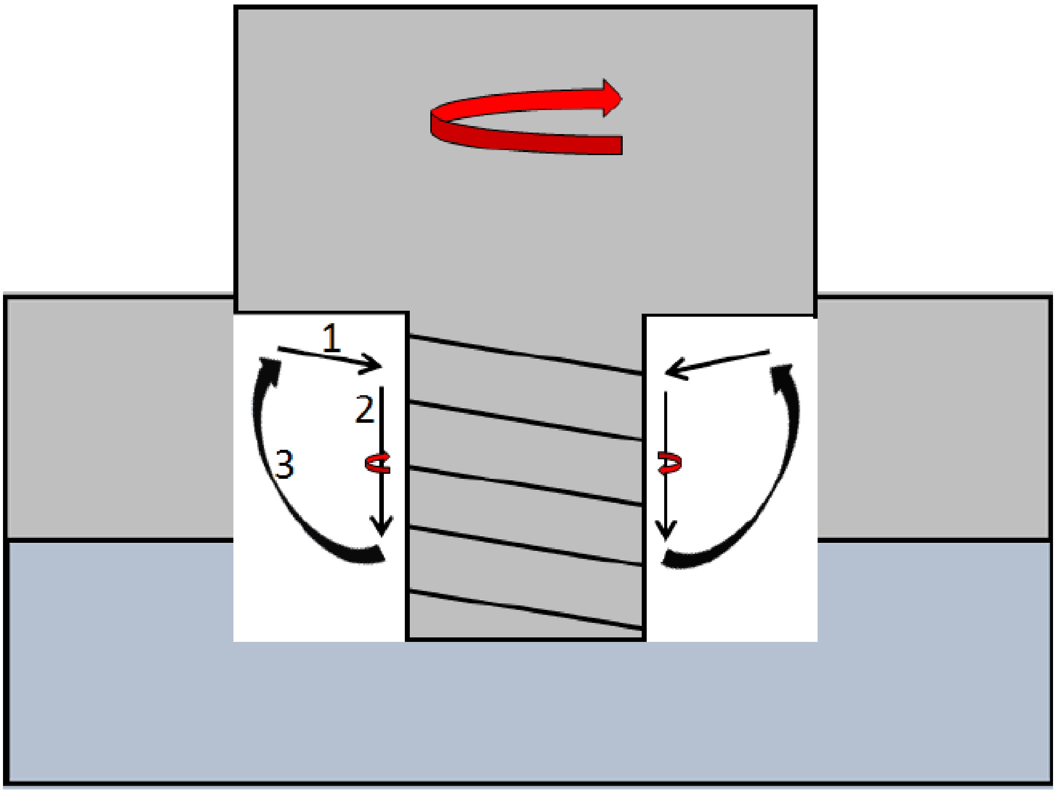

Figure 3 “Diagrammatic representation of material movement during the FSW process.” [3]

Solid-phase bonding is achieved through friction stir welding (FSW) by generating intense plastic deformation and localized frictional heat [4]. The mechanisms of metal flow and heat production in this method are strongly interconnected. Heat is primarily produced by the friction occurs at both the shoulder and the pin surfaces, although the majority of heat generation stems from the interaction between the shoulder and the top surface of the sheets. This heat softens the second workpiece, facilitating a metallic bond formed between the joined sheets. A slight tool inclination may be maintained to generate adequate frictional heat.

Accurately measuring the temperature of FSW welds is challenging; hence, numerous “finite element (FE) models have been developed to calculate temperature distributions resulting from plastic dissipation and frictional effects during the FSW process [5,6]. A moving heat source, caused by the friction between the rotating shoulder and the workpiece, is used to model heat transfer [7]. Research indicates that the maximum temperature near the weld is influenced by tool holding time, rotational speed, and transverse speed”.

Institutional Repository - Library & Information Centre - University of Thessaly
04/09/2026 08:51:35 EEST - 216.73.216.250

Ulysse utilized three-dimensional visco-plastic modeling to simulate the stir-welding process, revealing how welding speed affects temperature variations [8].

Similarly, Heurtier et al. [9] provided a comprehensive description of the thermal modeling of FSW, identifying two primary sources of heat generation: plastic strain and friction between the shoulder and the workpiece surface (excluding the contribution of pin friction). They proposed an equation to calculate the average power q, involving parameters such as the local coefficient of friction (μ), normal pressure (p), angular velocity (ω), and tool shoulder radius (R_S).

$$q = \frac{2\pi}{3}\mu\rho\omega R_s^3 \quad (1)$$

Appropriate heat input is critical in FSW, as it facilitates the formation of fine, dynamically recrystallized grains in the stir zone [10,11]. However, excessive heat can lead to grain coarsening. Thus, monitoring and controlling the temperature slightly above the dynamic recrystallization temperature ensures optimal weld quality.

The friction stir welding (FSW) process is known for its energy efficiency, environmentally friendly nature, and solid-state operation. These characteristics, combined with the favorable properties of friction stir welds related to their physical composition, mechanical behavior, and internal structure, as well as ongoing efforts within the FSW community to broaden its applicability across various materials, have driven significant advancements in tool designs, technologies, and materials. However, FSW still faces challenges such as low welding speeds, high forces applied during welding, significant rotational forces on the material being welded, the requirement for large and often cumbersome equipment, the gradual wear and tear of the welding tool, and the difficulties encountered when joining high-strength materials. To address these issues, continuous improvements and innovations have been made to the machines, tools, and processes involved in FSW. This section focuses on specific FSW techniques that utilize specially designed tools, such as Friction Stir Spot Welding (FSSW), Bobbin-Tool (BTFSW), Stationary-Shoulder (SSFSW), Reverse Dual-Rotation (RDRFSW), and Twin-Tool (TTFSW), along with a brief overview of other FSW methods.[12]

Institutional Repository - Library & Information Centre - University of Thessaly
04/09/2026 08:51:35 EEST - 216.73.216.250

2.2 Types of stir welding processes

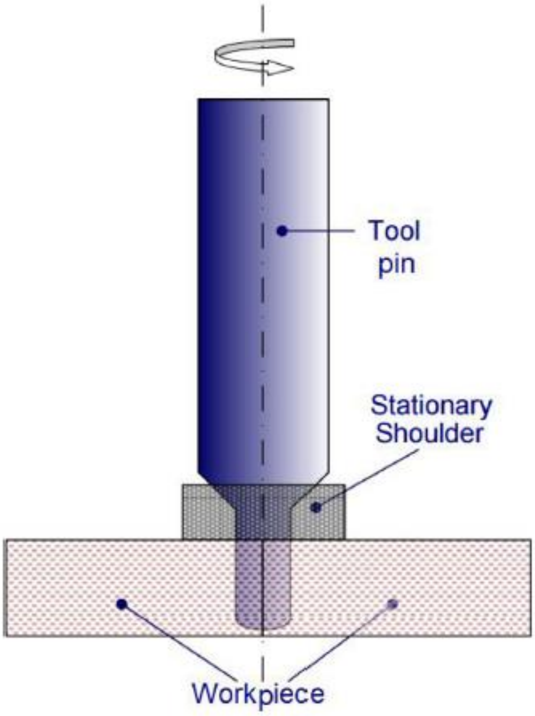

Figure 4 Diagram of the SSFSW process. [13]

2.2.1 Stationary-Shoulder Friction Stir Welding

"Stationary-Shoulder Friction Stir Welding (SSFSW)" was exploited at TWI to address the temperature difference throughout the thickness of the material challenges encountered in the friction stir welding of Titanium (Ti) alloys, known for their weldability difficulties. A graphic representation of SSFSW is provided in Figure 4. In this method, a spinning pin is embedded within a fixed shoulder that glides over the material's surface during the process. Consequently, the shoulder has minimal impact on deformation and generation of heat at workpiece's surface, whereas the rotating tool produces localized heat generated by friction, softening and stirring base material. This approach minimizes the size of the "Stir-Affected Zone (SAZ)", enhances process-stability, and improves the temperature and hardness distributions as well as the microstructural uniformity across the weld thickness.

Institutional Repository - Library & Information Centre - University of Thessaly
04/09/2026 08:51:35 EEST - 216.73.216.250

The primary parameters influencing the SSFSW and its produced joints include "tool profile and geometry, Rotational Speed (RS), Traverse Speed (TS), and Plunge Depth (PD)". Slower TS ensures a superior surface quality, whereas medium level speeds contribute to stronger joints.

Optimal rotation speeds, ranging from low to moderate, are critical for achieving desirable physical, mechanical, and microstructural properties in welded joints, as excessively high speeds can deteriorate these characteristics. Enhanced mechanical properties and microstructural uniformity are among the notable advantages of the process.

The magnified image obtained using an optical microscope for an Aluminum alloy 7075-T6 which has undergone the process is displayed in Figure 5(a). "The weld can be classified into distinct regions: the stir zone (SZ), thermo-mechanically affected zone (TMAZ), heat-affected zone (HAZ), and base material (BM)". The SZ exhibits a bowl-shaped or drum-shaped morphology, with the widest section occurring at medium thickness. Figure 5(b)-(e) illustrates the internal structure of the workpiece presenting all the zones mentioned above. Specifically TMAZ can be seen as a narrow and symmetrically positioned area around the SZ on mutually advancing and the retreating side.

Institutional Repository - Library & Information Centre - University of Thessaly
04/09/2026 08:51:35 EEST - 216.73.216.250

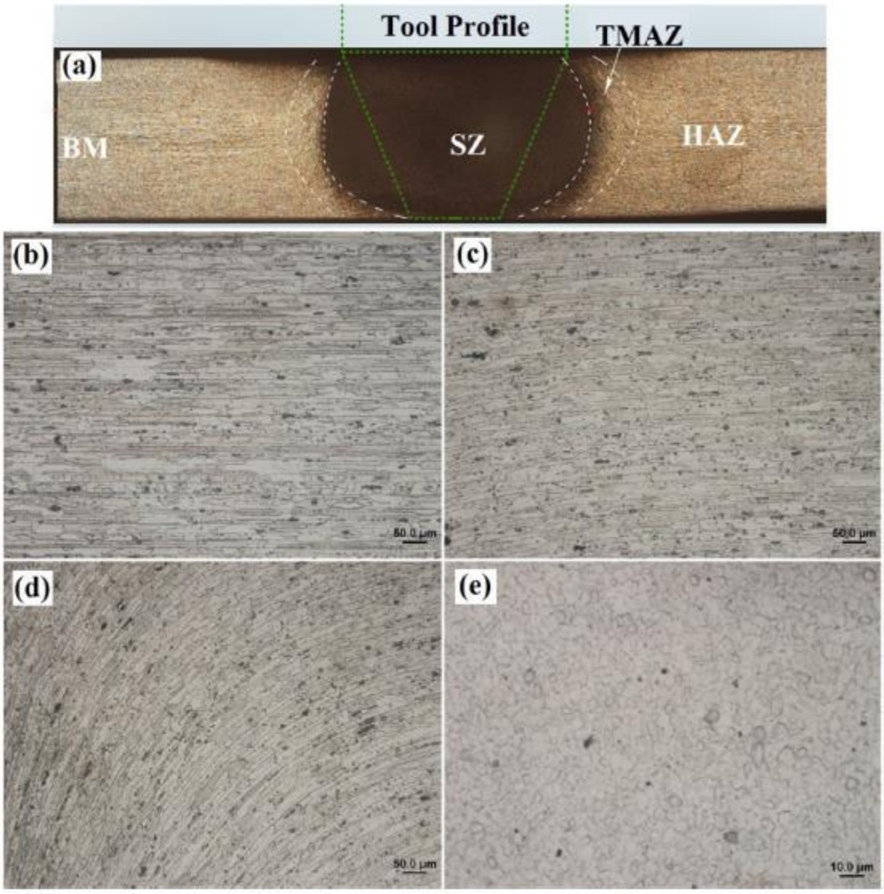

Figure 5 Optical micrographs of Stationary Shoulder FSW of 7075-T651 alloy

(a) “Macrostructure, (b) Base Material (BM), (c) Thermo-Mechanically Affected Zone (TMAZ), (d) Heat-Affected Zone (HAZ), (e) Stir Zone (SZ)”[14].

Grains in the Base Material are lengthened caused by the rolling process, while the structure within the Heat Affected Zone closely resembles that of the BM and remains largely unaffected by welding. The TMAZ demonstrates significant plastic deformation, with grains exhibiting a flow pattern indicative of material movement. Partial recrystallization is also observed within the TMAZ. The SZ is characterized by “refined, recrystallized grains that are homogeneous and equiaxed across the thickness”.

SSFSW has demonstrated considerable potential for welding aluminum alloys and has effectively mitigated overheating issues associated with titanium alloy welding. However, the practical application of SSFSW in welding iron and nickel alloys remains a challenge.

Institutional Repository - Library & Information Centre - University of Thessaly
04/09/2026 08:51:35 EEST - 216.73.216.250

2.2.2 Reverse Dual-Rotation Friction Stir Welding

High temperatures at the workpiece are a critical challenge in friction stir welding of large-thickness components, which compromises the microstructural and mechanical characteristics of the weld. This problem stems from the considerable difference in tangential velocity across the tool's radius. The problem can be mitigated by allowing the independent revolution of the shoulder and pin, enabling the tool-pin to achieve great rotational speeds while maintaining shoulder's peripheral RS. RDRFSW addresses this by independently rotating the shoulder and tool pin at dissimilar velocities in contrary directions. Additionally, the different directions of the shoulder and tool reduce the combined torque acting on the working material, thus minimizing fixture requirements. A diagram of the RDRFSW is illustrated in Figure 6(a).

Key process constraints influencing the properties of RDRFSW-welded joints include the RS of the shoulder, RS of pin, and TS. These parameters affect heat generation and distribution, and the deformation zone's size, subsequently impacting the joint's properties. A notable drawback of traditional FSW is the disparity in mechanical properties and microstructure between the “Advancing-Sides and Retreating-Sides of the process”. The reverse spins of shoulder and pin improve temperature symmetry throughout these sides, thereby reducing these differences and enhancing weld integrity. Joint properties in RDRFSW can be improved by simultaneously adjusting one rotational speed in tandem with the TS while keeping the other rotational speed unchanged, or by advancing the pin's Rotational Speed while reducing the shoulder's speed at a constant TS.

Figures 6(b)-(c) illustrate “the macrograph and representative microstructure of the RDRFSW joint. The joint can be classified into five distinct regions: the shoulder-affected zone (SAZ), stir zone (SZ), thermo-mechanically affected zone (TMAZ), heat-affected zone (HAZ), and base material (BM). Within both the stir zone (SZ) and the stir affected zone (SAZ), the grain structure exhibits recrystallization and a roughly equiaxed morphology”. However, the SAZ and SZ maintain distinct visual appearances due to the influence of reverse shoulder rotation. Notably, the grain dimensions within the SAZ is observed to be bigger than that within the SZ. Within the “thermo-mechanically affected zone (TMAZ)”, the grain structure exhibits an elongated morphology, aligning with the direction of

Institutional Repository - Library & Information Centre - University of Thessaly
04/09/2026 08:51:35 EEST - 216.73.216.250

applied shear stress, whereas grains in the Heat Affected Zone are coarser, closely resembling the grain size in the BM. Reverse rotation enhances refined grain structures not only at the Stir Zone but also at Stir Affected Zone. The “thermo-mechanically affected zone (TMAZ) and heat-affected zone (HAZ)” exhibit the presence of metastable, coarse precipitates. In contrast, the stir zone (SZ) is characterized by smaller, stable precipitates. [16]

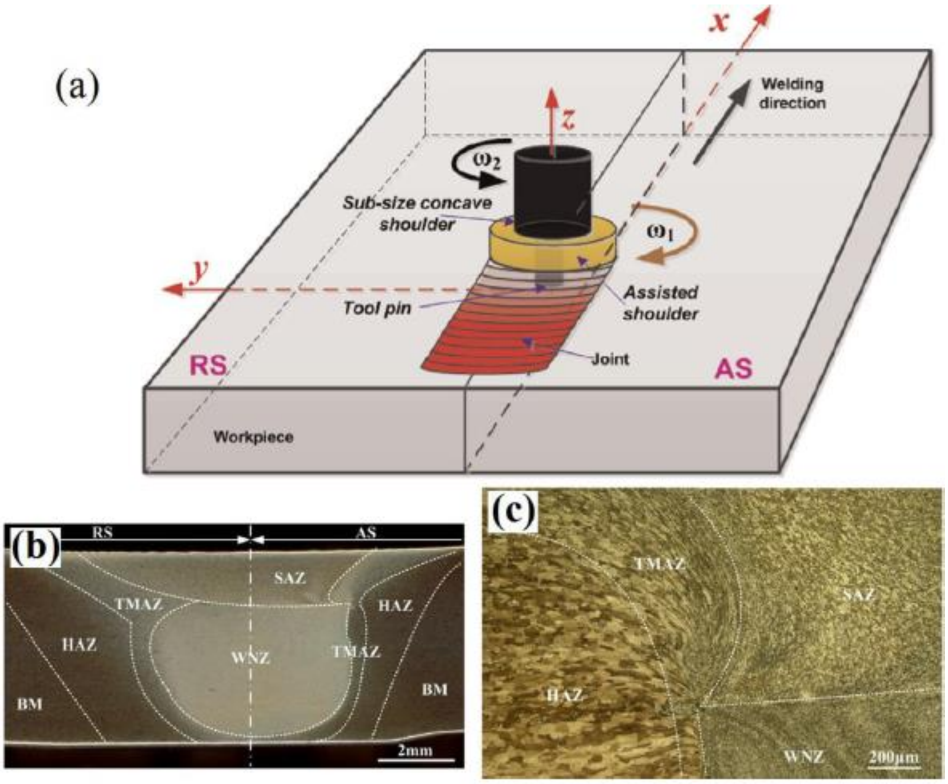

Figure 6 (a) Schematic of Reverse Dual Rotation FSW on 2219-T6[15] (b) Macrostructure image [16], and (c) Micro-structure [16].

RDRFSW has shown promise as a useful variant of FSW, but its application has so far been limited to aluminum alloys. Further investigation is warranted to evaluate the efficacy of this approach for processing a wider range of materials. A related welding technique involves “dual rotation speed friction stir welding (DRSFSW)”, where the shoulder and pin rotate independently at varying speeds while maintaining the same rotational direction. The key process parameters in DRSFSW are largely analogous to those employed in

Institutional Repository - Library & Information Centre - University of Thessaly
04/09/2026 08:51:35 EEST - 216.73.216.250

“reverse dual rotation friction stir welding (RDRFSW)”. The RS of the pin plays a pivotal role in forming the Stir Zone and OR. Counter-rotating shoulder and pin enhance weld properties by reducing microstructural asymmetry about the weld centerline. Higher rotational speeds of the pin improve process efficiency, whilst reducing shoulder speeds enhance weld formation.

2.2.3 Bobbin-Tool Friction Stir Welding

“The Bobbin-Tool Friction Stir Welding process” employs a “Bobbin-tool consisting of 2 shoulders” positioned on either side of the workpiece. A connecting pin extends between the “shoulders and traverses the entire thickness” of the workpiece throughout the welding process. Two categories of bobbin tools exist: one with a fixed gap between the shoulders and another adaptive design allowing an adjustable gap during welding. The self-reacting mechanism of the bobbin tool reduces or eliminates the need for downward axial force.

Figures 7(a) and 7(b) demonstrate the two types of tools used in the process. Figure 7(c) and figure (d) illustrate the process. Initiation can occur either at the plate-edge or through a pre-drilled hole between joined plates. It begins with low TS to initiate plastic deformation, followed by acceleration to a steady-state speed. Alternatively, prior to traversing the workpiece, the process may commence by ensuring adequate softening of the material surface which interacts with the spinning bobbin. Both shoulders help create heat by means of friction and material deformation, acting from opposing sides of the material. This design effectively confines reactive forces inside the tool itself, thereby mitigating compressive deformation of the tool-pin.

Institutional Repository - Library & Information Centre - University of Thessaly
04/09/2026 08:51:35 EEST - 216.73.216.250

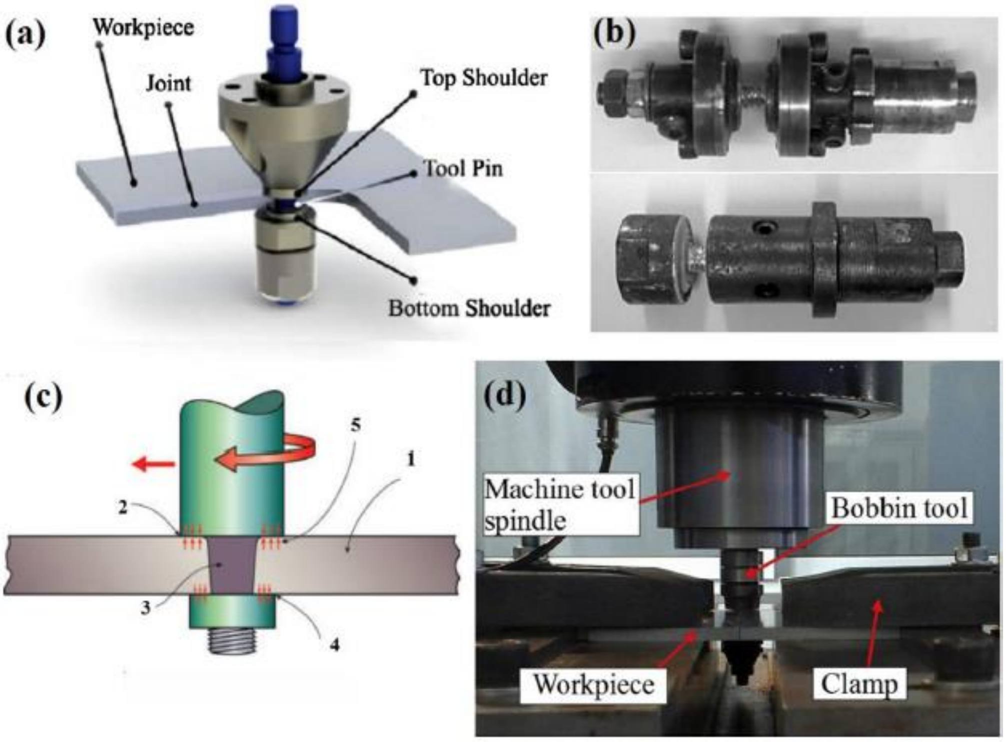

Figure 7 Bobbin-Tool process (a) “Schematic” [17], and (b) photo of tools [18]

(c) “Diagram that depicts: 1: Joining Parts, 2: Upper-Shoulder, 3: Tool-Pin, 4: Lower-Shoulder, 5: Applied forces” [19] (d) real life setup [20].

Key parameters in BTFSW include spindle RS and TS. Additional factors, such as dwell-time, the distance amongst the tool and the workpiece (tool gap), clamping arrangement, and the condition of the plates being joined, also significantly impact the characteristics of the welded joint. Furthermore, the specific design of the tool, its incorporated features, and the chosen process parameters all exert a significant influence on the final welding results. For aluminum alloys, recommended rotation speeds range from 450 up to 600rpm with TS from 75 to 100mm per min optimal for joining thin plates, typically ranging in thickness from 4 to 8 millimeters, and 170rpm to 300rpm with travel speeds of 100 to 500mm/min for thicker plates (around 25 mm). A rise in the ratio of RS/TS correlates with an enlargement of the grain dimensions in the weld. Conversely, lower temperatures, achieved through either reduced rotational speeds or increased traverse speeds, generally leading to improvements in both weld quality and overall mechanical properties.

Institutional Repository - Library & Information Centre - University of Thessaly
04/09/2026 08:51:35 EEST - 216.73.216.250

Figure 8(a) depicts a characteristic macrograph of a weld created via the BTFSW technique. The joint, like FSW, includes “the stir zone (SZ), thermo-mechanically affected zone (TMAZ), and heat-affected zone (HAZ)”. The SZ in BTFSW is shaped like a dumbbell or hourglass, characterized by a configuration akin to two FSW stir zones facing each other, but with a diminished shoulder width. At higher traverse speeds, the dumbbell shape becomes less distinct. The joint exhibits distinct upper and lower stir zones, characterized by recrystallized grains with an equiaxed morphology. Notably, the upper SZ displays a finer grain-structure compared to the lower SZ. The “thermo-mechanically affected zone (TMAZ)” exhibits a microstructure characterized by deformed, rotated, and elongated grains, exhibiting similarities to those observed in conventional friction stir welding (FSW). In contrast to conventional friction stir welding (FSW), where a characteristic "onion ring" structure is typically observed in the stir zone (SZ), BTFSW exhibits a distinct microstructural feature. Instead of the concentric rings, the central region of the SZ in BTFSW displays an elliptical region and a triangular region. These regions, magnified in Figure 8(b), result from insufficient deformation and stirring, with their sizes exhibiting opposite trends relative to heat input. Increased traverse speed enlarges the triangle region while reducing the ellipse region.

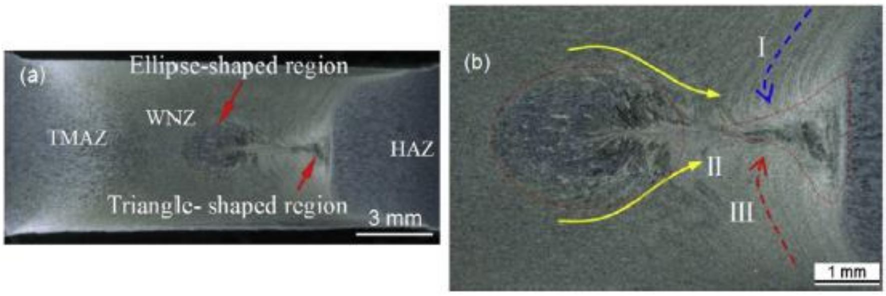

Figure 8 “Macrostructural image of the weld produced using the Bobbin Tool FSW process”. [20]

Institutional Repository - Library & Information Centre - University of Thessaly
04/09/2026 08:51:35 EEST - 216.73.216.250

BTFSW has been applied to aluminum, magnesium, and iron alloys, effectively addressing several limitations of FSW and enabling the successful welding of thick sections. For instance, the FSW process often requires a backing plate to support applied loads, limiting its flexibility, especially in welding closed hollow extrusions or complex structures. Additionally, root flaws may occur during FSW due to short tool pins or incorrect shoulder plunge depths. In contrast, BTFSW eliminates the need for a backing plate as the bobbin tool's bottom shoulder substitutes this function, while the pin carries most of the load. The pin's penetration across the full thickness of the workpiece ensures greater microstructural homogeneity and prevents root flaws. This capability allows BTFSW to weld thick sections from both sides simultaneously, enhancing process flexibility for intricate structures.

Advancements in friction stir welding have encompassed the development of innovative techniques, such as those employing counter-rotating twin-tools and self-supporting tooling systems. In each method, welding quality depends on tool rotation and traverse speeds. These approaches are still in early stages and require additional research for validation.

In addition to modified FSW processes, several innovative FSW variants incorporate auxiliary energy fields, such as thermal sources (e.g., electricity, laser, arc, or plasma) and mechanical sources (e.g., ultrasonic vibrations), to enhance the welding process. These auxiliary energy sources improve material flow, process efficiency, and weld quality by either complementing the heat-generation process, as observed in thermally assisted techniques, or directly soften the workpiece material, as exemplified by “ultrasonically assisted processes”. Experimental and numerical investigations into these auxiliary energy-assisted variants are ongoing and hold promises for future developments.

Institutional Repository - Library & Information Centre - University of Thessaly
04/09/2026 08:51:35 EEST - 216.73.216.250

2.2.4 Friction stir spot-welding

“Friction stir spot welding (FSSW)” is a variation of friction stir welding designed primarily for joining challenging-to-weld sheet materials in a lap joint configuration. This method is pretty similar to Friction Stir Welding but excludes tool's Transverse Movement. Also, it is a solid-state joining process that eliminates the need for consumables or shielding gases, thereby enhancing energy efficiency. The method was initially adopted by manufacturers such as “Sumitomo Light Metal Industries, Mazda, Kawasaki Heavy Industries, and Norsk Hydro” to replace riveting and reduce component weight.

Since its inception, it has been widely utilized for Spot-Welding a broad range of metals in various applications. Currently, several types of FSSW processes are in use, including conventional FSSW, “refill FSSW (RFSSW)”, and “pin-less” variants like “rotating anvil FSSW (RAFSSW)” and “double-sided FSSW”. Additionally, other FSSW process variations have been developed, commonly referred to as short FSW processes.

The stages of the procedure are illustrated in Figure9(a). Throughout the “plunge stage”, and while tool rotates, the threaded pin enters the overlapping sheets. Frictional heat created at the “interface between the tool and the upper workpiece” softens the material, while the threads facilitate material flow. When the “shoulder of the tool” touches the workpiece's surface, it exerts a substantial downward compressive force. The tool then advances progressively deeper into the workpiece and may pause briefly (“dwell stage”) before being withdrawn. This sequence creates a “solid-state bond to the sheets' interface”, as shown in Figure 9(a).

Institutional Repository - Library & Information Centre - University of Thessaly
04/09/2026 08:51:35 EEST - 216.73.216.250

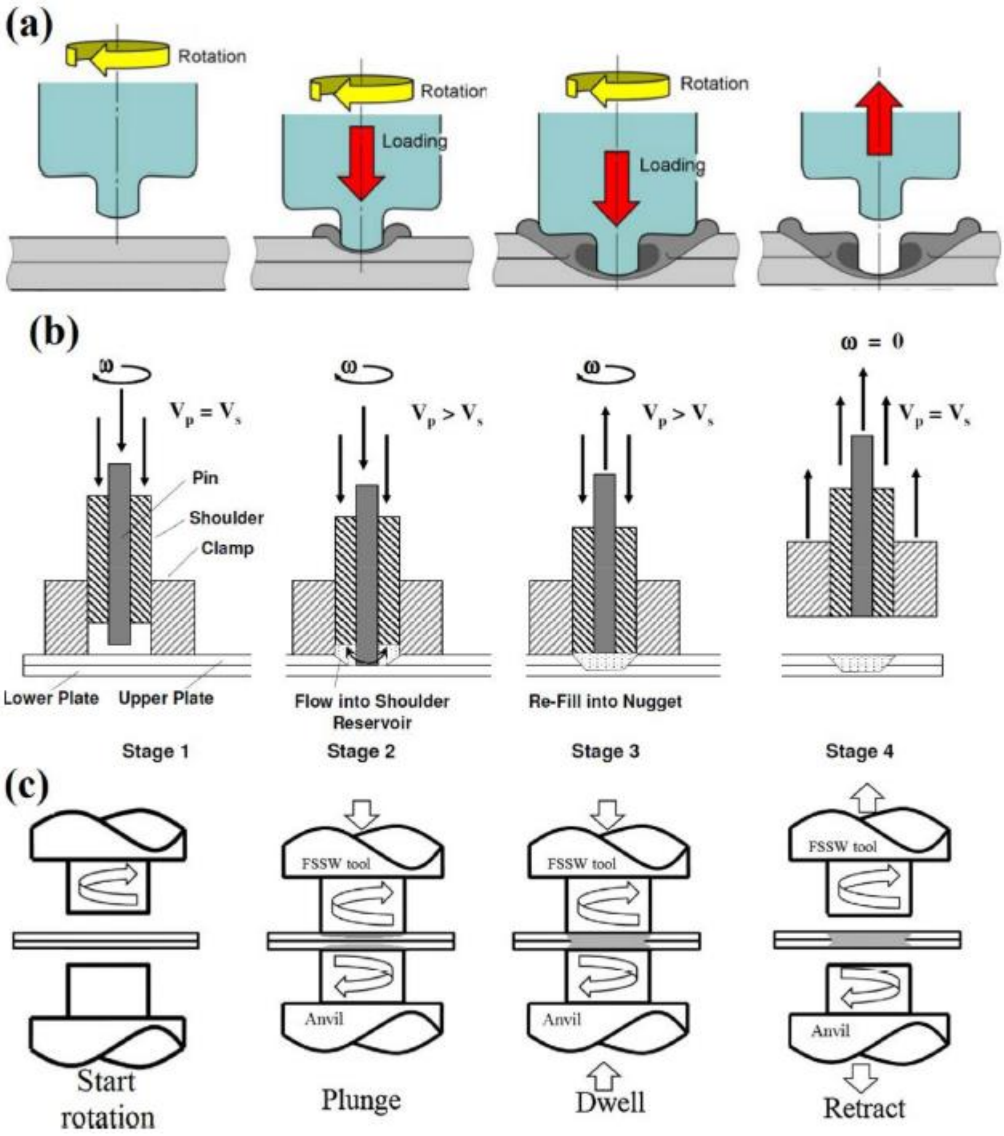

Figure 9 Diagrams of (a) "Friction Stir Spot Welding (FSSW)", (b) "Refill Friction Stir Spot Welding" [13], and (c) "Double-Sided FSSW".

Throughout the "plunge stage", material located underneath the pin is displaced upwards towards its boundary [21], and "bonding initiates even before the pin fully penetrates the lower sheet, driven by material deformation and diffusion at the pin tip". Material flow during this process is characterized by rotational, horizontal, and vertical movements [22]. Although the dwell stage is optional in FSSW, the process inherently leaves an exit hole at the joint due to tool "retraction". This "exit-hole" might be addressed through specific tool designs or "post-processing" techniques.

Institutional Repository - Library & Information Centre - University of Thessaly
04/09/2026 08:51:35 EEST - 216.73.216.250

2.2.5 Refill Friction Stir Spot-Welding

"Refill Friction Stir Spot-Welding (Refill FSSW)" is an enhanced version of FSSW method, designed to construct joints without creating an "exit-hole" in the joint. The process is illustrated in the stages shown in Fig. 9(b). In this variant, a specialized system is used to create the weld while maintaining a flush surface, effectively preventing an exit hole. This system includes three main pieces: "a clamp-ring, a shoulder, and a pin", each of which operates individually during the process.

Initially, the "clamp" secures the overlapping material sheets in place. The "rotating shoulder" then engages at the upmost material's surface, as the pin is maintained in a retracted state. Heat generated by friction amongst the shoulder and specimen softens the material. Once enough heat is generated, subsequently, the "pin is plunged into the workpiece, while the shoulder retracts to accommodate the material displaced by the advancing pin". Following a short "dwell-time", the pin is withdrawn, and the shoulder is then lowered back towards the material being joined. This action reintroduces the displaced material within the weld region, filling any potential "exit-hole". The process is finalized upon the complete retraction of the pin within the shoulder.

2.2.6 Rotating Anvil FSSW and Double-Sided FSSW

RAFSSW and "double-sided FSSW" are cost-effective alternatives to traditional FSSW, utilizing "pin-less" tools. Rotating Anvil FSSW is a "single-sided", "pin-less" FS Spot Welding technique that relies solely on a rotating shoulder to generate heat and apply substantial forging loads to achieve Spot-Welding. An anvil component is utilized to counteract the forces generated during the welding process. This method does not create an exit hole, but it is limited to welding sheets up to 1mm thick.

"Double-sided FSSW" is an enhanced version of RAFSSW, designed for welding thicker sheets. A representation of this procedure is displayed in Figure 9(c). In this method, the materials joined, are secured in a lap configuration, are simultaneously penetrated from

Institutional Repository - Library & Information Centre - University of Thessaly
04/09/2026 08:51:35 EEST - 216.73.216.250

opposite sides. A rotating tool shoulder engages the top workpiece, while an anvil penetrates the bottom workpiece. During the “dwell stage”, both the tool shoulder and the anvil continue to rotate and exert forging pressure. This creates the necessary frictional heat and deforms the material, facilitating the spot-welding process. Material flow occurs underneath the tool-shoulder towards its boundaries, then downwards, and finally back towards the centerline of the weld. The material displaced downwards by the “shoulder” and upwards by “the rotating anvil” converge at the interface, resulting in the formation of the weld joint.

2.2.7 Short-Traverse FSSW processes.

“Short-Traverse FSSW” processes, such as “stitch FSSW” and “swing FSSW”, employ a small traverse of tool following the principals of the initial FSSW operation. This minimal tool feed is employed to generate joints with larger surface areas, which results in higher strength. These processes are depicted in Figure 10 and are highly suitable for implementation in robotic systems.

In “stitch FSSW”, the tool-holder executes a circular or octagonal trajectory around a central axis. This controlled movement results in a weld joint length ranging from 8mm to 18mm, as depicted in Figure 10(a). In “swing FSSW”, the tool holder executes a short, circular swinging motion within a limited angular range around its central axis. This motion, driven by a cam mechanism, results in the formation of a short, 5millimeter “stitched” joint, as illustrated in Figure 10(b). Joints made by swing FSSW typically exhibit higher strength compared to those made by non-swing FSSW

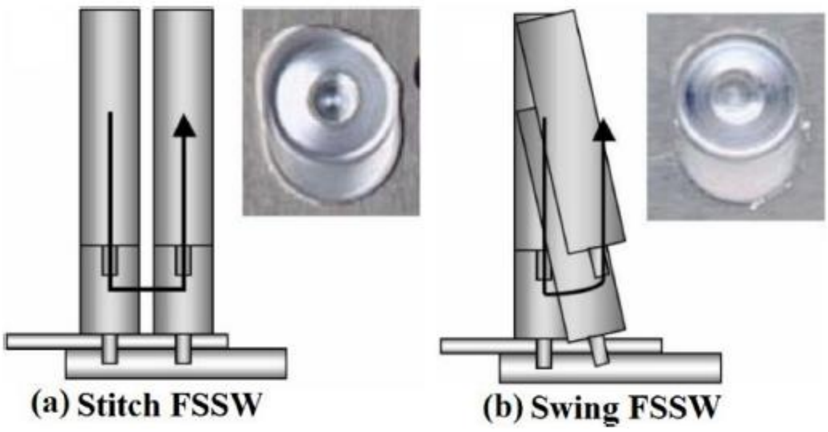

Figure 10 Short traverse Friction Stir Spot Welding processes (a) “stitch FSSW”(b) “swing FSSW” [23]

Institutional Repository - Library & Information Centre - University of Thessaly
04/09/2026 08:51:35 EEST - 216.73.216.250

2.3 Types of joints produced from FSW

Friction stir welding (FSW) is most effectively applied to “butt and lap joint configurations”. An example of a basic “square butt joint” is illustrated in Figure 11(a). In this setup, two plates or material sheets of identical thickness “are positioned on a backing plate and securely clamped to ensure the joint faces remain aligned during welding. Special attention is required during the initial tool plunge, as significant forces are involved, which could cause separation of the plates in the butt joint arrangement. The rotating tool is inserted into the joint line and moves along it while the tool's shoulder maintains close contact with the plate surfaces, resulting in a weld along the abutting edges”.[24]

In contrast, “for a standard lap joint, two overlapping plates or sheets are similarly clamped onto a backing plate. The rotating tool is plunged vertically through the upper plate into the lower plate and then traversed in the desired direction, fusing the two layers together (Figure 11(d)). Additional joint configurations can be created by combining butt and lap joint techniques. Furthermore, alternative joint designs, such as fillet joints (Figure 11(g)), can be utilized to meet specific engineering requirements”.[24]

Notably, no extensive preparation is necessary for Friction Stir Welding when working with butt or lap-joints. Plain sheet-metal plates can be readily welded in these configurations without significant concern for their surface condition.[24]

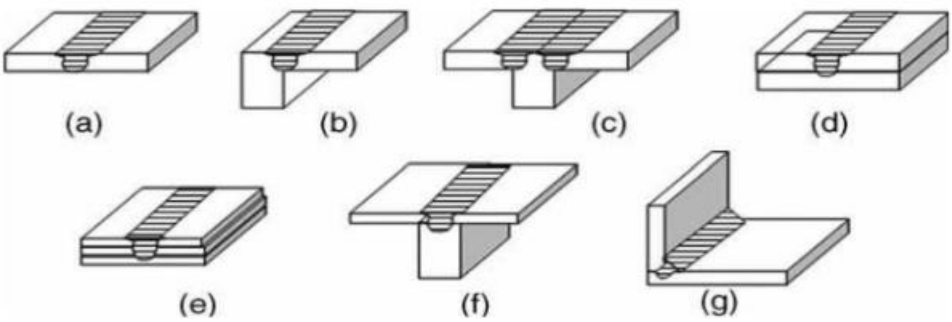

Figure 11 “Different designs of joints for friction stir welding:(a) Square butt joint, (b) Edge butt joint, (c) T-butt joint, (d) Lap joint, (e) Multi-layer lap joint, (f) T-lap joint, (g) Fillet joint”. [24]

Institutional Repository - Library & Information Centre - University of Thessaly
04/09/2026 08:51:35 EEST - 216.73.216.250

2.4 Materials usually undergoing FSW

Friction stir welding (FSW) is progressively utilized in large-scale productions across a range of industries, necessitating the welding of a wide array of materials. Aluminum alloys remain the primary candidates for FSW applications, while advancements in tool design and material have expanded its potential to include other metals and alloys. Recent developments have enabled FSW "to be utilized for joining materials such as copper, lead, magnesium and their respective alloys, stainless steel varieties like AISI 304L" [25], and high-melting-point metals including titanium, nickel, and their derivatives. Certain welding tools incorporate additional cooling or heating mechanisms, as well as gas shielding, to accommodate the stringent thermal and wear resistance requirements of these materials. According to Aissani et al. [26], a high gripping force on the workpiece and, in some cases, the integration of an absorber within the tool, are necessary to mitigate vibrations during welding. These specialized tools are not only effective for high-strength materials but also widely applied in aluminum alloy welding.

Composite materials, particularly metal-matrix composites (MMCs), can also be assembled using friction stir processing (FSP). For instance, Azizieh et al. [27] applied nano-powder into a surface groove to produce an AZ31/Al_2O_3 nanocomposite. After multiple passes of FSP, the nanoparticles achieved a more uniform distribution. Optimal microstructural properties were observed at a high RS of 1200rpm and four stir rounds. Additionally, FSP has been employed to develop Functionally Graded Materials (FGM) [28]. Marode further utilized "silicon carbide (SiC) and graphite (Gr) nanoparticles to enhance the properties of AZ91 magnesium alloy composites" [29]. "Multi-layered laminates can also be fabricated via FSP without defects". For example, Hassan described the "Friction Stir Additive Manufacturing (FSAM) technique to produce laminates using AA7075-T651" [30], and this procedure was applied by Hassan and Pedapati to create AA5083 laminate-structures [31].

Numerous studies have examined "the influence of welding parameters and joint efficiency for various materials", as summarized in Table 1. This table highlights the significant advancements in FSW applications for a diverse range of alloys and materials. It is evident that joint efficiencies vary, with pure metals generally exhibiting higher efficiencies compared to

Institutional Repository - Library & Information Centre - University of Thessaly
04/09/2026 08:51:35 EEST - 216.73.216.250

alloys. However, this trend does not extend to MMCs. Aluminum alloys, which typically melt at temperatures ranging from 463 to 671 °C, differ from magnesium alloys with lower melting points. Table 1 also reveals variations in melting temperatures and joint efficiencies among materials, which are influenced by processing parameters and the dissolution of alloying elements, as some components disintegrate at temperatures below the base material's melting-point. [32]

During the recrystallization process, which occurs after the tool passes the welding point, retained heat promotes grain refinement in the material. Various methods have been developed to optimize joint performance by reducing grain size. For example, lower temperatures can be accomplished by incorporating water cooling within the fixture, and a water-cooled backing plate or frame can further enhance cooling efficiency [33]. In FSW, tangential speed ranges from 0 at the pin's centerline to its maximum at the shoulder's limit. Once shoulder's diameter is large, this speed differential can cause low-melting-point materials or alloys to begin melting, adversely affecting their mechanical and microstructural properties. To address this, Li and Liu proposed "a dual-rotational tool, enabling differential speeds between the tool pin and shoulder". [16] This innovation allows the pin to spin at an optimal velocity without disrupting the shoulder's peripheral speed, resulting in improved joint efficiency compared to conventional FSW methods.

In MMCs, particles are intensely mixed and bonded when effectively welded with aluminum alloys. This process facilitates the evolution of refined grain structures and sizes, driving the development of MMCs using FSP. However, as indicated in Table 1, welding may not always achieve complete fusion along the thickness at the joint line. Certain experiments involving aluminum alloys revealed that FSP did not consistently outperform FSW [34]. Thus, such conclusions should be drawn cautiously.

Institutional Repository - Library & Information Centre - University of Thessaly
04/09/2026 08:51:35 EEST - 216.73.216.250

Table 1 The welding parameters and joint effectiveness of different materials. [35]

Work pieces materials and	Tool geometry	Tool material	Welding parameters				Joint or processing efficiency	N revolution/mm
			Feed (mm/min)	Rotational speed (rpm)	Force (kN)	Tilt angle (degree)		
AA2219-T6	Conical threaded pin with concave rotational sub-size and outer moving shoulder	/	100	800-900	/	2.5	69%	8.5
AA2219-T87	Square tool profile	High carbon steel	45.6	1600	12	/	61%	35.1
AA2024	Square pin profile	Tool Steel H13	60	900	9.9	2	87%	15
FSP of AA3003-H18	Cylindrical pin	Tool Steel H13	100	1200	/	2.5	54%	12
AA5083-H321	Flute threaded pin		85	266	/	2.5	85%	3.1
AA6082-T6	Cavity shoulder (concave) and cylindrical pin	56NiCrMoV7-KU	460	1810	/	2	77%	3.9
AA6351	Cylindrical tapered	High speed steel (WC-Co)	115	1350	/	2	68.8%	11.7
AA6005C-T5	Cylindrically	/	350	1200	/	0	82.1%	3.4
AA7075-T651	Tapered (conical) threaded the helix to the right once and to the right once more	/	100	1600	/	/	63%	16.0
AA7075-T6	Concave shoulder with cylindrical pin tool	Tool Steel H13	40	1300	/	3	75.8%	32.5
AA7039	/	High carbon steel	40	460	6.5	/	83.3%	11.5
AA2024-0 and AA5754-H22	Cylindrically screw thread pin	/	5	2000	/	/	66.93%	400.0
AA5083 and Pure Copper	Cylindrical pin	Tool Steel H13	32	825	/	3.5k	74%	25.8
Pure Copper and AA1350	Concave shoulder with conical threaded pin	/	80	1000	/	2.5	74%	12.5
Magnesium AlloyAZ31B-H24	Scrolled shoulder with left hand threaded prope	Tool Steel H13	1200	1000	/	0.5	62% tensile shear	0.8
Magnesium AlloyAZ31B-H24	Scrolled shoulder with right hand threaded prope	Tool Steel H13	1800	2000	/	/	78%	1.1
Al-Mg-Si Alloy	Screwed pin and hybrid shoulder	/	800	1800	8	/	82.8%	2.25
Dissimilar AA6063 and Metal Matrix Composites Al-B4C	Conical unthreaded	WC-Co Alloy	100	2000	9.8E-6 on MMC Al-B4C and 9.8E-5 on AA6063 side	3	100%	20.0
AA 6061-T6 and 430Stainlesssteel	Incomplete cone-shaped pin	Tungsten carbide–cobalt	80	560	/	3	62.8%	7
Titanium alloy Ti-Al6V4 and AA2024	Concave shoulder with threaded tapered pin	Standard tool steel coated with a voidex excessive wear	80	800	/	/	73%	10.0
Oxide Desperit Strengthen MA956	Tapered cylindrical	Hybrid Carbide WC-Co face and W-Ni-Fe shank	51	1000	/	3	125%	19.6
Acrylonitrile Butadiene Styrene ABS	Threaded cylindrical pin tool with shoe shoulder geometry assistant to provide heat	CK45 Steel and using a shoe made from common Structural Steel	20	1600	/	0	88.8%	80.0
Martensitic Steels	Cylinderical pin	WC-based material	150	400	/	3	92%	2.67
AISI 304 Stainless steel	Equilateral triangle pin and shank with mill cutter	Cemented carbide specifications: K10, 94% WC and 6% Co	60	950	9	1.5	85.14%	15.8
Copper DHP	Scrolled shoulder with threaded cylindrical pin	/	160-250	1000	7	0	100%	4.9
Pure copper	/	SKD61	200-800	<1300	9.81	3	100%	1.6
Pure Titanium	Threaded cylinder	Shoulder made from tungsten (W) and a pin made from tungsten carbide (WC)	60	1500	/	1	100%	25.0
Electro-galvanized mild steel (EG) to magnesium alloy AZ31	Scrolled convex shoulder and cylindrical pin with curved tip at the end of the pin	Tool Steel H13	100	700	6.5	0	80%	7.0
HSLA-65 Steel	Cylindrical with tapered end tip	W-25%Re pin with Mo-TZM shoulder	76.2	400	/		108%	5.2
Ni-Al Bronze Alloy	Threaded conical pin with concave shoulder	Nickel- Alloy super alloy	50	1200	/	3	100%	24.0
Mg-10Gd-3Y-0.5Zr casting	Threaded conical pin	/	50	800	/		100%	16.0
Cu-Ni alloy and Low-carbon steel (SS400) with Ni coating assistant	Cylindrically	High speed steel SKH51	10	800-1400	/	1	Shear strength will be 2.9 times that without Ni coating	110.0

Institutional Repository - Library & Information Centre - University of Thessaly
04/09/2026 08:51:35 EEST - 216.73.216.250

Chapter 3. Process Optimization in Stir Welding

3.1 Factors influencing weld quality and mechanical properties

The final quality and durability of the weld are determined by numerous factors and variables. Among these, “the design of the tool, plunge depth, pin configuration (threaded or unthreaded), and shoulder and tool” attributes play a pivotal role. Additionally, “welding speed and tool rotational speed” are two critical parameters that significantly impact the welding outcome.

Specifically, design constraints such as the “pin profile and shoulder geometry” are key determinants of welding quality in FSW, as they effect material movement, shoulder structure, and the connection area amongst tool and workpiece. A well-designed shoulder promotes efficient heat transfer and effective material mixing, thereby enhancing weld quality. Similarly, the pin profile governs the stirring action and defect formation. An optimized pin profile facilitates consistent material flow and minimizes defects, thereby improving the welding process's overall quality [36].

Various studies have researched the impacts of these factors on weld quality. Liu and Li [37] examined the influence of the shoulder’s condition—for both stationary or moving. They observed that increasing the rotational speed of the tool from 600 to 900 rpm exacerbated certain defects, attributing these issues to the stationary shoulder. Nonetheless, using this shoulder type offered some advantages, including a slight improvement in joint efficiency, while appropriate rotational speeds could result in defect-free welds. “For both similar and dissimilar materials”, the influence of these factors remains largely consistent. Bisadi et al. [34] shown the importance of tool RS in determining weld quality for lap joints between AA5083 and commercially pure copper sheets. Their findings indicated that defects were prevalent at both excessively low and high welding temperatures, which were influenced by the “frictional interaction between the rotating tool and the workpieces”.

Sundarama and Murugan [38] investigated the tensile performance of a joint between AA2024-T6 and AA5083. Their experimental study employed various tool geometries, revealing that “tapered hexagonal pin profiles produced the highest tensile strength and elongation, whereas straight cylindrical pins resulted in the lowest values”. Elangovan and Balasubramanian [39,40] also found that square pin profiles outperformed other shapes in tensile testing. Their research further emphasized the importance of shoulder diameter, demonstrating that maintaining the diameter within an optimal range is crucial for achieving effective joint performance. Excessive heat generation, often caused by friction and stirring, necessitates careful consideration of shoulder geometry during design to avoid overheating [38,41,42].

Institutional Repository - Library & Information Centre - University of Thessaly
04/09/2026 08:51:35 EEST - 216.73.216.250

The volume of heat generated during the FSW is affected by the forces acting on the tool-workpiece setup. Arora et al. [42] estimated the torque, as well as the extent of “sticking and sliding at the interface” between the tool and the workpiece. They noted that torque and heat generation are interdependent. The heat Q produced per unit area at the interface, was calculated as follows:

$$Q = [(1 - \delta)\xi\tau + \delta\mu_f P_N](\omega r - v sin\theta) \quad (2)$$

Here, “ ξ represents mechanical efficiency, ω is the tool's rotational speed (in rad/s), P_N denotes the applied axial pressure, τ indicates the shear yield strength, while μ_f and δ are the friction coefficient and spatially variable fraction slip, respectively. The radial distance is r and v is the welding speed”. The parameters μ_f and δ were further derived using

$$\delta = 0{,}31 \exp\left(\frac{\omega r}{1.87}\right) - 0.062 \ (3)$$

$$\mu_f = 0.5 \exp(\omega r \ x \ \delta) \ (4)$$

The tangential velocity ωr “was measured in m/s, with parameter boundaries set between 0.1 and 1.6 m/s. Heat generation depends primarily on the shoulder diameter and rotational speed, with (ωr−vsinθ) being the critical factor in Eq. 2. For optimal welding conditions, ωr must exceed vsinθ. Notably, the geometry of the pin exerts a limited effect on heat generation and torque [25]. However, when considering identical welding parameters, it becomes evident that tool shape design plays a critical role in welding strength and quality” [42].

Institutional Repository - Library & Information Centre - University of Thessaly
04/09/2026 08:51:35 EEST - 216.73.216.250

3.2 Tool Optimization

3.2.1 Tool Geometry

“Advancements in tool design have been achieved through extensive research at various welding institutes. Numerous modifications to tool geometry have been implemented to enhance the welding process.

Tool geometry is one of the most critical factors influencing the development of the FSW process. It significantly affects material flow and directly determines the traverse rate at which friction stir welding can be performed. An FSW tool typically comprises a shoulder and a pin, as illustrated schematically in Fig. 12. The tool serves two primary purposes: (a) localized heating and (b) facilitation of material flow. During the initial phase of the plunge, heat is primarily generated through friction between the pin and the workpiece, with additional heating resulting from material deformation. The tool continues to plunge until the shoulder comes into contact with the workpiece, at which point friction between the shoulder and the workpiece contributes the most to heat generation. From a heating perspective, the relative dimensions of the pin and shoulder are of primary importance, whereas other design attributes play a secondary role. The shoulder also confines the heated material within its boundary.”

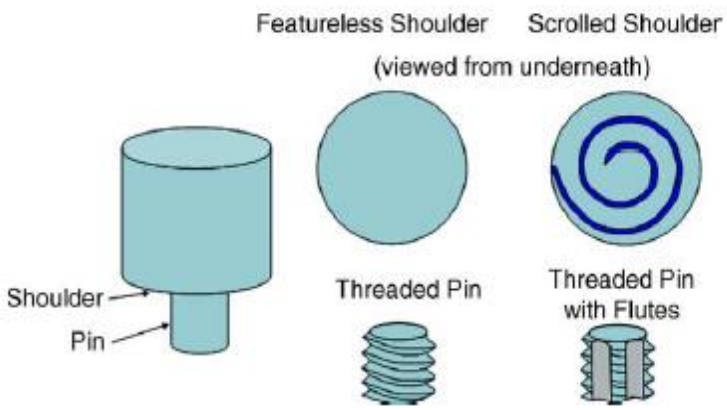

Figure 12 Diagrammatic representation of a FSW tool. [1]

“The second function of the tool is to stir and move the material. The uniformity of the microstructure, mechanical properties, and the process loads depend heavily on the tool's design. Typically, tools with concave shoulders and threaded cylindrical pins are preferred”. [1]

“With advancements in understanding material flow, tool geometry has evolved substantially. Innovative features have been introduced to enhance material flow, mixing, and reduce process loads. For instance, the “Whorl™ and MX Triflute™ tools”, developed by TWI,

Institutional Repository - Library & Information Centre - University of Thessaly
04/09/2026 08:51:35 EEST - 216.73.216.250

are depicted in Figure 13”. According to Thomas et al. [43], the pins in these tools are designed as frustums, displacing less material compared to cylindrical pins with identical root diameters. “The Whorl™ reduces displaced material volume by approximately 60%, while the MX Triflute™ achieves a 70% reduction. These tools are designed to: (a) lower welding forces, (b) enable smoother material flow, (c) create a downward augering effect, and (d) increase the interface between the pin and the softened material, thereby increasing heat generation. These advancements have made it possible to friction stir weld aluminum plates up to 50 mm thick in a single pass using these tools. Additionally, a 75 mm thick 6082Al-T6 plate was welded in two passes, each achieving approximately 38 mm penetration. Thomas et al. [43] identified the dynamic-to-static volume ratio of the pins as a key factor in ensuring sufficient material flow paths”. When using pins with nearly identical root diameters and lengths, “this ratio is approximately 1.1:1 for conventional cylindrical pins, 1.8:1 for Whorl™ pins, and 2.6:1 for MX Triflute™ pins when welding 25 mm thick plates.”

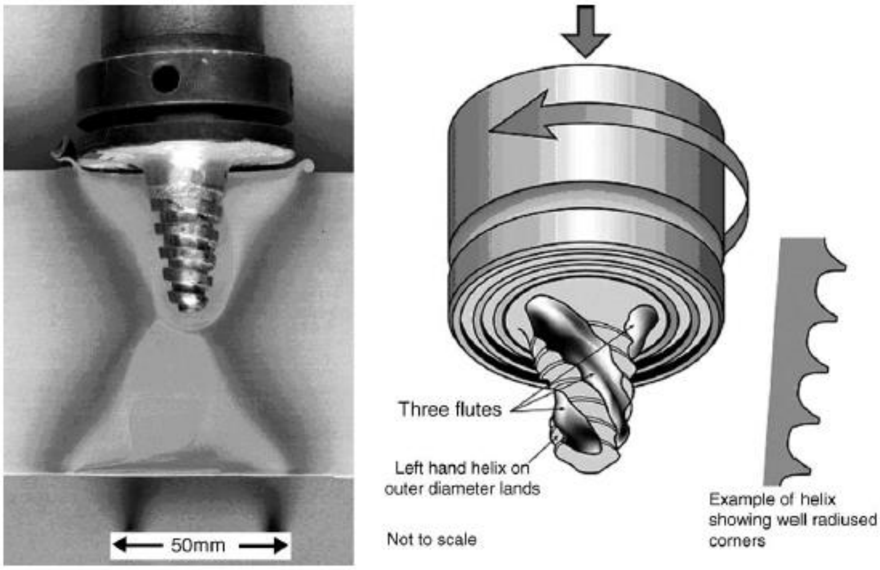

Figure 13 “WorlTM and MX TrifluteTM tools developed by TheWelding Institute (TWI), UK” [43]

In lap-welding process, “conventional cylindrical threaded pins often lead to excessive thinning of the top sheet, significantly impairing bend properties” [44]. Additionally, “the weld interface's width and the notch's angle at the weld edge are critical for applications where fatigue performance is a primary concern. To address these issues, two novel pin geometries—Flared-Trifute™ (with flared-out flute lands) and A-skew™ (with the pin axis inclined relative to the spindle axis)”—were developed, as shown in Figures 14 and 15.

Institutional Repository - Library & Information Centre - University of Thessaly
04/09/2026 08:51:35 EEST - 216.73.216.250

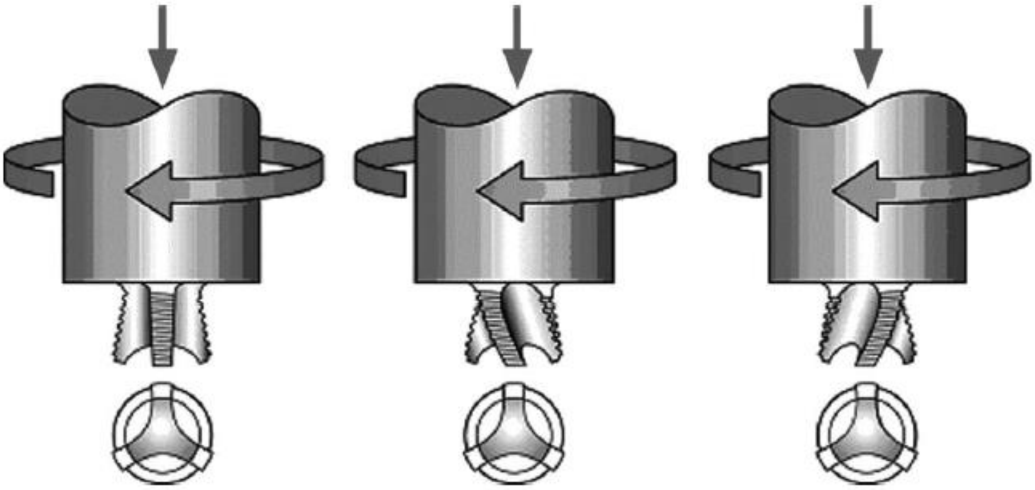

Figure 14 “Flared-TrifluteTM tools developed by TWI: (a) neutral flutes, (b) left flutes, and (c) right hand flutes” [44]

These designs aim to: (a) enhance the “swept-to-static volume ratio of the pin for better material flow, (b) expand the welding region through flared flute lands or skewed pin action, (c) improve oxide fragmentation and dispersal at the weld interface, and (d) provide orbital forging at the weld root, enhancing weld quality in this area. Compared to conventional threaded pins, Flared-Trifute™ and A-skew™ pins demonstrated over a 100% increase in welding speed, approximately a 20% reduction in axial force, a significantly expanded weld region (190–195% of plate thickness versus 110% for conventional pins), and a reduction in upper plate thinning by more than four times [45]. Furthermore, the Flared-Trifute™ pin substantially reduced the notch angle at the overlapping plate/weld interface, while the A-skew™ pin produced a slight downturn in the outer weld interface regions, both of which improved joint properties [44,45]. Thomas and Dolby [45] concluded that these pins are well-suited for lap, T, and similar welds, where the joining interface is perpendicular to the machine axis.”

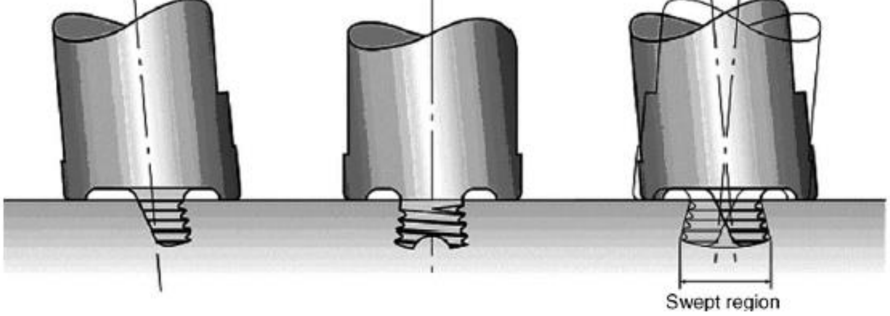

Figure 15 “A-Skew^{TM} tool developed by TWI: (a) side view, (b) front view, and (c) area covered by the skewing motion.” [44]

Institutional Repository - Library & Information Centre - University of Thessaly
04/09/2026 08:51:35 EEST - 216.73.216.250

Various shoulder profiles have also been developed by TWI to accommodate several materials and joining constraints (Figure 16). These designs have a better mechanical interlocking among the tool shoulder and the material by locking softened material inside specialized re-entrant features.

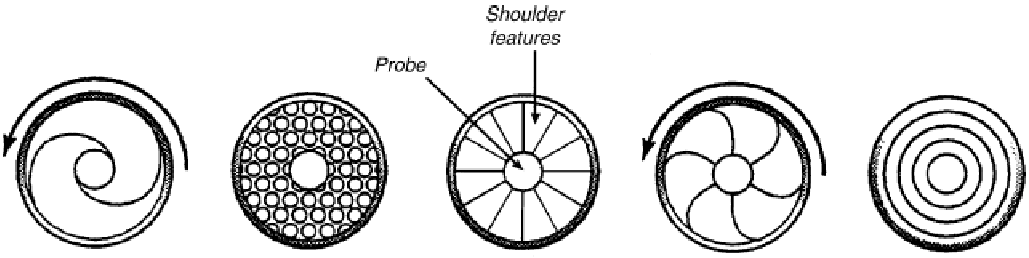

Figure 16 Tool shoulder profiles, observed from the underside. [43]

Given the substantial influence of tool shapping on material flow, the relationship between material movement and the resultant microstructure changes with every tool design. Developing a structured approach to tool development is essential. Computational methods, such as “finite element analysis (FEA)”, can provide insights into material flow and axial force distribution. Although some companies have conducted internal R&D in this area, these findings are not widely available in the public domain. A deeper understanding of the correlation between microstructure evolution and process constraints remains challenging without detailed information on tool designs. Tool geometries and their use in special processes are displayed in Table 2.

Institutional Repository - Library & Information Centre - University of Thessaly
04/09/2026 08:51:35 EEST - 216.73.216.250

Table 2 Key advancements in the design of tool shapes used in FSW. [35]

Descriptions and features of tools
Bobbin tool
• Has an extra backup part instead of the backup plate.
• Can be used for welding curved plates by using shoulder and backup parts that have concave or convex shapes.
Tool with supporting arm
• The arm is used to preserve the plates at the welding line.
• The arm can also be modified to provide heat for welding materials and alloys with high melting temperatures.
Retractable tool
• This tool can be retracted automatically into the shoulder to avoid hole defects at the end of the welding process.
• The tool moves vertically, rotationally, and linearly.
• However, additional equipment is needed to control this tool. It is manufactured by the NASA Marshall Space Flight Center.
Shoe heater tool
• The shoe is used to provide additional heat.
• It is suitable for welding materials with low-friction coefficients, such as ABS material.
Twin-stir tool
• Reduces the forces required for fixing the workpieces.
• Has high-quality joining results.
• Unfortunately, it produces two-hole defects.
Three different variants of this instrument were produced at the welding institute: parallel, tandem, and staggered twin-stir.
Stationary shoulder tool
• There are two shoulders on this tool; the one closest to the pin rotates while the other remains motionless.
• Removes the flash defects
• Lessens the required torque
• This tool requires a careful selection of the welding parameters to prevent additional defects caused by the stationary shoulder.
Tungsten carbide tool
• It provides a cooling factor that decreases the wear.
• Typically used for welding harder alloys and materials.
• A cooling bracket at the outside shoulder and an internal heater to raise the temperature at the stir point are features of some models.
• It has the ability to protect gases.

Institutional Repository - Library & Information Centre - University of Thessaly
04/09/2026 08:51:35 EEST - 216.73.216.250

3.2.2 Tool material

The material used for FSW tools must exhibit superior rigidity and strength relative to the workpiece. “Additionally, the mechanical properties of the tool, including strength and thermal performance, should be high to ensure effective and uniform heat dissipation” [46]. Tools designed for “joining soft materials, such as aluminum and magnesium alloys, are relatively easier to manufacture with the desired properties. Commonly used materials for such tools include high-speed steel, low-carbon steel, and H13 tool steel, which are commercially available and effective across a range of process parameters” [47]. These materials demonstrate excellent performance with minimal wear and material degradation during welding. “Among them, H13 tool steel is widely regarded as a reliable option for welding aluminum and magnesium alloys with thicknesses ranging from 0.5 to 50mm“[48, 49].

In “structural applications, especially in industries like defense, aerospace, oil and gas, and heavy manufacturing, there is a high demand for tools that offer extended service life and deliver satisfactory weld quality. However, when dealing with harder materials like steel and titanium, further research and improvement of tool materials remain necessary. Advanced tool materials, including tungsten carbide and polycrystalline cubic Boron Nitride (PcBN), have proven effective for welding high-strength materials like steel, copper, and titanium. For commercial FSW applications, the selected tool material must also be cost-effective, durable, and structurally robust” [50].

The selection of tool materials, along with their performance analysis in terms of welding quality and cost efficiency, continues to be a critical area of focus. Developing tools that balance these factors is vital to enhancing the efficiency and applicability of FSW processes. Table 3 presents the typical combinations of alloy types and corresponding tool materials commonly utilized.

Table 3 Suitable pairs of materials for tool design and part material. [35]

Type of alloy	Thickness (inch)	Tool material
Al Alloys	<0.50	Tool Steel, WC-Co
	<1.02	MP159
Magnesium Alloys	<0.24	Tool Steel, WC
Copper and Copper Alloys	<2.00	Nickel alloy, PCEN(a), Tungsten alloys
	<0.40	Tool Steel
Titanium Alloys	<0.24	Tungsten Alloys
Stainless Steel	<0.24	PCBN, Tungsten Alloys
Low-alloy Steel	<0.40	WC, PCBN
Nickel Alloys	<0.24	PCBN

(a) Polycrystalline Cubic Boron Nitride

Institutional Repository - Library & Information Centre - University of Thessaly
04/09/2026 08:51:35 EEST - 216.73.216.250

3.3 Optimization Techniques for Stir Welding

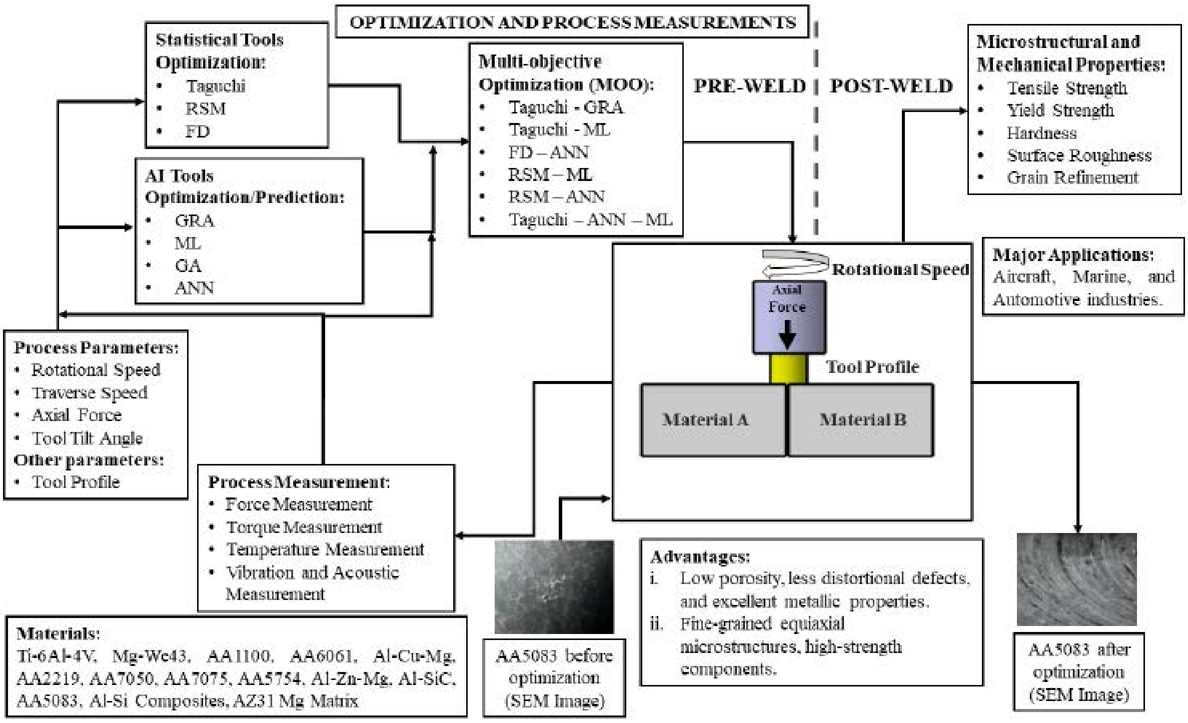

Figure 17 “Schematic representation of the optimization and measurement methods applied in the FSW process”. [51]

Optimization algorithms are integral components of the optimization process, functioning as numerical simulators to accurately represent physical models requiring optimization. These algorithms can be broadly categorized as either deterministic or stochastic. “Deterministic algorithms operate based on predefined rules, producing consistent outputs for a given input without incorporating randomness. In contrast, stochastic algorithms involve randomness in their operation, leading to variable outputs for the same input. The incorporation of randomness at various stages of an algorithm is often referred to as heuristics or, in some instances, metaheuristics” [52]. This section provides an overview of the optimization techniques applied thus far in FSW. Figure 18 illustrates the diverse combinations that can be employed to achieve optimisation.

Institutional Repository - Library & Information Centre - University of Thessaly
04/09/2026 08:51:35 EEST - 216.73.216.250

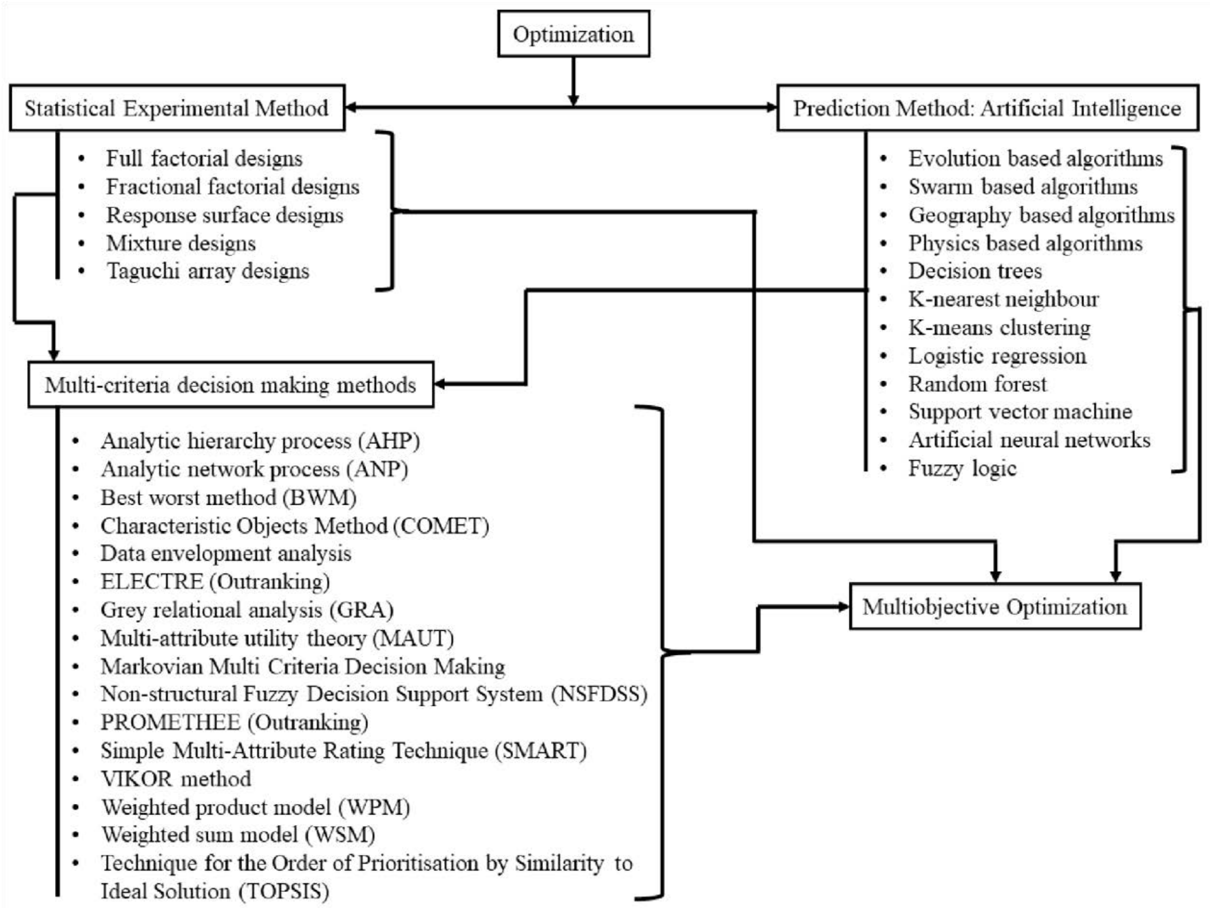

Figure 18 Various arrangements that can be utilized for conducting optimization.[51]

3.3.1 Statistical Tools

Taguchi Optimization

The Taguchi method, formed by Dr. Genichi Taguchi in 1978, is a statistical approach aimed at enhancing the quality of manufactured products. This method involves the design of experiments (DoE) to create robust systems [53]. The Taguchi optimization process comprises eight sequential steps:

- Identifying the elementary function for the method.
- Determining factors such as noise, testing conditions, and quality attributes.
- Establishing the criterion function.
- Categorizing the various elements, so as to assign appropriate values.
- Selecting the appropriate orthogonal matrix for conducting multiple experiments.

Institutional Repository - Library & Information Centre - University of Thessaly
04/09/2026 08:51:35 EEST - 216.73.216.250

- Performing the experiments.
- Analyzing the data and predicting the optimal performance level.
- Verifying the experimental results and planning future actions.

The parameters selected during this process can significantly influence FSW joints, material properties, microstructure, and grain refinement. Proper parameter settings are crucial in achieving desirable outcomes. Optimization tools facilitate the development of inter-relationships among various parameters, enabling their analysis [54]. These tools generate the optimal combination of data for implementation in the process. In Figure 19 is shown how Taguchi optimization method works.

Korgal investigated the grain alteration but also the tensile strength of AA4032 alloy with the Taguchi method combined with ANOVA analysis [55]. One of its main advantages (of Taguchi meth.) is that prioritize the average operation value instead of merely ensuring results fall within specified limits. This approach simplifies narrowing down the primary process parameters. Taguchi’s orthogonal arrays (OAs) reduce the number of required experiments to less than 0.3% of the original experimental set. However, this method has limitations: It neither assesses every possible configuration of procedure parameters nor considers dynamic variations in values. Additionally, operates exclusively in offline optimization mode, serving as a foundational step in process development.[51]

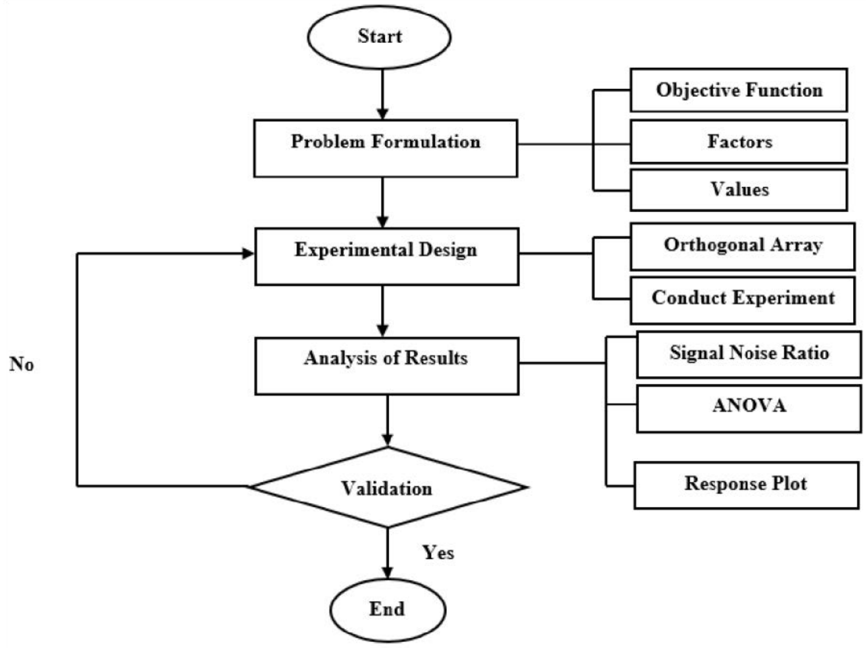

Figure 19 Flow diagram of the Taguchi optimization process. [51]

Institutional Repository - Library & Information Centre - University of Thessaly
04/09/2026 08:51:35 EEST - 216.73.216.250

Taguchi L18 experiments were performed to join an AA2014 aluminum alloy in six millimeters of thickness, an AZ31 Mg alloy and Al–SiC composite utilizing an alloy steel tool, varying parameters such as rotational speed (RS) (600 to 1200rpm), pin profile (tapered and non-tapered), traverse speed (TS) (20 to 35mm/min), and preheating. The analysis revealed that tool rotation significantly influenced tensile strength, whereas the tool pin shape had minimal impact [56]. A tapered, unthreaded high-speed steel (HSS) tool was employed to join five millimeters thick AA6351 and AA5083 plates coated with copper and zinc. Coating thickness was found to significantly affect tensile strength, with optimal parameters being a TS of 20 mm/min, RS of 1300rpm, and 50 µm of copper coating on both sides, resulting in tensile strengths of 141–149.5 MPa [57].

Taguchi L9 experiments, involving Rotational Speed (1000 to 1600rpm), TS (3to5mm/s), and axial force (5–7 kN), were performed for butt welding AA6063 pipes. Results indicated that traverse speed had a 62.75% impact and axial force a 50.43% impact on residual stresses in the welded joint [58]. Another Taguchi L9 experimental setup, varying RS (1000to1400rpm), Feed Rate(FR) (14to18 mm per min) tool shapes (tapered, threaded, and cylindrical), analyzed AA5451 plates employed in marine applications. “The threaded pin profile exhibited superior performance in tensile strength, hardness, joint efficiency, and microstructure” [59].

A Taguchi experimental design with parameters Rotational Speed(710to1400rpm), Traverse Speed (16to40mm/min) and stay time (8–22s), using an H-13 die-steel-tool with a cylindrical-pin, was employed for Al-Li (AA 8090) alloy joints. Higher TS and dwell time enhanced ultimate tensile strength (UTS) by reducing “heat flow into the weld zone”, while increasing RS significantly improved hardness. Scanning electron microscopy (SEM) analysis showed improved grain density near the weld line, leading to greater properties. Ductile fracture characterized by dimpled morphology was found in joints areas [60].

Optimization of parameters including Rotational Speed (700to1100rpm), Axial-Force (1.5–2.5kN), Tilt-Angle(1–3°), and pin profile: tapered-threaded was carried out for dissimilar butt welding of AA 6061 and AA 7075 alloys. Results demonstrated that impact strength increased with RS up to 1000 rpm and tilt angle, but declined thereafter [61]. Also studied the influence of pin shapes (cylindrical, triangular, square) with Rotational Speeds of

Institutional Repository - Library & Information Centre - University of Thessaly
04/09/2026 08:51:35 EEST - 216.73.216.250

450to1120rpm, Traverse Speeds of 100 to 250mm per minute and tilt-angles of 1 to 3° on the corrosive performance of AA1080 alloy. Pins with smooth surfaces exhibited better corrosion resistance. SEM analysis revealed greater corrosion in samples welded with triangular pins compared to those with cylindrical pins, which showed higher corrosion resistance due to finer grain size [62].

"Multi-objective optimization using grey relational analysis (GRA)" was conducted for AA6982-T6 parts to evaluate the effect of the shoulder dimensions in diameters from 14 to 18 mm, "plunge depth (PD) from 0 to 0.4 mm, and fixture placement from 30 to 90 mm, on surface roughness (SR), nugget zone (NZ) hardness, and Ultimate Tensile Strength". Results indicated that increasing shoulder diameter initially increased SR but decreased it beyond a critical value. Maximum hardness, SR, and UTS were achieved at a fixture position of 60mm and a shoulder diameter of 14mm with a PD of 0.2mm [63].

Taguchi L9 experiments were also applied to optimize parameters like pin shapes: tepered, cylindrical and tri-flute, Rotational Speed from 900 to 1400rpm and Traverse Speed from 37.5 to 47.5 mm/min for 5 mm thick AA6061 alloy butt joints. "Optimal conditions were found at Rotational Speed of 1400rpm, Traverse Speed of 37.5 mm per min and tapered pin achieving tensile strengths more than 286 MPa, hardness of 77.96HRA, and welding temperatures of approximately 559.9°C " [64]. Additionally, Taguchi L9 were carried out with "tapered cylindrical cam tri-flute tools featuring left-hand threads for AA2519-T87 (15.4 mm thick plates), shoulder diameters from 23 to 29 mm, Rotational Speeds from 450 to 710 rpm, and Traverse Speeds between 31.5 and 50 mm/min". Reduced RS values minimized tunneling defects, and the SZ/TMAZ interface exhibited high-density Al_2Cu coarser particles.

The outcome derived from the review of the existing studies on the Taguchi method summarized as follows: [51]

1. The Taguchi matrix design provides an economic framework for optimization and parameter analysis.
2. The design of experimental matrices in the Taguchi method varies, with the choice of matrix depending on the investigator's discretion. The investigator must consider factors such as individual, curvature, and interaction effects, as well as levels influencing responses, during the selection of an orthogonal array or matrix.
3. The method is designed to optimize only a single response variable at a time.

Institutional Repository - Library & Information Centre - University of Thessaly
04/09/2026 08:51:35 EEST - 216.73.216.250

4. An optimum parameter for one response may not align with another response.
5. Optimal conditions vary across materials due to differences in material properties.
6. Key constraints such as “tool material and geometry, shoulder dimensions, Rotational-Speed(RS), axial force, Traverse-Speed(TS), tool tilt angle, tool vibration, probe penetration, feed rate” significantly influence the properties of the joint.
7. Many studies neglect the interaction effects between factors, likely due to the limitations of reduced experimental trials or specific matrix designs.
8. The Taguchi method identifies factor levels that produce optimal conditions but often results in a local rather than a global solution.

Advantages and Limitations [51]

-Advantages

1. The Taguchi method prioritizes performance values over the performance limits or range values of individual parameters.
2. It simplifies the experimental process by narrowing down critical process parameters through limited trials, focusing on their influence on performance.
3. The method facilitates experimental trials to assess the importance of individual influences and their interactions.
4. It accommodates the study of both continuous and discrete responses.

-Limitations

1. Taguchi’s orthogonal arrays (OA) do not account for every possible pattern of process constraints and fail to incorporate dynamic variations in parameter values.
2. The approach is primarily designed for offline optimization, making it less effective for real-time applications.
3. It is often used at the early steps of process development.
4. The limited number of experimental matrices restricts the method’s ability to evaluate all interactions among factors.
5. The focus on a one-time improvement often leads to suboptimal or localized solutions.

Institutional Repository - Library & Information Centre - University of Thessaly
04/09/2026 08:51:35 EEST - 216.73.216.250

6. Taguchi's method relies on empirical equations without fully developing mechanistic models, which limits process insights and results in local optimization.
7. The absence of intrinsic modeling in the method hampers its ability to provide comprehensive process understanding.
8. The Taguchi method requires supplementary optimization techniques, such as GRA, TOPSIS, MOORA, artificial intelligence (AI), or machine learning (ML), to simultaneously optimize multiple objectives.
9. When applied to multi-objective optimization, the method depends on subjective judgment, resulting in less efficient models.

Response Surface Methodology (RSM)

The "Response Surface Methodology (RSM)", developed by Box and Wilson in 1951, is a technique designed to collect data and establish relationships between input and output variables [65]. It develops correlations between dependent and independent variables by employing various regression models [66]. This approach is based on an empirical model derived from experimental data, often represented by regression equations [66,67]. The standard regression model can be expressed as:

$$y = f\,(x_1, x_2, \ldots . x_{n-1}, x_n) + \varepsilon \quad (5)$$

"where *y = output variable*

f = function

$x_1, x_2, \ldots, x_n$ = *input variable*

ε = error".

Advantages of RSM

1. It allows the collection of extensive information with a limited number of experimental trials.
2. The collected data is utilized to construct models that effectively correlate input and output variables.

Institutional Repository - Library & Information Centre - University of Thessaly
04/09/2026 08:51:35 EEST - 216.73.216.250

3. It offers a graphical representation of data to illustrate the relationships between inputs and responses in a process.
4. The methodology facilitates the analysis of “individual, quadratic (linear or nonlinear), and interaction effects of factors on responses”.
5. It is capable of optimizing multiple responses by identifying appropriate combinations of input variables.

Limitations of RSM

1. The methodology does not deliver insight into the mechanism of the procedure.
2. Its regression models are typically limited to 1st or 2nd order polynomials, which may not capture all effects.
3. An expanded set of independent-variables necessitates additional experimental trials, potentially lowering prediction accuracy.
4. The technique is most effective for analyzing and optimizing processes with a limited number of independent variables.

RSM is usually used in the following applications:

1. **Welding Process Optimization:**
   RSM was applied to establish correlations between input variables such as rotational speed (650–850 rpm), traverse speed (10–50 mm/min), tool tilt angle (1–3°), and pin profile (cylindrical, tapered, threaded) and the output variable (maximum tensile strength) for friction stir welding (FSW) of tailored blank sheets of AA1100 and AA6061 alloys [68]. The model achieved a high predictive capability with an R^2 value of 0.96. It was observed that tensile strength increased with rotational speed, traverse speed, tilt angle, and pin profile up to a middle value but decreased thereafter. Fine and equiaxed grains were identified in the stir zone, while deformed non-recrystallized grains were observed in the TMAZ region.
2. **“Friction Stir Spot Welding”:**
   The Box–Behnken design, a subset of RSM, was employed to relate inputs such as rotational speed (1300–1700 rpm), plunge depth (2.2–2.8 mm), and sleeve moving

Institutional Repository - Library & Information Centre - University of Thessaly
04/09/2026 08:51:35 EEST - 216.73.216.250

rate (0.75–1.25 mm/s) to lap shear fracture load (LSFL) for AA6061-T6 aluminum alloy [65]. The model generated a polynomial-equation that accurately calculated LSFL values in agreement to the experimental results. Optimal conditions yielded a maximum LSFL value of 7934N at 1506rpm with 1.01mm/sec sleeve rate, and 2.46mm plunge depth.

3. **Double-Side FSW:**
   RSM was utilized to study the influence of Rotational Speed between 1100 and 1500 rpm, Traverse Speed of 2.4 to 4 mm/s and pin geometries, square and pentagonal tapered, on the material properties of bobbin tool friction stir welded aluminum-alloys (AA6082-T6) [69]. Pentagonal tapered pins achieved superior strength (155 MPa), hardness (87 HV), and toughness (1.91 kg(f)m) compared to tapered square pins. Here was exhibited a finer grain structure with that tool geometry in the area affected by the process.
4. **Tensile Strength Analysis:**
   The RSM technique optimized parameters such as RS from 1200 to 1400rpm, TS (75 to 125mm/min and axial-forces between 5 and7 kN to enhance the tensile properties of FSW joints involving AA 8011 and AA 6062 alloys [70]. Axial force contributed 90% to tensile strength, while traverse speed had minimal significance. Tensile strength increased with higher rotational speed up to a point before declining.
5. **Mechanical Properties Optimization:**
   Taguchi L18 experiments were conducted on butt-welded AA 6061 joints to analyze the effect of RS from 560 to 1800rpm, TS of 50 to 150 mm per min, tool tilt angles between 0 and 5° and material of tool, having as specimens carbon steel, stainless steel and anti-heat steel, on the material properties [71]. RSM optimization yielded maximum tensile strength (200 MPa) and hardness (110 HV). The grains in the TMAZ appeared elongated and deformed, with elliptical grains and onion ring structures noted in the NZ.

RSM, combined with the Taguchi method, minimizes experimental trials while providing detailed insights into the effects of individual, curvature, and interaction factors. The RSM optimizer also facilitates multi-objective optimization by assigning weights to various responses, enhancing its utility in process analysis and optimization.

Institutional Repository - Library & Information Centre - University of Thessaly
04/09/2026 08:51:35 EEST - 216.73.216.250

In contrast to the Taguchi method, RSM utilizes empirical equations, which are frequently employed to predict and optimize outcomes.

Advantages and Drawbacks of RSM

Advantages:

1. Provides extensive information with minimal experimental effort.
2. Facilitates the construction of models and graphical representations to associate process constraints and responses.
3. Identifies optimal conditions for multiple responses.
4. Offers detailed insights into quadratic factor effects on responses.
5. Develops empirical equations for prediction and optimization.

Drawbacks:

1. Does not explain underlying process mechanisms.
2. Limited to first- or second-order polynomial fits, unable to model systems with complex curvature.
3. Increasing independent variables necessitates more experiments, reducing prediction feasibility.
4. Ineffective for solving nonlinear, multi-modal, or multi-objective optimization problems.
5. Quadratic response surfaces are limited to three or fewer responses.
6. May not be cost-effective for certain manufacturing applications.
7. Empirical equations require continuous differentiability for optimal solutions.
8. RSM predicts only one output at a time.
9. Machine learning techniques, discussed later, can address some of these shortcomings.

Institutional Repository - Library & Information Centre - University of Thessaly
04/09/2026 08:51:35 EEST - 216.73.216.250

Factorial Design (FD)

Factorial Design (FD) is a robust experimental approach, especially suited for studies involving more than two factors. This method evaluates all combinations of factor levels. For instance, if a factor has xxx levels and another has yyy, then xyxyxy combinations can be tested. Typically, experiments involve nnn replicates [72]. It is particularly favored for designs with fewer parameters [73].

1. **Application 1: Properties of AA7475-T7 Lap Joints**

“The mechanical and microstructural properties of friction stir welded (FSW)” lap joints of AA7475-T7 were analyzed using “Full Factorial Design (FFD)”. A total of 27 experiments were conducted, varying three factors: (RS:1000–1400rpm), (TS:20–36mm/min), and plunge speed rate (PSR: 0.04–0.08mm/s), each at three levels [74]. “RS had the most significant impact on ultimate tensile strength and toughness”. Optimum conditions found with Rotational Speed at 1400rpm, Traverse Speed at 30mm per minute and PSR at 0.06mm per sec, and all these yielded the ultimate tensile strength and the hardness at 172.88MPa and 200 HV respectively, compared to initial conditions of 130MPa and 125HV.

2. **Application 2: FSW of Aluminum Plates (AA 1100)**

“The mechanical and microstructural characterization of friction stir welded AA1100 aluminum” rolled plates was performed using a two-level FFD. Eight experiments were conducted with varied Rotational Speeds from 1100 to 1500rpm, Traverse speeds between 20 and 60mm per minute and plunge depth (PD) of 0.1 to 0.5mm [75]. Regression models were developed to estimate the impact of factors on joint strength. Results showed RS had the most influence on axial compression and rotational torque forces, with notable decreases in these forces detected. Microstructural analysis indicated grain size improvement with changes in RS (from 0.48 at 0.36 μm) and TS (from 0.45 at 0.40 μm), while grain size increased for PD (from 0.40 at 0.46 μm). The” base metal (BM) displayed elongated grains along the rolling direction, while the heat-affected zone (HAZ) and BM

Institutional Repository - Library & Information Centre - University of Thessaly
04/09/2026 08:51:35 EEST - 216.73.216.250

zones showed no significant grain size change. The thermomechanically affected zone (TMAZ) exhibited deformed patterns, and the nugget zone (NZ) showed fine equiaxed grains.

At 1100 rpm, microhardness around the NZ periphery dropped to 38 HV. Increasing RS (1100–1400 rpm) initially improved tensile strength" but declined at 1500 rpm due to reduced material flow stress and void defects from excessive heat.

3. **Application 3: Polycarbonate Butt Joints**

FFD experiments were also used to analyze the strength of polycarbonate butt joints. Parameters tested included RS, TS and pin geometry [76]. Axial force and torque were recorded, and K-type thermocouples were employed to measure temperatures on the advancing and retreating sides, 9 millimeters from the process centerline. Maximum UTS was achieved with a "square pin profile at a Rotational Speed of 1800rpm and a Traverse Speed of 20 mm per min. The pin with the lower peak temperatures and cooling rates was the triangular profiled" [76].

Summary and Insights from FFD

The literature confirms that FFD provides in-depth understandings into the Friction Stir Welding technics. Also, the cost of FFD experiments is significantly lower such as "central composite designs (CCD) and Box Behnken (BBD)". Optimal responses in CCD are often at the extreme corners of factor levels, while BBD is better suited for middle-range optimization.

3.3.2 Artificial Intelligence (AI)

Artificial intelligence refers to the capability of computers to perform tasks requiring reasoning, generalization, and learning from prior events. To function autonomously, AI systems must undergo training, which involves feeding data into the system, enabling it to analyze problems, incorporate previous knowledge, apply logic, and deliver optimal solutions. AI is extensively applied in various fields worldwide, including healthcare, election forecasting, cybersecurity, traffic management, autonomous robotics, underwater exploration, and more.

For efficient performance, AI employs various techniques. In friction stir welding (FSW), AI has primarily been utilized to adjust process variables for optimal performance and

Institutional Repository - Library & Information Centre - University of Thessaly
04/09/2026 08:51:35 EEST - 216.73.216.250

determine the most advantageous settings. AI techniques are broadly categorized into "artificial neural networks (ANN), machine learning (ML), hybrid approaches and fuzzy logic". These techniques significantly decrease the processing expense of optimisation tasks. By processing large datasets, AI enables the execution of complex operations while minimizing errors and computation time. Additionally, automation is a key advantage of employing AI in such applications.

Artificial Neural Networks (ANNs)

In recent years, scientists have incorporated "Artificial Neural Networks, Genetic Algorithms, Machine Learning" techniques alongside Taguchi optimization methods. ANNs are utilized to predict the affect of FSW parameters on the quality characteristics of the final part. Drawing inspiration from the biological structure of neural nodes, ANNs employ pre-existing datasets utilized for network training using specific input parameters, referred to as neurons, and forecast the corresponding outputs [77]. By learning from data pairs of inputs and corresponding outputs, ANNs establish sophisticated, nonlinear relationships through the application of algorithms. However, their main drawbacks include significant computational demands, the potential for overfitting, and a "black-box" nature, where the internal workings remain obscure. The central feature of ANNs mirrors the function of the human mind, with researchers and scientists developing mathematical models based on the neuro-physical structure of the brain. Several models of artificial cells and networks have been proposed [78].

Typically, the architecture of an ANN involves three layers: the input-layer, where neurons represent process variables; the hidden-layers; and the output-layer, where neurons correspond to the output quality characteristics. The number of neurons in the hidden layers is determined by the training data [79]. Additionally, network parameters include biases (which help produce constant outputs during training), weights (which represent the strength which layers are connected with), and transfer functions (they generate outputs based on the inputs from the previous layer.). During learning process, the weights are adjusted within the network's structure. The operation of the network is

Institutional Repository - Library & Information Centre - University of Thessaly
04/09/2026 08:51:35 EEST - 216.73.216.250

affected by the arrangement of single and numerous layers [80]. The network undergoes numerous training iterations with different sample sets, leading to refined outputs. Figure 20 illustrates the architecture of an ANN.

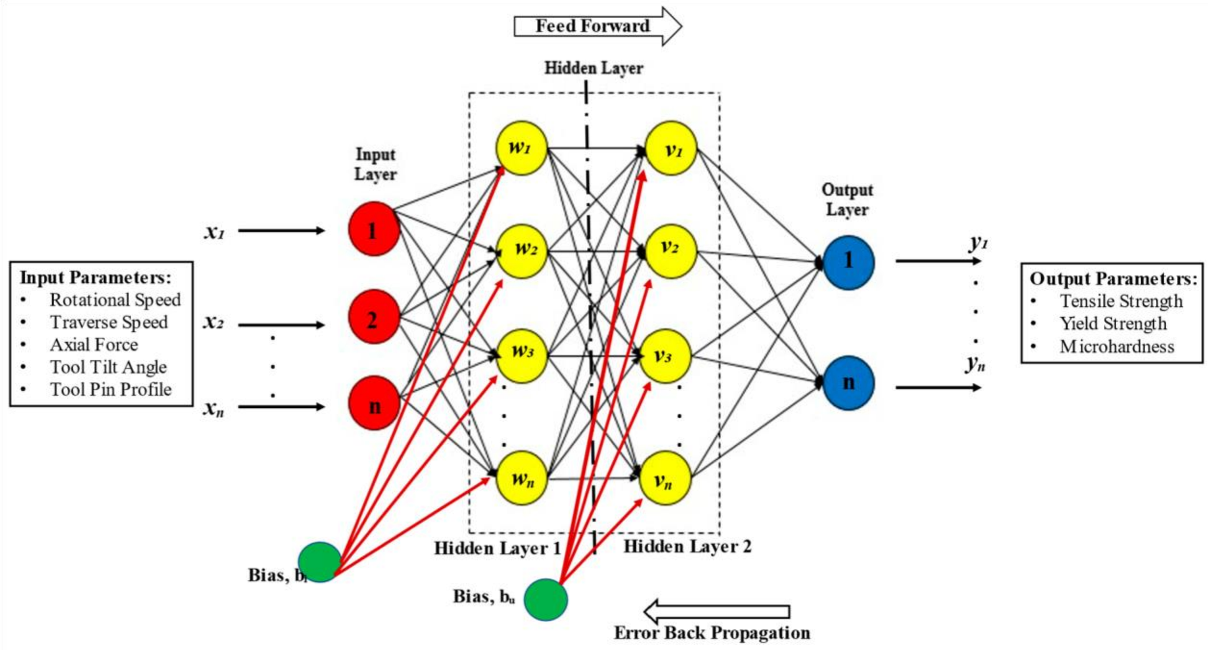

Figure 20 Schematic representation of an AN Network [51]

The transfer function is expressed with the mathematical formula given below: [80]

$$\emptyset(x) = \frac{2}{1+e^{-2x}} - 1 \text{ (6)}$$

$$\psi(x) = \frac{1}{1+e} - x \text{ (7)}$$

$$x(x) = linear(x) \text{ (8)}$$

The amount of nodes and hidden-layers in an ANN is determined using the error-minimization criterion throughout the train procedure. To avoid data dispersion, input values are normalized to a range between 0 and 1, achieved by dividing all values by the maximum parameter value, resulting in a normalized output [79].

A controlled learning method, specifically the back-propagation algorithm, is employed to train the ANN. Data are provided to the input layer, where transfer functions are applied to compute the outputs. The results from the input-layer are then passed to the hidden-layer, where further transfer-functions generate the hidden layer outputs. These outputs are fed into the final layer, which delivers final outputs through transfer functions.

Institutional Repository - Library & Information Centre - University of Thessaly
04/09/2026 08:51:35 EEST - 216.73.216.250

The choice of transfer function is at the discretion of the researcher, as no universal standard exists. Mean squared errors are calculated to assess the discrepancy among observed (targeted or experimental) values and the predictions made by the network [81].

The data groups are split, with 65% to 75% used for training and the rest 15% to 30% dedicated to checking and authenticating the network. The objective of the BP algorithm is to minimize the error as much as possible [79, 81]. In Figure 20, "x_1, x_2, x_3" represent input constraints, "w_1, w_2, w_3" denote the weighted averages of the first hidden-layer, "v_1, v_2, v_3" are the weighted averages of the second hidden-layer, and "y_1, y_2, y_3" are the output parameters.

"Finite Element Method (FEM) simulations were conducted to gather data for optimization, and multi-objective optimization of FSW parameters was carried out using an ANN" [82]. ANNs were combined with "multi-objective particle swarm optimization (MOPSO)" to establish the rotational and traverse speed for an Aluminum butt joint [83]. Throughout the learning phase, the Backpropagation algorithm adjusted network parameters by reducing errors with a trial-and-error method used to fine-tune them. The network design consisted of "2 input-layer neurons, 6 hidden-layer neurons, and 2 output-layer neurons". The output layer's neurons represented tensile shear (TS), rotational speed (RS), tensile shear force, and hardness. MOPSO identified the ideal solutions. The resulting values of "Rotational Speed 1182.11rpm and Traverse Speed 11mm per min produced pick hardness and ultimate tensile strength (UTS) of 96HV and 265MPa", respectively. [83]

A CEL (coupled EulerianLagrangian) numerical approach model was employed to research the effects of RotationalSpeed and TraverseSpeed on base material's temperature, von-Mises stresses, heat transfer, and deformation strain [84]. The ANN design, configured as 2input-10hidden-4output, trained using Backpropagation with 25 simulation data-sets, and 12 data-sets were used for prediction accuracy. The model predicted a plastic strain of 1.25%, temperature of 0.164%, heat flux of 0.2%, and von-Mises stress of 0.3%. High temperatures and residual stresses were detected on the retreating side of the weld. Increasing Rotational Speed led to larger grain sizes thanks to higher values of temperature, heat transfer, more stress, and plastic strain. Testings were conducted using various setups for traverse speeds (15 to 35mm per min), Rotational Speed (from 800 to 1000rpm), with "H13 steel tool (cylindrical threaded and square profiles)", to test the joint strength of AA 6061-T6 [85]. The cylindrical threaded pin, a Rotational Speed of 1000revolutions per

Institutional Repository - Library & Information Centre - University of Thessaly
04/09/2026 08:51:35 EEST - 216.73.216.250

minute, and the TraverseSpeed of 15mm per minute resulted in greater yield strength (YS) of 78.4MPa and Ultimate Tensile-Strength 107.49MPa. “The square pin, with Rotational Speed of 900rpm and a Traverse Speed of 25mm per min”, yielded YS 121.79Mpa and UTS of 151.61MPa. The ANN calculations closely aligned with the experimental outcomes.
AA 6063-O and AA 2014-T6 aluminum plates were joined to test strength and hardness of joint [86]. The ANN's predictions for these properties were very similar to the outcomes of the experiment. The increasing significance of ANNs in manufacturing demonstrates their potential for further exploration.

Advantages and Limitations of Artificial Neural Networks (ANNs)

“The significant benefits of ANNs are outlined as follows [87]:

1. The ability to store information across the entire network, handle missing data, and perform parallel processing efficiently.
2. ANNs can model processes by establishing linear or nonlinear relationships between response variables.
3. They effectively address limitations associated with low-order polynomial equations and datasets that include noise or missing information, leading to better predictions.
4. The ANN framework is capable of predicting multiple outputs concurrently.
5. ANNs can be utilized for both online and offline monitoring of processes.

However, ANNs also have notable limitations, including:

1. The weights between network layers are used without direct knowledge of their physical implications during modeling.
2. Tuning architectural parameters such as the quantity of hidden layers, learning rates, momentum constants, TF, and biases is necessary for accurate predictions.
3. A major drawback lies in determining the optimal size and structure of the network.
4. ANNs are considered "black-box" models, meaning that the relationships between input and output parameters are not explicitly understood, and implementing them in hardware can be expensive” [88].

Institutional Repository - Library & Information Centre - University of Thessaly
04/09/2026 08:51:35 EEST - 216.73.216.250

Machine Learning in FSW

Advancements in the field have paved the way for developing new software tools capable of extending industry's capabilities afar from traditional constraints. "Machine learning (ML)" is a data-centric methodology that leverages algorithms to create models and derive insights from observed patterns [89]. ML employs three primary techniques—supervised, unsupervised, and reinforcement learning—to make inferences and propose optimal solutions [90].

Algorithms like the image-pyramid and image-reconstruction were utilized to analyze AA6060-T5 aluminum plates that have undergone FSW [92]. A set of four welded samples was produced using parameter sets of Rotational Speeds from 1500 to 2000rpm, Traverse Speed from 200 to 400mm per minute, and Axial Forces between 1.5 and 2.5kN. During each iteration, the image dimensions were reduced by a factor of 1.2 in both width and height. Noise removal was performed with a threshold value of 0.8. Grayscale images were used as masks, while eroded images acted as markers. Edge detection was carried out using the Sobel approximation. By applying image processing techniques cracks and defects identified in the structure and recommended utilizing neural networks for improved and optimized outcomes.[92]

For tensile strength predictions for AA 7039 joints with FSW, ML algorithms such as "Gaussian Process Regression (GPR), Support Vector Machines (SVM), Artificial Neural Networks (ANN), and Linear Regression (LR)" were implemented using specific input parameters for RS,TS,Tilt Angle(1325–1812rpm,WS:26–43mm/min,1.3–2°). The application of 70% of the data for training reduced RMSE, achieved a higher correlation coefficient, and enhanced predictions for unknown datasets. Pick tensile strength of 477MPa was achieved at Rotational Speed of 1325rpm, Traverse Speed of 35mm per min, and a tilt angle of 1.65°. A comprehensive analysis of ML and AI algorithms demonstrated their accuracy in optimizing processes. Many researchers employed experimental design techniques to collect data for training networks and subsequently used these algorithms to foretell outputs after known inputs. Unlike the "Response Surface Methodology (RSM)", ANNs can predict multiple outputs simultaneously from extensive datasets.

Institutional Repository - Library & Information Centre - University of Thessaly
04/09/2026 08:51:35 EEST - 216.73.216.250

Various welding processes, including “Friction Stir Welding (FSW), Electron Beam Welding (EBW), Submerged Arc Welding (SAW), and Gas Tungsten Arc Welding (GTAW), were optimized by using regression-derived objective functions combined with the quasi-oppositional-based Jaya algorithm (QO-Jaya)” [93]. Comparisons of “Jaya algorithms and their variants with Genetic Algorithms (GA), Teaching-Learning-Based Optimization (TLBO), and Simulated Annealing (SA)” highlighted their effectiveness. For instance, process parameters of a FSW (tool, RS, TS, and AF) were optimized to improve corrosion resistance [94]. The QO-Jaya algorithm achieved computationally an efficient solution, resulting in a 5.73 % enhancement in corrosion resistance compared to alternative approaches.

Central-Composite Design(CCD) was tested with multiple sets of input parameters, such for RS, TS, and AF, focusing on the mechanical properties of FSW joints made from AA 7075 alloys [95]. A “hybrid model combining Adaptive Neuro-Fuzzy Inference System (ANFIS) and Simulated Annealing (SA) algorithm” was developed. The model was developed using 31 experimental datasets and validated with 10 previously unseen datasets. The ANFIS framework utilized “five layers (input–product–normalization–defuzzification–output)” and was based on Takagi–Sugeno fuzzy rules.

The output from the ANFIS model was fed into the SA algorithm, which yielded the highest mechanical properties under optimal conditions: “square pin profile, RS at 1400 rpm, WS at 1.75 mm/s, and AF at 7.5kN”. This setup facilitated simultaneous optimization of single and multiple responses.

FSW parameters (RS and WS) for aluminum alloy joints (AA5083 and AA7075) were also optimized using Genetic Algorithms (GA) to maximize tensile strength [95]. An empirical model established correlations between input parameters (RS-WS) and ultimate tensile strength (UTS). The optimal GA settings (population size: 25, elite count: 2–8, crossover rate: 0.8) yielded a UTS of 294.388MPa at RS:500rpm and WS:50mm/min. Variations in GA parameters, however, led to suboptimal results.

Machine Learning Algorithms in Welding Process Optimization

“Machine learning algorithms such as Decision Trees (DT), Random Forest (RF), and XGBoost” were applied to predict yield strength (YS) in AA6061-T6 joints using inputs like Rotational Speed, TA, Traverse Speed, shoulder diameter (SD), pin diameter (PD), hardness of tool, and thrust force [96]. The training dataset comprised 75% of the data, while the

Institutional Repository - Library & Information Centre - University of Thessaly
04/09/2026 08:51:35 EEST - 216.73.216.250

testing dataset accounted for 25%. The XGBoost model demonstrated superior precision of 95.24%, outperforming DT-RF models, which achieved 90.48%.

In another study, machine learning models, including “Linear Regression (LR), Polynomial Regression (PR), Support Vector Regression (SVR), Decision Tree Regression (DTR), and Random Forest Regression (RFR)”, were employed to predict the performance of dissimilar butt-welded AA 7050 and AA 2014A FSW joints [97]. The input variables included RS:1000to1600rpm, TS:30to70, and TA:0.5to2.5°. The models trained on 90 % of the datasets and tested at the rest, achieving reduced errors in MSE, MAE, and RMSE. Experimental data showed defects like tunneling at RS of 1000 rpm due to insufficient heat generation. Proper material mixing was observed at higher RS values, with peak temperatures less than 300°C.

Advantages and Limitations of Machine Learning

Machine learning techniques effectively handle high-dimensional data, offer adjustable parameters, and enhance classification performance. They reveal hidden relationships within datasets, adapt to dynamic systems, and accommodate evolving environments [98]. However, ML models are limited by their "black-box" nature, as they lack transparency in the underlying processes. Furthermore, ML models trained for one process are not directly transferable to others due to variations in stochastic weights and biases. Selecting the most appropriate algorithm and preprocessing data accurately are critical steps in successful optimization.

Institutional Repository - Library & Information Centre - University of Thessaly
04/09/2026 08:51:35 EEST - 216.73.216.250

3.3.3 Multi-Objective Optimization Using Nature-Inspired Algorithms

Multi-objective optimization in FSW processes has been successfully carried out using various nature-inspired algorithms, including "Genetic Algorithm (GA), Particle Swarm Optimization (PSO), Artificial Bee Colony (ABC), Harmony Search (HS), and Ant Colony Optimization (ACO)". These algorithms are modeled after natural phenomena to address optimization problems involving two or more objectives simultaneously.

For example, "the hybrid fuzzy–grey Taguchi method was employed to optimize the FSW of dissimilar aluminum-copper (Al/Cu) joints" [99]. Experiments used Taguchi's L16 orthogonal array with input factors such as rotational speed (RS), welding speed (WS), pin diameter (PD), and tool pin offset. By transforming multiple outputs into a single objective using the fuzzy–grey method, the outcome showed that in the heat-affected zone (HAZ), the grain size for aluminum was 70.7 µm, while for copper, it was 71.50 µm. Similarly, in the thermo-mechanically affected zone (TMAZ), grain sizes were 51.98 µm (aluminum) and 60.6 µm (copper). In the nugget zone (NZ), the grain size was 46.61 µm for aluminum and copper, compared to base metal grain sizes of 73.64 µm (aluminum) and 228.64 µm (copper). The use of advanced fuzzy sets enhanced the accuracy of the results. [99]

In other experimental setup, the "dragonfly algorithm" used to optimize the FSW parameters for AA6082-T6 aluminum joints [100]. Parameters such as RS, tool tilt angle, and WS were used. MATLAB (version R2021a) was utilized for simulation. The optimal parameters resulted in UTS of 221.6MPa and impact strength of 14 MPa, respectively. Experimental results closely matched the optimization predictions.

In a study using Taguchi L27 experiments, different tool materials (steel, PCBN, and tungsten) and tool configurations were evaluated to optimize parameters for tensile and impact strength. The results demonstrated high agreement amongst experimental and optimized values, validating the reliability of the approach.

For dissimilar AA 6061 and AA 2024 alloy FSW, Taguchi L9 experiments were employed [101]. Grey relational analysis (GRA) and dragonfly algorithms were used for multi-output optimization. Microstructural analysis revealed finer grains in the NZ compared to the TMAZ and HAZ.

Another investigation utilized Taguchi L16 experiments to optimize the weld of AA 6061 joints [102]. Parameters included RS, TS, penetration depths and tilt angles. The use of

Institutional Repository - Library & Information Centre - University of Thessaly
04/09/2026 08:51:35 EEST - 216.73.216.250

“a cylindrical, tapered pin made of H13 tool steel” demonstrated enhanced joint efficiency and microhardness. By integrating the “neighborhood cultivation genetic algorithm (NCGA)” with “adaptive neuro-fuzzy inference systems (ANFIS)”, optimized conditions (Rotational Speed:560rpm, Traverse Speed:90mm/min, penetration-depth:0.9mm, and tilt-angle:2°) achieved a 17 % reduction in specific weld energy, a 2.3 % increase in joint efficiency, and a 6.4 % increase in microhardness.

“Central composite design (CCD) under the response surface methodology (RSM)” framework was employed for optimizing FSW parameters and pin for aluminum-magnesium alloys [103]. Surface roughness and tensile strength were analyzed, revealing that a straight cylindrical pin with RS (1200 rpm) and TS (20 mm/min) achieved the lowest surface roughness (4.9 µm). Conversely, higher tensile strength (137 MPa) was achieved with RS at 1000rpm and TS at 40 mm/min. Microstructural studies highlighted dendritic grains in the base metal (BM) and equiaxed grains in the stir zone (SZ).

Taguchi experiments were also conducted on AA 2024-T4 joints [104]. “Weighted-principal component analysis(WPCA)” employed to convert multiple outputs just in a single objective. Artificial neural networks (ANN) were trained using backpropagation (BP) and Levenberg-Marquardt (LM) algorithms, with datasets comprising 70% training, 15% validation, and 15% testing. Optimized parameters—D/d ratio of 3, RS of 1180rpm, and TS of 17mm/min—yielded the highest UTS of 108.105MPa (20% improvement) and hardness of 76 (a 25% improvement).

Another study [105] optimized strength properties like yield strength (YS) and impact strength for AA6082-T6 joints using Taguchi experiments. Grey relational analysis (GRA) was combined with ANN models trained using BP and LM algorithms. The ANN achieved a pick grey relational grade (GRG) of 0.508 under optimal conditions: of RS=1002rpm, tilt angle=1.5°, and TS between 1 and 2 inches/s. Among different tool pin profiles, conical and pyramidal shapes yielded better results. Microstructural validation supported the optimized parameters.

Institutional Repository - Library & Information Centre - University of Thessaly
04/09/2026 08:51:35 EEST - 216.73.216.250

Advantages and Limitations of ANFIS

The “Adaptive Neuro-Fuzzy Inference System (ANFIS)” is well-suited for managing extensive datasets derived from nonlinear or dynamically complex systems. This system proves invaluable for modeling scenarios where no direct relationship exists between input and output variables. Additionally, ANFIS can integrate data from multiple sources, thereby enhancing the efficiency and accuracy of model development.

A critical aspect of applying ANFIS is the careful identification and representation of input–output variables, as this significantly influences the model's performance. However, a major drawback of ANFIS is its reliance on large datasets for both training and validation. Without sufficient data, the model may suffer from underfitting, which compromises its predictive accuracy [80,106].

Institutional Repository - Library & Information Centre - University of Thessaly
04/09/2026 08:51:35 EEST - 216.73.216.250

3.4 Process Measurement

The demand for superior-quality products necessitates continuous monitoring throughout manufacturing processes. To enhance process efficiency, industries increasingly adopt advanced technologies. Sensors play a pivotal role in enabling continuous monitoring, providing real-time data to adjust parameters and improve the mechanical properties of components manufactured by friction stir welding (FSW). Real-time monitoring ensures smoother production processes and helps detect failures at an early stage [107].

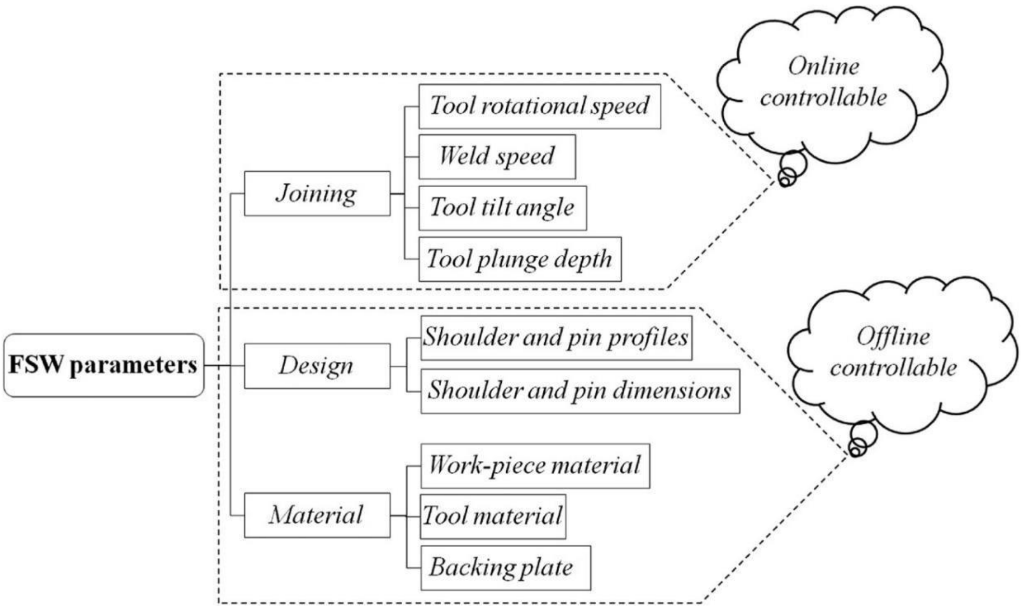

Figure 21 Categorization of procedure factors. [108].

Process monitoring relies on constant feedback from sensors and can be conducted through two primary methods: online and offline. For FSW, "process-parameters are grouped into three categories: (i) joining-parameters, (ii) material-parameters, and (iii) design-parameters". Heat creation, influenced by joining-parameters such as "rotational speed (RS), traverse speed (TS), tilt angle, and plunge depth (PD)", is regulated using online monitoring. For instance, "tilt-angle increases the flow of plasticized material. Rotational speed and welding speed are particularly crucial for determining the quality of the joint".

Design parameters, including tool profiles and dimensions, remain consistent during the process and significantly impact the welded specimen's properties. Material parameters, such as "the properties of the workpiece, tool material, and backing plate", are also constant

Institutional Repository - Library & Information Centre - University of Thessaly
04/09/2026 08:51:35 EEST - 216.73.216.250

throughout the procedure [109]. Figure 21 illustrates the sorting of different process parameters managed through on-line and off-line processes, while Figure 22 depicts the placement of various sensors in FSW machines.

The procedure starts by recognizing the key parameters and deciding on the appropriate sensors to capture data. Once sensor signals are acquired, processing methods are employed to isolate relevant features. These signals reveal alterations occurring throughout the process, aiding in error identification and effective process control. “By analyzing the sensor data, operators can make informed adjustments to ensure optimal performance” [107,108].

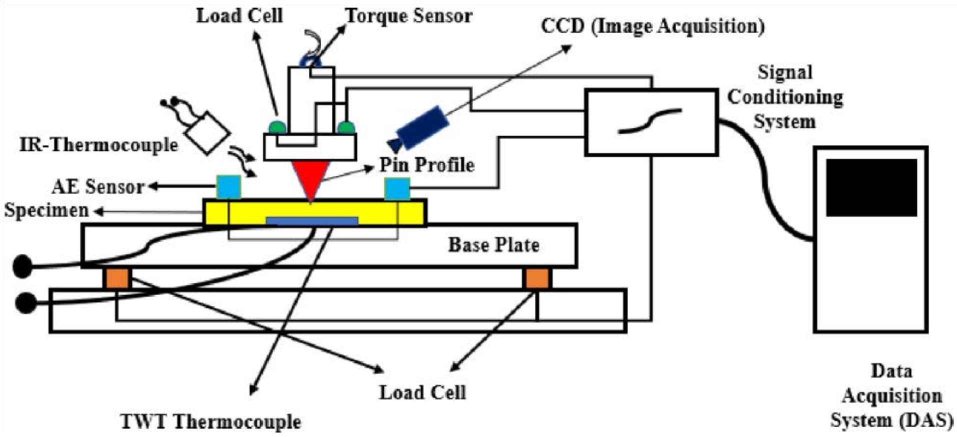

Figure 22 Measuring devices placement in FSW machinery.
(“AE:acoustic emission, IR:infrared, CCD:charge-coupled device”). [110]

Babalola et al. [111] explored “on-site process monitoring approaches for FSW machines” through three case-studies: (i) AA 2014 with AA 6063 with a thickness of 6 mm, (ii) AA6063T6 using Ø50 mm pipes, and (iii) AA1100 also with 6mm thickness. Two of these studies employed charge-coupled devices(CCD) during tests, eliminating repetitive experiments to address reliability concerns. The authors used a cause-and-effect approach to identify three critical factors ensuring strong welds: “(i) Base material fixture mechanism, (ii) tool condition-health, (iii) FSW-machinery compliances”. To minimize errors associated with clamping and tools, regular maintenance of spindles, mechanical-fixtures, and clamping-fixtures is necessary. Key contributors to machine rigidity issues include “wear and tear of meshing gears, gradual deterioration of machine drives, and insufficient lubrication”.

Institutional Repository - Library & Information Centre - University of Thessaly
04/09/2026 08:51:35 EEST - 216.73.216.250

Axial force monitoring is essential in force control mode, while tool plunge depth (PD) should be observed in position control mode. Tilt angle and RS, in both modes, are basic parameters demanding monitoring.

Integrating sensors with FSW machines enables the collection of data such as temperature, power, torque and force. Acquisition of data in real-time and analysis facilitate performance prediction. Signal processing combined with machine learning (ML) algorithms enhances weld quality. For instance, acoustic emission sensors paired with image processing techniques were applied to monitor FSW of AA6082-T6 [112]. Another study [113] employed the “best first tree (BFT)” algorithm to group information collected from vibrational analyses conducted on tools throughout the Friction Stir Welding of AA 5202. This experiment, accomplished at two different RS. First at 1400rpm and then at 1800rpm with a constant TS of 30mm/min, used a piezoelectric accelerometer to capture tool vibrations. 12 datasets collected and used to train the “BFT” setup. BFT improved grouping accuracy to 93 %. Furthermore, a “support-vector machine” (SVM) algorithm to group FSW images taken during the welding of Al2024. Throughout the process the algorithm extracted features from FSW figures, achieving a precision of 95.8 % when distinguishing between good and defective welds.

3.4.1 Measurement of Forces

During Friction Stir Welding tools encounter forces in longitudinal, lateral, and axial directions. Axial forces created when tool begins rotation and plunges into the workpiece, counteracting the employed axial force exerted by the tool shoulder. Longitudinal power arises while the tool moves linearly, while asymmetric material movement around the pin is caused by the interaction of lateral and axial forces [48,114]. Measuring forces and torque in the FSW tools is crucial for three reasons: a high torque corresponds to increased process power requirements, higher loads accelerate tool wear and deformation, and tool wear can lead to weld defects and compromised joint properties [115,116]. Sensors for force measurement are typically positioned in two locations: firstly, on the machine's workbench and secondly on the tool head, tool, or spindle. However, force sensors are influenced by welding conditions, such as “rotational speed (RS), plunge depth (PD), and traverse speed

Institutional Repository - Library & Information Centre - University of Thessaly
04/09/2026 08:51:35 EEST - 216.73.216.250

(TS)” [108,117]. To mitigate uncertainties, the implementation of an “adaptive PID controller” can be utilized. Torque sensors, which show a steady increase in torque during welding regardless of axial force fluctuations, are more reliable for predicting tool positions. Among the parameters, “Rotational Speed and axial force” are most essential for force and torque measurement.

Zuluaga-Posada introduced at her research [118] an innovative device to measure force following the “Ulrich” method to measure axial force. Two potential designs were proposed: (a) positioning the sensor right on the spindle, (b) installing the setup on the workbench. This setup incorporated 2 load cells, a balancing mechanism, and a flat ballbearing within a frame, with an option to add a load cell for Traverse-force measurement. Experiments were conducted using 36 different properties patterns for RS (600to1600rpm), TS (40to140mm/min), Plunge-Speed at 30 mm/min, Tilt Angle at 0°, and dwell time at 20s). Pick axial force appeared throughout the plunge stage, stabilizing during the weld and dwell stages. Radiographic inspections exposed defects such tunnels and wormholes at FSW area. In another study [119] Kistler dynamometers were used to monitor tool positions during welding. Axial forces were recorded against tool offsets using box-and-whisker plots. A “general-regression NN” was developed with input signals, predicting forces from 30 welds performed under varying parameters. The network produced an absolute error and standard deviation of 0.42mm and 0.508mm per sample.

Das et al. [116,120] investigated the use of torque and force sensors in defect detection during the process. Experiments on AA1100 alloy (6 mm thickness) with an L9 design were conducted to achieve butt joint configurations, using SS-316 for tool material. “Eddy current sensors” collected spindle and feed signals from motors, while another sensor monitored the spindle motor voltage. Tool RS signals were obtained using a non-contact laser tachometer probe. Regression models demonstrated strong predictive performance, with coefficients of determination of 0.9998 for ultimate tensile strength and 0.9781 for yield strength. Spindle motor current-signals proved more valuable in foreseeing ultimate tensile strength and yield strength. In [121], “Discrete-Wavelet Transform” (DWT) was applied to identify flaws based on torque and force signals in welding AA1100 aluminum alloy (2.5 mm thickness). A three-level hierarchy was used to divide the signals employing a “Daubechies-wavelet of 4th order”. A “strain-gauge sensor” captured load data in the z-direction, with meridian filters preprocessing the raw sensor data before DWT application.

Institutional Repository - Library & Information Centre - University of Thessaly
04/09/2026 08:51:35 EEST - 216.73.216.250

Welds performed at RS: 500 rpm, feed rate: 50mm/min, tilt-angle: 0°, and PD: 0.05 mm generated a load of 603.06 N and exhibited surface defects.

Arya et al. [122] studied the AA6063 joint, focusing on forces and parameters. A compression-type load cell monitored horizontal and vertical forces, while an "S-type" load-cell captured additional data. The study found that shear force increased during plunging, indicating material softening beneath the FSW tool. Vertical force rose with higher Plunge Depth, suggesting increased rubbing between the base plate and shoulder of tool. Square pin profiles generated a smaller amount Vertical-Force compared to other profiles such as triangular and cylindrical. In [123], experiments on AA 5052-H34 FSW using a square-tool shape assessed tool forces via a piezoelectric dynamometer. Temperatures increased alongside with Rotational Speed, reducing although yield-stresses. Pick radial force occurred at a 45° welding direction for all parameter combinations.

From the literature, Torque and Force measurements are pivotal for studying energy consumption, tool lifespan, and weld quality. Constraints such as "Plunge Depth, pin profile, Rotational Speed, Traverse Speed, and dwell time" affect directly the forces generated and the resultant joint properties.

3.4.2 Temperature Measurement

Temperature is an essential parameter in the FSW process, influencing microstructure evolution and weld quality. It is typically measured using pyrometers, thermocouples, or resistance temperature detectors (RTDs). The transient nature of welding temperature makes its accurate measurement essential. Fehrenbacher, in his study [124], came up with a "closed-loop" control system that automated the procedure by varying rotational speed, while De-Backer [125] implemented a "proportional-integral controller" (PIC) with rotational speed as the primary variable, showing its significant impact on temperature readings.

In another study [126], temperature sensors, such as thermocouples, were embedded at various locations, including "the tool, workpiece, and at the tool-workpiece interface". The stir zones in welds were identified as the hottest regions. Standard methods for temperature measurement involved embedding thermocouples within the workpiece or

Institutional Repository - Library & Information Centre - University of Thessaly
04/09/2026 08:51:35 EEST - 216.73.216.250

under the rotating pin. However, uncertainties arose due to “thermocouple displacement and plastic deformation in the stirring zone” [127].

“Wire type thermocouples” enclosed in Stainless-Steel sheaths were employed for “tool-embedded temperature” monitoring [124]. This setup incorporated “closed-loop control and wireless data acquisition. A laser operating at a maximum power of 200 W in continuous mode provided input voltage pulses, while an oscilloscope captured temperature and laser pulse data”. The Seebeck effect, using chromel-alumel K-type thermocouples, measured the temperature at tool-material interfaces in both FSW and turning processes [129,130]. Calibration for specific tool-workpiece combinations revealed a Seebeck coefficient of 12Volts/Kelvin, with copper coating significantly affecting measurements. A discrepancy of 60–90 K was observed between measured and modeled tool-workpiece interface temperatures, highlighting the need for correction factors to improve accuracy.

Temperature at the tool-workpiece interface was analyzed for its impact on the quality of welds [131]. A wireless closed-loop control system monitored in real-time temperatures at the interface. Thermocouples, embedded in specimen holes using electrical discharge machining (EDM), directly contacted the workpiece material. Data was recorded at angular resolutions from 17° to 41°, with spindle RS and a sampling-rate of 250Hz, capturing 8.8–21 measurements per tool rotation. Tool temperatures were influenced by factors such as “Rotational Speed, plunge depth, traverse speed, and thermal boundary conditions”. FSW quality was also evaluated in studies examining welds of 175millimiteres length between aluminum workpieces (AA 606-T6), involving 29-factorial tests and additional experiments on different backing plates (steel, Ti, Cu). The temperature reported at the interface of the weld was significantly affected by RS and Boundary-Conditions, and was crucial for UTS and weld quality, with UTS varying between 25% to 76% of the parent material.

Residual stresses, which affect microstructure, fatigue life, and corrosion resistance, were reduced using laser-assisted and cold FSW techniques for AA5754H111 plates [132]. Eddy current testing [133] and acoustoelastic techniques at frequencies of 3.5 and 5 MHz were used to evaluate residual stresses in FSW joints of 7050-T7451 aluminum alloy [134]. Quadratic equations were developed to estimate AZ80A Mg joint temperatures [135], and numerical analyses using COMSOL software validated experimental results. Experiments were conducted with different traverse speeds, axial forces, and RS, with traverse speed

Institutional Repository - Library & Information Centre - University of Thessaly
04/09/2026 08:51:35 EEST - 216.73.216.250

contributing the most (41.65%) to temperature evolution. Peak temperatures of 368°C, resulting from high RS and axial forces with low traverse speeds, led to high-quality welds.

Numerical investigations, such as those on 304L Stainless-Steel [136], modeled the procedure as a “3D non-Newtonian fluid”, incorporating heat from tool-plate friction and plastic deformation. Simulations conducted with “ANSYS-Fluent” matched experimental records, identifying defects like wormholes and flashes. Traverse speed was a key factor in defect formation. These studies aim to minimize experimental costs and predict temperatures in welded zones, ensuring controlled microstructure evolution, reduced residual stresses, and improved mechanical properties of welds.

3.4.3 Vibration and Acoustic Measurements

Acoustic sensing methodologies exhibit superior efficacy in comparison vibration sensing techniques, particularly when sensing higher frequencies [108]. When the threshold exceeds 45dB, higher-frequency acoustic emission (AE) waves in the 100–270 kHz range become more frequent [137]. The ability of acoustic sensors to detect these high-frequency phenomena makes them useful for monitoring defects during the welding process. However, managing the large volume of data generated during monitoring is a challenging task.

In [137], Experimental investigations were undertaken to observe acoustic emissions and assess the impact of different tool pin profiles (made of SS-316) on the UTS of AA 6063-T6 joints. Each tool underwent three experiments under specific weld parameters (TS of 40mm per minute, RS of 1000rpm, and Plunge Depth of 0.3mm) for reliability. The process was monitored through an examination of its characteristics in both the time and frequency domains. The square-profiled pin generated greater UTS(196MPa) thanks to its increased number of edges, significant amplitude and considerable duration. The AE constraints, such as the total event count, the signal's rise time, and the acoustic energy waveforms, contributed to a higher UTS, ranging from 175-200 MPa.

In another study [138], the Acoustic Emission method was used for real-time observation of data by fitting two sensors 70mm apart on either side of the butt joint. The Fourier transformation method was used to identify the cause of inadequate contact at the “tool shoulder-workpiece” interface. A “couplant” was employed to optimize acoustic wave

Institutional Repository - Library & Information Centre - University of Thessaly
04/09/2026 08:51:35 EEST - 216.73.216.250

propagation, while a band-pass filter with a range of 10–400kHz and a 40dB gain preamplifier reduced mechanical noise. Two frequency bands were observed. In the low-frequency band (100-170 kHz), a correlation was found between increasing temperature and elevated thermal stresses, resulting in a higher "power spectral density (PSD)". The PSD exhibited a pronounced increase in the higher frequency range (220-260kHz) as the workpiece's temperature neared its melting point. Sudden peaks in the wavelet transform plot indicated changes in the contact interface between the tool shoulder and the piece. The short-time Fourier transform provided limited insights into the "thermomechanical conditions, while the wavelet transform effectively analyzed the time-frequency characteristics of AE signals, which were related to tool movement and weld quality in AA6061 alloy" [139]. Silicon rubber served as the acoustic coupling medium in the AE sensor setup, and a 20-kilohertz frequency filtered mechanical noise. Daubechies wavelets helped nullify extraneous signals. The AE signals were primarily created by friction between the tool and material and thermoactivated deformation of the materials. Variations in band energy during FSW gave more certain indications of the influences of gaps.

In addition to AE-based monitoring, machine vision systems are used in process monitoring. These systems employ pattern recognition algorithms applied to a series of digital images to assess process effects. Machine vision is vital for ensuring high-quality product production, with the potential for integrating "machine learning (ML), artificial-neural-networks (ANN)", and signal processing methods to optimize values during process.

Summary

Key observations from the study include:

- Material parameters such as "workpiece material, tool material, and backing plate" maintained at a constant level during the process.
- In force control, the axial force exerted by the tool should be closely monitored. Conversely, the depth to which the tool penetrates the workpiece should be controlled through position feedback. While these are the primary control modes, the tilt angle of the tool and its rotational speed (RS) from the desired path are vital parameters that require continuous tracking in both modes.
- The tool encounters forces in the lateral, axial, and longitudinal directions. Throughout the plunge process, an axial force is generated as the tool rotates in the material, which is counteracted by the employed axial-force from the tool's shoulder.

Institutional Repository - Library & Information Centre - University of Thessaly
04/09/2026 08:51:35 EEST - 216.73.216.250

Tool's linear movement effects in a longitudinal-force, and the interaction of axial and longitudinal forces leads to a lateral force, creating uneven flow distribution around the tool.

- Among the process parameters, rotational speed (RS) exerts the most significant influence on temperature measurement during FSW.
- The predominant approach for temperature measurement in FSW research utilizes embedded thermocouples positioned in close proximity to the rotating pin within the workpiece.
- Spindle rotational speed and the surrounding thermal environment significantly impact the temperature distribution at the joint interface.
- Acoustic sensors excel at detecting high-frequency events compared to vibration-sensors. In Friction Stir Welding, they have been successfully employed to identify gap defects and analyze tool wear. However, effectively managing and analyzing the substantial volume of data generated during AE monitoring presents a significant challenge.

Institutional Repository - Library & Information Centre - University of Thessaly
04/09/2026 08:51:35 EEST - 216.73.216.250

Chapter 4. Microstructural and Mechanical Characterization

4.1 Macrostructure of FSW Joints

The unique “thermo-mechanical” conditions during the friction stir welding (FSW) often lead to the creation of a distinctive "Onion Ring" structure in the joint, as Figure 23 shows. The welded joint comprises four distinct regions progressing from the center to the edge: “the nugget zone (NZ), thermo-mechanically affected zone (TMAZ), heat-affected zone (HAZ), and base metal (BM)”. These regions exhibit varied characteristics due to differences in material movement. The HAZ is defined by grains with no deformation in shape and shows evidence of grain coarsening caused solely by thermal effects. Consequently, the structural traits of the BM and HAZ are largely alike. The TMAZ is subjected to higher thermal exposure and moderate material flow, resulting in elongated grains. Furthermore, the TMAZ exhibits asymmetry between the “advancing side (AS) and the retreating side (RS)”, with the AS undergoing more intense material flow. On the boundary between the TMAZ and NZ, banded structures are observed, which are prominently visible on the AS but less distinct on the RS. In the NZ, located beneath the tool, numerous fine grains are formed, with the bottom region exhibiting finer grains compared to the upper zone. These equiaxed fine grains are widely understood to result from recrystallization.[3]

Figure 23 Macrostructure of FS weld [3]

Institutional Repository - Library & Information Centre - University of Thessaly
04/09/2026 08:51:35 EEST - 216.73.216.250

4.2 Microstructure of FSW Joints

4.2.1 Distribution of Grain-Size

Grain refinement in "friction stir welded" (FSWed) joints is widely attributed to recrystallization and deformation geometry. The deviation in heat input and geometric distortion across different zones of the weld results in a heterogeneous grain size distribution. In the "heat-affected zone (HAZ)", which is located far from the stirring tool, grains are slightly coarser in comparison to those in the "base metal (BM)". This is likely because of the absence of "plastic deformation", with the material experiencing only thermal exposure, which promotes grain growth. Conversely, "grain refinement in the thermo-mechanically affected zone (TMAZ)" is primarily influenced by shoulder friction. This zone contains partly "recrystallized refined grains" and some elongated grains oriented alongside the stirring direction, forming a gradient in grain dimensions. This unique microstructure in the TMAZ arises from insufficient heating or strain to facilitate full dynamic recrystallization during FSW [140].

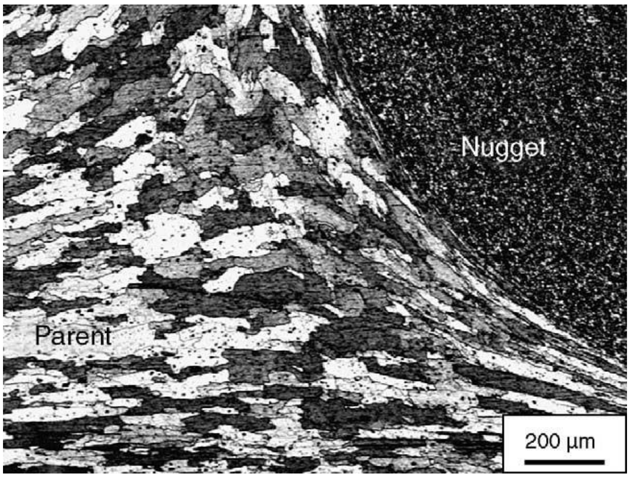

Figure 24. Depict of TMAZ in FSP of 7075Al [47]

Institutional Repository - Library & Information Centre - University of Thessaly
04/09/2026 08:51:35 EEST - 216.73.216.250

Additionally, the advancing side (AS) displays slightly coarser grains in comparison to the retreating side (RS), which is ascribed to greater strain on the AS [141].

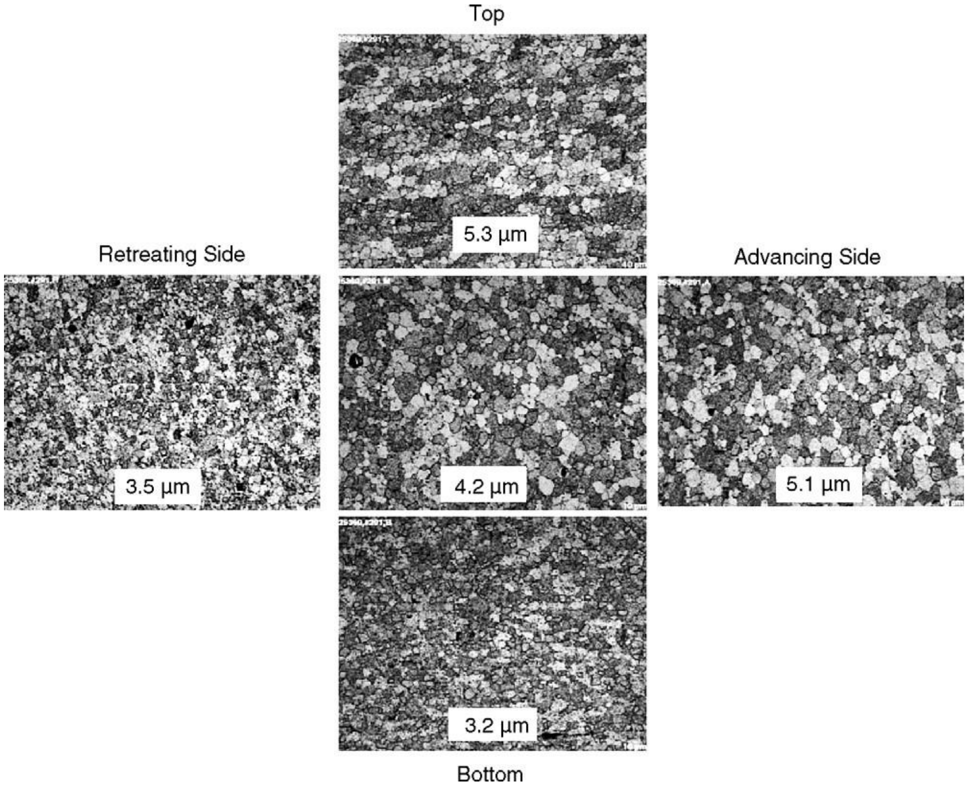

Figure 25 Distribution of grain sizes at different locations within the 7050 Aluminum alloy's weld nugget (mean grain-size in µm). [25]

In the "stir zone (SZ)", the material undergoes severe plastic deformation and high-temperature subjection, leading to substantial grain refinement. The microstructure in this zone is predominantly composed of dynamically recrystallized grains with a uniformly small grain size. This distinctive characteristic of SZ is linked to the "dynamic recrystallization" caused by the intense plastic deformation during FSW. Studies have observed a great proportion of "high-angle grain boundaries (HAGBs)" (approximately 97.5%) in SZ after Friction Stir Welding in cast Mg-Al-Zn alloys [142], providing evidence of dynamic recrystallization. Furthermore, research indicates that dynamic recrystallization produces both "low-angle grain boundaries (LAGBs) and high-angle grain boundaries (HAGBs)" [143].

In some cases, however, grain growth occurs in the SZ after welding, assigned to the "ultrafine-grained base material", which is unstable under the thermal cycling of the process. The heat produced by plastic deformation delivers the necessary drive-force for recovery,

Institutional Repository - Library & Information Centre - University of Thessaly
04/09/2026 08:51:35 EEST - 216.73.216.250

resulting in grain growth [144]. Su noted that "the evolution of grain structure in the SZ is influenced by the initial grain boundary structure, grain size, and dislocation density of the base material" [145]. Materials with "ultrafine grains, high dislocation density, and abundant high-angle boundaries" are particularly prone to grain growth during FSW. This phenomenon can be explained by recovery processes that reduce defect density within grains, promoting their growth [146]. Additionally, the initial hardness of the material also impacts grain size, as observed by Chang et al. [147]. Softer materials result in reduced heat input during welding.

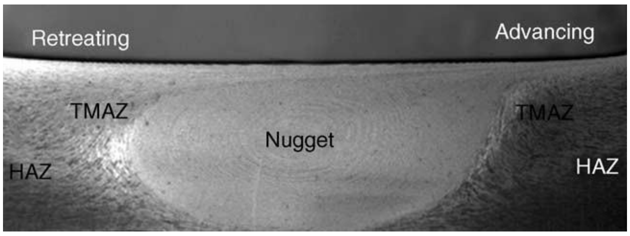

Figure 26 A representative macrograph displaying different microstructural zones (7075Al-T651).[1]

4.2.2 Nugget Zone

The severe "plastic deformation and frictional heating" occurring throughout friction stir welding (FSW) lead to the formation of a "recrystallized, fine-grained" microstructure in the stirred zone. This area, often described to as the "nugget zone (or weld nugget) or dynamically recrystallized zone (DXZ)", is characterized by fine grains. In certain FSW situations, an "onion ring structure" has been noted within the nugget zone (Figures 26-27b). Typically, "the recrystallized grains in this area have a low dislocation density" [1]. Researchers have stated the presence of high sub-boundary density, subgrains and dislocations within the small "recrystallized grains of the nugget zone". The interface between the recrystallized nugget zone and the base material tends to be more diffuse on the "retreating side" of the tool, while it is notably sharp on the "advancing side".

Institutional Repository - Library & Information Centre - University of Thessaly
04/09/2026 08:51:35 EEST - 216.73.216.250

Shape of Nugget Zone

The figure of the nugget zone differs depending on factors such as "processing parameters, tool geometry, workpiece temperature, and the material's thermal conductivity". Two primary nugget zone shapes have been identified: "basin-shaped nuggets, which broaden near the upper surface, and elliptical nuggets". Sato et al. [148] observed basin-shaped nuggets in the FSW of 6063Al-T5 plates and attributed their formation to "the intense deformation and frictional heating at the upper surface caused by contact with the cylindrical tool shoulder". In contrast, Rhodes and Mahoney et al. [11] stated "elliptical nugget zones in welds made from 7075Al-T651".

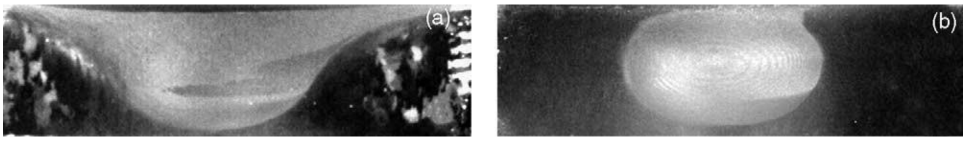

Figure 27 "Impact of RS and TS on nugget shape: (a) 300 rpm, 51 mm/min and (b) 900 rpm, 203 mm/ min (standard threaded pin)(FSPA356)" [1]

Recent studies "on the effects of FSP parameters on the microstructure and properties of cast A356" [47] revealed that "lower tool rotation rates (300–500 rpm) produced basin-shaped nugget zones, while higher rotation rates (>700 rpm) resulted in elliptical nugget zones" (Figure 27). These findings demonstrate that nugget zone shapes can be altered using the same tool geometry but varying processing constraints.

Reynolds [149] explored the correlation amongst nugget size and pin size, reporting that "the nugget zone is slightly larger than the pin diameter, except at the weld's bottom, where the pin tapers into a hemispherical end". Furthermore, it was noted that "increasing the pin diameter resulted in a more rounded nugget zone shape, with the maximum diameter located at the weld's midsection".[149]

4.2.3 Grain Size

Dynamic recrystallization during friction stir welding (FSW) "results in the formation of fine, equiaxed grains in the nugget zone" [1]. Several factors influence the recrystallized grain

Institutional Repository - Library & Information Centre - University of Thessaly
04/09/2026 08:51:35 EEST - 216.73.216.250

size, including "FSW parameters, tool geometry, material composition, workpiece temperature, vertical pressure, and cooling methods".

Benavides et al. [150] studied "the impact of workpiece temperature on the grain size in FSW 2024Al". Their findings revealed that "reducing the initial temperature of the workpiece from 30°C to -30°C using liquid nitrogen cooling lowered the peak temperature from 330°C to 140°C at a point 10 mm from the weld centerline. This change reduced the grain size from 10 μm to 0.8 μm". Similarly, Su et al. [151] achieved "bulk nanostructured 7075Al with an average grain size of 100 nm using a mixture of water, methanol, and dry ice for rapid cooling".

Kwon et al. [152,153] utilized a "cone-shaped pin with a sharp tip" to minimize frictional heat through FSW of 1050 Aluminum alloy. "A peak temperature of 190°C was recorded at a tool rotation rate of 560 rpm and a traverse speed of 155 mm/min, resulting in a grain size of 0.5 μm". Likewise, Mishra and Charit [96] reported "a grain size of 0.68 μm in FSP of cast Al–Zn–Mg–Sc using a small-diameter tool with a threaded pin at 400 rpm and 25.4 mm/min traverse speed". These observations align with recrystallization principles, which indicate that lower annealing temperatures produce finer recrystallized grains.

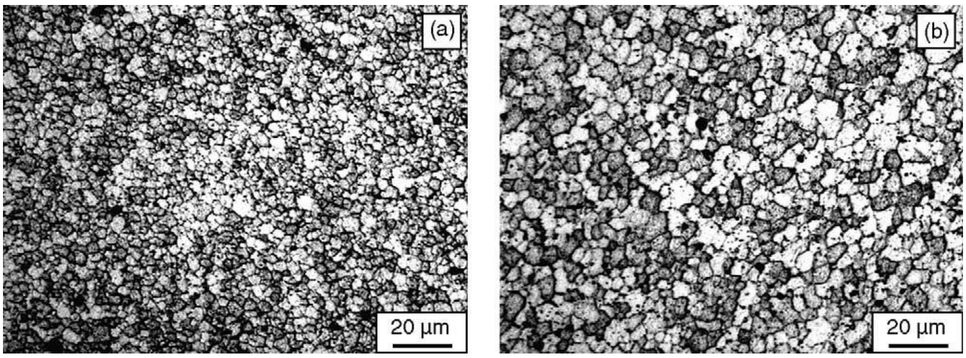

Figure 28 "Impact of RS and TS on nugget grain size (7075Al-T7651): (a) 350 rpm, 152 mm/min (b) 400 rpm, 102 mm/min".[1]

Recent researches by Li [154], Sato [148], and Kwon [152,153] examined how parameters applied on the process affect the microstructure of aluminum alloys under FSW and FSP. "Reducing the tool rotation rate at a constant traverse speed or lowering the ratio of tool rotation rate to traverse speed consistently decreased the recrystallized grain size". For example, Kwon et al. [152,153] observed "grain sizes of 0.5 μm, 1–2 μm, and 3–4 μm at rotation rates of 560 rpm, 980 rpm, and 1840 rpm, respectively, with a constant traverse

Institutional Repository - Library & Information Centre - University of Thessaly
04/09/2026 08:51:35 EEST - 216.73.216.250

speed of 155 mm/min". Similarly, Sato et al. [148] reported "grain sizes of 5.9 µm, 9.2 µm, and 17.8 µm in FSW 6063Al at rotation rates of 800 rpm, 1220 rpm, and 2450 rpm, respectively, with a constant traverse speed of 360 mm/min".

Whenever the process performed at higher "tool rotation rates or higher ratios of tool rotation rate to traverse speed" increases the deformation level and peak temperature during the thermal cycle. While greater deformation reduces recrystallized grain size, higher peak temperatures promote grain size increase. A study on FSP of 7050 Aluminum alloy showed that newly recrystallized grains, initially 25–100 nm, grew to 2–5 µm after heating for 1–4 minutes at 350–450°C [1]. Consequently, the resulting grain size depends on whether deformation or peak temperature dominates the process.

The grain dimensions also varies inside the weld zone. It typically increases approaching the uppermost part of the weld and decreases toward the centerline and the bottom, linking to the heat distribution within the zone. Mahoney et al. [47] reported a "grain size gradient in a 6.35 mm-thick FSP 7050Al, with average sizes of 3.2 µm at the bottom, 5.3 µm at the top, 3.5 µm on the retreating side, and 5.1 µm on the advancing side. Similarly, in a 25.4 mm-thick plate of FSW 2519Al, the grain sizes were 12 µm, 8 µm, and 2 µm in the top, middle, and bottom regions, respectively".

This alteration in grain size is accredited to differences in the "temperature profile and heat dissipation" within the nugget zone. The portion of the workpiece that rests on the backing plate experiences lower peak temperatures and shorter thermal cycles, which inhibit grain growth and result in finer grains. As the plate becomes thicker, the temperature gradient between the top and bottom of the weld also increases, amplifying grain size differences.

Institutional Repository - Library & Information Centre - University of Thessaly
04/09/2026 08:51:35 EEST - 216.73.216.250

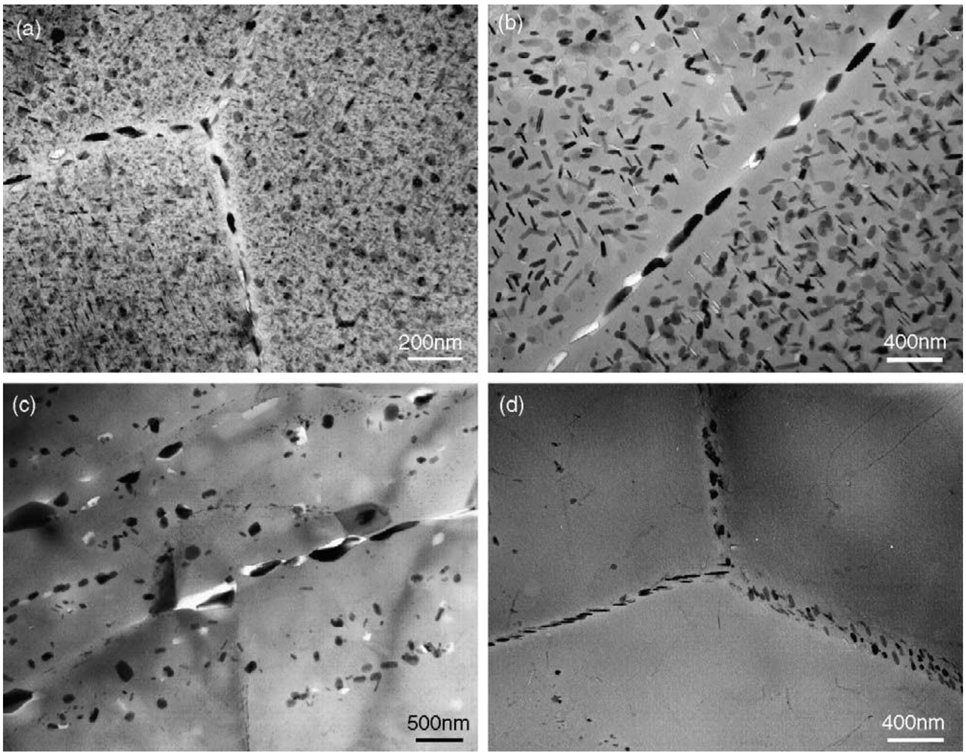

Figure 29 “Microstructures of precipitates within the grain interior and along the grain boundaries in: (a) base metal(BM), (b)Heat Affected Zone (HAZ), (c)Thermo-mechanically affected zone (TMAZ) near HAZ, and (d) TMAZ near nugget zone
(Friction Stir Welding on Al 7050-T651,RS: 350 rpm, TS: 15 mm/min)” [155].

4.2.4 Thermo-Mechanically Affected Zone (TMAZ)

A distinct feature of the FSW processes is the formation of a transitional zone, known as the “thermo-mechanically affected zone (TMAZ)”, situated between the base material and the nugget zone. This region is depicted in Figure 26. Throughout FSW, the TMAZ undergoes both thermal exposure and mechanical deformation.

A usual microstructure of the TMAZ is shown in Figure 24, revealing a greatly deformed structure. The elongated grains from the parent material are observed to follow an “upward flow pattern around the nugget zone”. Despite experiencing plastic-deformation, recrystallization does not occur in the TMAZ due to insufficient strain levels. However, some “dissolution of precipitates” has been reported in this zone, as illustrated in Figure 29 (c)-(d), attributed to the high temperatures encountered throughout FSW [155]. The extent of this dissolution is influenced by the specific thermal cycle within the TMAZ.

Institutional Repository - Library & Information Centre - University of Thessaly
04/09/2026 08:51:35 EEST - 216.73.216.250

4.2.5 Heat-Affected Zone (HAZ)

Located beyond the thermo-mechanically affected zone (TMAZ) is the "heat-affected zone (HAZ)", which experiences a thermal cycle without undergoing any plastic deformation (Figure 26). Mahoney referred to the HAZ as the region where the temperature exceeds 250°C in heat-treatable aluminum alloys[148]. Grain structure within the HAZ remains unchanged from the parent material. However, thermal exposure above 250°C significantly influences the precipitate structure.

Recent studies by Jata et al. [156] examined "the impact of friction stir welding (FSW) on the microstructure of 7050Al-T7451 aluminum alloy". Their findings indicate that even that the welding procedure has minimal impact on subgrain size within the HAZ, it causes "coarsening of strengthening precipitates and expands the precipitate-free zone (PFZ) by approximately five times its original size". Su, using detailed TEM analysis of FSW 7050Al-T651, observed similar effects, including precipitate coarsening and PFZ widening (Fig. 29b). Likewise, Heinz and Skrotzki reported notable precipitate coarsening in the HAZ of 6013 aluminum alloy under FSW. [155]

4.3 Properties of FSW joints

4.3.1 Residual Stresses

In contrast to FSW throughout fusion welding techniques, local heat application and mechanical constraints generate complex "thermal and mechanical stresses" in the joint area and surrounding material, often resulting in residual stresses nearing the yield-strength of the base material. Conversely, FSW, a low-temperature solid-state method, generally produces lower residual stresses. Furthermore, the clamping used in the process introduces most of the times enhanced structural support for the plates while being welded relative to usual welding methods, limiting contraction in the "weld nugget and heat-affected zone" during cooling. However this restraint generates longitudinal and transverse residual stresses, which

Institutional Repository - Library & Information Centre - University of Thessaly
04/09/2026 08:51:35 EEST - 216.73.216.250

significantly influence post-weld mechanical properties, especially fatigue. Consequently, investigating residual-stress distribution in Friction Stir Welded parts is crucial.

Mahoney et al. [157] measured “residual stress in FSW 7050Al-T7451, C458 Al–Li alloy, and 2219Al using the X-ray diffraction $\sin^2\psi$ method”. Their findings revealed:

1. “Residual stresses in FSW welds were considerably lower than those in fusion welds.
2. The transition region between fully and partially recrystallized zones exhibited higher residual stresses compared to other regions.
3. Longitudinal residual stresses were tensile, whereas transverse stresses were compressive.

   These low stresses were attributed to reduced heat input during FSW and the recrystallization-induced stress accommodation” [157].

Donne et al. [158] used various techniques, including “cut compliance, X-ray diffraction, neutron diffraction, and synchrotron radiation”, to study “residual stress in FSW 2024Al-T3 and 6013Al-T6 welds”. Key observations included:

1. “Good agreement between different measurement techniques.
2. Longitudinal residual stresses consistently exceeded transverse ones, irrespective of pin diameter, tool rotation rate, or traverse speed.
3. Residual stresses followed an "M"-shaped distribution across the weld, with maximum tensile stress approximately 10 mm from the weld centerline.
4. Similar stress profiles were observed on the weld’s top and root sides.
5. Larger pin diameters widened the M-shaped distribution, while slower welding speeds reduced tensile stress magnitudes.
6. Residual stresses in small samples were 30–60% of the weld material's yield strength and 20–50% of the base material's yield strength”. [158]

Peel et al. [159] studied “FSW 5083Al using synchrotron X-ray diffraction” and found:

1. “Longitudinal stresses exhibited an "M"-shaped distribution, while transverse stresses peaked at the weld center.
2. The nugget zone experienced tension in both directions.

Institutional Repository - Library & Information Centre - University of Thessaly
04/09/2026 08:51:35 EEST - 216.73.216.250

3. Maximum tensile stresses occurred at the tool shoulder edge, 10 mm from the weld centerline.
4. Longitudinal stress increased with tool traverse speed, whereas transverse stress showed no significant trend.
5. A mild asymmetry was noted, with 10% higher longitudinal stress on the advancing side.
6. Maximum longitudinal and transverse stresses were 40–60 MPa and 20–40 MPa, respectively".

Residual stresses in FSW aluminum alloys remained below 100 MPa, significantly lower than fusion welding stresses and the alloys' yield strength. This reduced stress leads to minimal distortion and improved mechanical properties.[159]

Apart from aluminum alloys stainless steel has been investigated under FSW. For 304L, Reynolds et al. [160] measured residual stress using neutron diffraction. Observations included:

1. "Stress patterns resembled those in fusion welding, with high longitudinal tensile stress and low transverse stress.
2. Maximum longitudinal stresses were near the base metal's yield strength, comparable to fusion welding in austenitic stainless steels.
3. Increasing tool rotation rate from 300 to 500 rpm slightly widened the high-stress range without affecting overall distribution.
4. Longitudinal stress varied minimally with depth, whereas transverse stress exhibited significant depth variation, transitioning from positive at the crown to negative at the root due to rapid cooling from contact with the backing plate".

The differences in stress distribution and magnitude between FSW aluminum alloys and steel likely arise from variations in yield strength with temperature and deformation effects from the tool's trailing edge. [160]

4.3.2 Hardness

Aluminum alloys are categorized as either "heat-treatable or non-heat-treatable". It is has been known from a series of experiments that the hardness variation in friction stir welds

Institutional Repository - Library & Information Centre - University of Thessaly
04/09/2026 08:51:35 EEST - 216.73.216.250

differs significantly between these two types of alloys. For “heat-treatable aluminum alloys”, FSW often results in a softened region near the weld centerline. This softening is attributed to “the coarsening and dissolution of strengthening precipitates caused by the thermal cycle of the FSW process” [1].

Sato et al. [148] studied the hardness-profiles of 6063Al-T5 after FSW and found that “hardness was predominantly influenced by precipitate distribution rather than grain size”. A usual hardness-profile throughout the weld zone is illustrated in Figure 30, including “the average hardness of solution-treated base material for comparison”. Substantial softening was observed across the weld zone in contrast to the parent material in the T5-condition. Notably, the lowest hardness was located approximately 10mm away from the joint center.

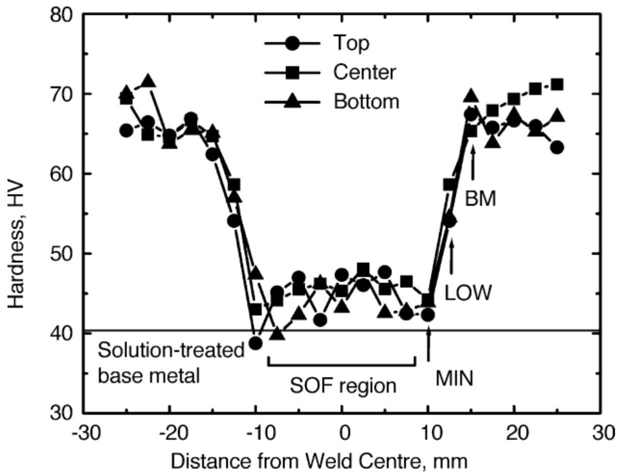

Figure 30 “Usual hardness profile across the FSW of Al 6063-T5” [148].

Sato et al. [148] identified four regions in the hardness profile: “BM (base material hardness), LOW (reduced hardness region), MIN (minimum hardness region), and SOF (softened region)”. The microstructure of these regions revealed two precipitate types: “needle-shaped precipitates (~40 nm, partially or completely coherent with the matrix) and rod-shaped precipitates (~200 nm, with low coherency)”. The material properties of 6063Al are primarily affected by the density of needle-shaped precipitates.

- **BM Region:** “The precipitate microstructure (type, size, and distribution) resembled that of the base material, resulting in similar hardness.
- **LOW Region:** A reduced density of needle-shaped precipitates and increased density of rod-shaped precipitates caused a decrease in hardness.

Institutional Repository - Library & Information Centre - University of Thessaly
04/09/2026 08:51:35 EEST - 216.73.216.250

- **MIN Region:** Only a low density of rod-shaped precipitates remained, eliminating the hardening effect of needle-shaped precipitates and reducing the solid-solution hardening effect, leading to minimum hardness.
- **SOF Region:** Complete dissolution of precipitates occurred, with hardness slightly higher than the base material due to smaller grain size and a higher density of sub-boundaries".[148]

In contrast, FSW generally does not cause softening in non-heat-treatable aluminum alloys [1]. "For 5083Al-O containing small particles, the hardness profile was relatively uniform" [1]. "For 1080Al-O, which lacks second-phase particles, hardness in the nugget zone was slightly higher than the base material, with the maximum hardness observed in the TMAZ" [1].

Studies investigating hardness and microstructure in FSW joints of "non-heat-treatable aluminum alloys" have identified key factors:

- **5083Al-O:** Svesson et al. [130] notified "fine equiaxed grains in the nugget zone, a lower density of large particles (1–10 μm), and a higher density of small particles (0.1–1 μm). The hardness profile was mainly influenced by dislocation density, as strain hardening is the dominant strengthening mechanism".
- Sato noted that "fine recrystallized grains formed in the nugget zone, while the TMAZ contained recovered grains with subgrain structures. Both small and large Al6(Mn,Fe) particles were present in the nugget zone and base material. Hardness was governed primarily by Orowan strengthening, driven by the distribution of small particles rather than grain size (Hall–Petch relationship)".
- **1080Al-O:** Sato found that "the nugget zone comprised recrystallized grains with low dislocation density, while the TMAZ had recovered grains with subgrain structures. The hardness profile was influenced by contributions from grain boundaries, particle dispersion, and substructure".

4.3.3 Impact of FSW on "Microstructure and Mechanical Properties"

Friction stir welding (FSW) causes substantial microstructural changes inside and all-around the stirred-zone, including the "nugget zone, thermomechanically affected zone

Institutional Repository - Library & Information Centre - University of Thessaly
04/09/2026 08:51:35 EEST - 216.73.216.250

(TMAZ), and heat-affected zone (HAZ)”. These changes substantially influence the mechanical properties of the welds. The sections below briefly review mechanical properties such as fatigue, ductility, strength, and fracture toughness.

Mahoney studied “the room-temperature tensile properties of FSW 7075Al-T651”. Samples were extracted from the nugget-zone in two orientations: longitudinal (parallel to the weld) and transverse (normal to the weld). “Longitudinal specimens consisted entirely of recrystallized nugget grains, while transverse specimens incorporated microstructures from the parent material, HAZ, TMAZ, and nugget zone”[11]. Table 4 presents a summary of the longitudinal tensile properties observed within the nugget zone.

Table 4 Longitudinal tensile properties of nugget zone of a FSWed Al 7075-T651. [11]

“Condition	UTS (MPa)	YS (MPa)	Elongation (%)
Base metal, T651	622	571	14.5
As-FSW	525	365	15
Postweld age treatment	496	455	3.5”

- **As-Welded Condition:** A decrease in YS and UTS was observed in the nugget-zone, while elongation remained unaffected. The strength reduction was accredited to the loss of “pre-existing dislocations and the dissolution of fine hardening precipitates”.
- **Postweld Aging (121°C/24 h):** Aging restored a significant portion of YS but reduced UTS and ductility. The yield strength improvement was linked to the increased of fine hardening precipitates, while reduced ductility was attributed to “precipitate-free zones (PFZs)” forming at grain boundaries [11].

Transverse Orientation:

Table 5 presents a summary of the transverse tensile properties. of FSW 7075Al-T651. Compared to the unwelded material, the transverse samples exhibited substantial reductions in strength and ductility, which were also lower comparing to those in the longitudinal orientation. Post-weld aging did not improve strength and further decreased ductility. Failures consistently occurred as shear-fractures in the HAZ.

Institutional Repository - Library & Information Centre - University of Thessaly
04/09/2026 08:51:35 EEST - 216.73.216.250

Table 5 Tensile characteristics in transverse direction of FSWed Al 7075-T651 [11]

“Condition	UTS (MPa)	YS (MPa)	Elongation (%)
Base metal, T651	622	571	14.5
As-FSW	468	312	7.5
Postweld age treatment	447	312	3.5”

The low strength in the HAZ was caused by coarse precipitates and PFZ formation. During tensile testing, most strain occurred in the HAZ, reaching 12–14% strain before necking and fracturing, while the nugget zone experienced only 2–5% strain. This localized strain resulted in low overall strength and ductility for transverse samples.

Post-weld Heat Treatments in 6063-T5 Aluminum:

Sato et al. [148] evaluated the effects of “post-weld treatments on the transverse tensile properties of FSW 6063-T5 aluminum”. Treatments included “post-weld aging (175°C/12 h) and solution heat treatment with aging (SHTA, 530°C/1 h + 175°C/12 h)”.

- **As-Welded Condition:** Strengths and ductility were lowest.
- **Post-weld Aging:** Improved strengths and ductility slightly beyond the base material.
- **SHTA:** Significantly increased strengths above the base material while nearly fully restoring ductility.

The Effect of Process Parameters on Tensile Properties

Biallas et al. [161] researched “the influence of FSW parameters on the tensile properties of 2024Al-T4”, summarized in Table 6. With a constant “tool traverse speed/rotation rate ratio, increasing the rotation rate enhanced yield strength, ultimate strength, and ductility”. Thinner plates exhibited higher strength and joining efficiency than thicker plates.

Institutional Repository - Library & Information Centre - University of Thessaly
04/09/2026 08:51:35 EEST - 216.73.216.250

Table 6 “Tensile characteristics of base material and welded joints in both longitudinal (L) and transverse (T) directions of FSWed Aluminum plates with 4mm and 1.6mm thickness (2024-T3)” [161]

“Material	Rotation rate (rpm)	Traverse speed (mm/min)	YS (MPa)	UTS (MPa)	Elongation (%)	UTS_{FSW}/ UTS_{base}
Base-4 mm-L			424	497	14.9	
FSW-4 mm-L	800	80	279	408	6.6	0.82
FSW-4 mm-L	1000	100	296	423	8.1	0.85
FSW-4 mm-L	1250	125	304	432	7.6	0.87
Base-1.6 mm-L			325	472	21.0	
FSW-1.6 mm-L	1200	120	301	424	6.3	0.90
FSW-1.6 mm-L	1800	180	315	434	6.9	0.92
FSW-1.6 mm-L	2400	240	325	461	11.0	0.98”

Comparison of Joining Efficiency Across Alloys

Table 7 summarizes transverse tensile strengths and welding efficiencies of FSW joints in multiple aluminum alloys. Joining efficiencies for heat-treatable alloys ranged from 65–96%, while non-heat-treatable alloys like 5083Al achieved efficiencies of 95–119%. Notably, FSW demonstrated higher joining efficiency than conventional fusion-welding, especially for heat-treatable alloys.

Institutional Repository - Library & Information Centre - University of Thessaly
04/09/2026 08:51:35 EEST - 216.73.216.250

Table 7 “Efficiency of friction stir weld joints for different aluminum alloys”. [1]

“Alloy	Base metal UTS	Friction stir weld UTS	Joint efficiency (%)
AFC458-T8	544.7	362.0	66
2014-T651 (6 mm)	479–483	326–338	68–70
2024-T351 (5 mm)	483–493	410–434	83–90
2219-T87	475.8	310.3	65
2195-T8	593.0	406.8	69
5083-O (6–15 mm)	285–298	271–344	95–119
6061-T6 (5 mm)	319–324	217–252	67–79
7050-T7451 (6.4 mm)	545–558	427–441	77–81
7075-T7351	472.3	455.1	96
7075-T651 (6.4 mm)	622	468	75
6056-T78 (6 mm)	332	247	74
5005-H14 (3 mm)	158	118	75
7020-T6 (5 mm)	385	325	84
6063-T5 (4 mm)	216	155	72
2024-T3 (4 mm)	478	425–441	89–90
7475-T76		465	92
6013-T6 (4 mm)	394–398	295–322	75–81
6013-T4 (4 mm)	320	323	94”

Insights from Mini Tensile Specimens

Large-specimen tests reflect the weakest regions of the weld and average strain over various zones but do not reveal localized tensile properties. Recent studies by von Strombeck and Mishra used mini tensile specimens to assess localized properties. Key findings for FSW 7075Al alloy include:

1. **Nugget Zone:** “Yield strength was 80% of the base material, ultimate strength approached 100%, and ductility improved due to the fine-grained microstructure.
2. **Nugget/TMAZ Transition:** Strength remained similar to the nugget, but ductility decreased as the TMAZ retained deformed structures.
3. **TMAZ/HAZ Transition:** Strength dropped significantly (~60% of the base material) in the HAZ (12 mm from the weld centerline). The decline was not accompanied by increased ductility.
4. **Retreating vs. Advancing Side:** The retreating side exhibited lower strength, consistent with observed fracture locations”. [148]

Institutional Repository - Library & Information Centre - University of Thessaly
04/09/2026 08:51:35 EEST - 216.73.216.250

4.4 Fatigue

Applications like aerospace structures, transportation vehicles, platforms, and bridges require materials with excellent fatigue properties. Understanding fatigue performance of FSW joints is crucial thanks to their extensive potential in engineering applications. Consequently, research interest in this field has grown, with studies focusing on the relationship between applied stress and the number of cycles a material can endure before failure (S-N), along with the progression of fatigue cracks (FCP).

S–N Behavior

1. **Comparison of Fatigue Strength:**
   - Compared to the base material, FSW welds generally exhibit lower fatigue strength at 10^7 cycles, suggesting a higher likelihood of fatigue crack initiation. Irving and Bussu [162] demonstrated that "transverse FSW specimens exhibit lower fatigue strength compared to longitudinal specimens. Nevertheless, the fatigue performance of FSW welds surpasses that of MIG and laser welds" [1]. For instance, Figure 31 illustrates the "S–N curves for FSW welds, laser welds, MIG welds, and base metal in 6005Al-T5", showing that "the finer and more uniform microstructure" produced by FSW results in superior properties compared to fusion welding methods.

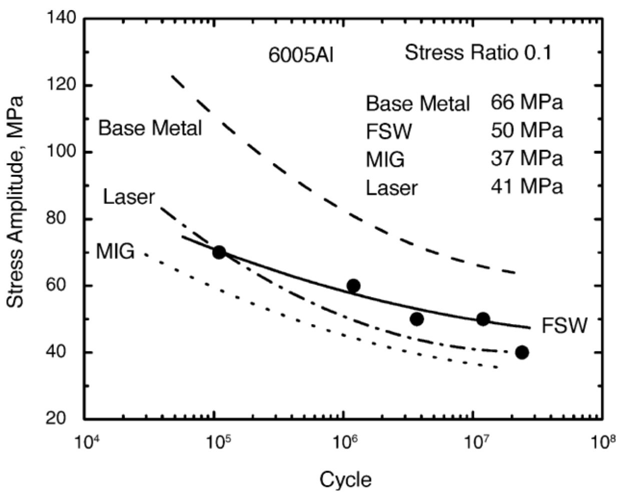

Figure 31 S–N curves for different welding methods
(FSW, Laser and MIG) (6005-T5)
[162]

Institutional Repository - Library & Information Centre - University of Thessaly
04/09/2026 08:51:35 EEST - 216.73.216.250

2. **Impact of Surface Quality:**
    - Surface condition significantly influences the fatigue performance of FSW welds. Hori et al. [162] reported that increasing the tool traverse speed/rotation rate (n/v) ratio reduces the fatigue strength due to the formation of non-welded grooves on the weld's root side. However, when these grooves are removed, the fatigue strength remains unaffected by changes in the n/v ratio. Furthermore, Bussu and Irving found that skimming a 0.5 mm layer from both the root and top sides eliminates surface irregularities, resulting in fatigue strength comparable to the base metal for both transverse and longitudinal specimens. Similarly, Magnusson and Källman [163] observed that milling a 0.1–0.15 mm layer from the top side substantially enhances fatigue strength. These findings indicate that surface crack nucleation limits fatigue life and that successful FSW welds are free from internal defects.
3. **Influence of FSW Parameters:**
    - The correlation amongst FSW parameters and fatigue strength is complex, with no consistent trends reported. Hori et al. [162] found that for a fixed n/v ratio, fatigue strength remained unaffected by tool traverse speed. Conversely, Biallas et al. [161] observed that for a constant n/v ratio, increasing tool rotation rate and traverse speed improved the fatigue strength of 2024Al-T3 FSW welds, particularly in thinner specimens. For instance, S–N data for 1.6 mm thick welds produced at a rotation rate of 2400 rpm and a traverse speed of 240 mm/min fell within the scatter band of the base metal.
4. **Effects of Low Plasticity Burnishing (LPB):**
    - LPB treatment significantly enhances the fatigue-life of FSW welds. Jayaraman reported an 80% increase in high-cycle fatigue endurance for FSW 2219Al-T8751 joints due to the introduction of a deep compressive residual stress layer at the surface. Additionally, the polished surface finish achieved through LPB contributes to improved fatigue properties, consistent with findings that surface crack nucleation primarily governs fatigue performance.
5. **Corrosion-Fatigue Interaction:**
    - Friction stir welds (FSW) usually exhibit lower fatigue resistance in air compared to the base material, however fatigue life and thresholds of 2519Al-

Institutional Repository - Library & Information Centre - University of Thessaly
04/09/2026 08:51:35 EEST - 216.73.216.250

T87 after FSW and the base material were comparable in a 3.5% NaCl solution[1]. This suggests that surface corrosion products influence fatigue crack initiation and underscores the complexity of the interplay between FSW and corrosion in fatigue performance.

6. Conclusion

Despite their slightly lower fatigue performance compared to base materials, FSW welds exhibit superior fatigue properties relative to conventional fusion welding methods. Surface treatments, parameter optimization, and corrosion considerations are vital in enhancing the fatigue-life of FSW joints. Overall, the fatigue characteristics of FSW aluminum alloys demonstrate significant promise for various engineering applications.

Table 8 “Transverse tensile characteristics of FSW welds in different **steels** at ambient temperature” [1]

“Materials	Conditions	UTS (MPa)	YS (MPa)	Elongation (%)	Reduction in area
12% Cr steel	Base metal	–	–	–	–
	FSW welds	539–541	–	–	–
Low carbon steel	Base metal	–	–	–	–
	FSW welds	453–457	–	–	–
AISI 1010	Base metal	463	310	33.9	22
	FSW welds	476	331	22	31
304L	Base metal	483	172	–	–
	FSW welds	621	340”	–	–

Institutional Repository - Library & Information Centre - University of Thessaly
04/09/2026 08:51:35 EEST - 216.73.216.250

4.5 Defects in Microstructure

Defects during the FSW process typically arise from inappropriate choice of input parameters, such as “tool design and dimensions, rotational speed, welding speed, plunge depth, and tool tilt angle”. These defects are often associated with either insufficient or excessive heat generation. If temperature remains at low levels, the material remains insufficiently softened for effective welding. Conversely, excessively high temperatures can alter the weld microstructure and negatively affect the material's mechanical properties. Additionally, improper material transport can occur due to “a loss of traction on the leading and trailing sides of the tool” [164]. The following sections address the key defects.

Ribbon Flash

This defect appears as a ribbon-like structure on the weld’s top surface, caused by material expulsion. It typically results from excessive plunge depth, which generates excessive heat, or from a synthesis of high rotational speed (RS) and low travel speed (TS). This defect causes a reduction in material thickness (Figure 32(a)). To mitigate ribbon flash, choosing a proper plunge depth, a concave-shaped shoulder, or a proper tilt angle is essential [165].

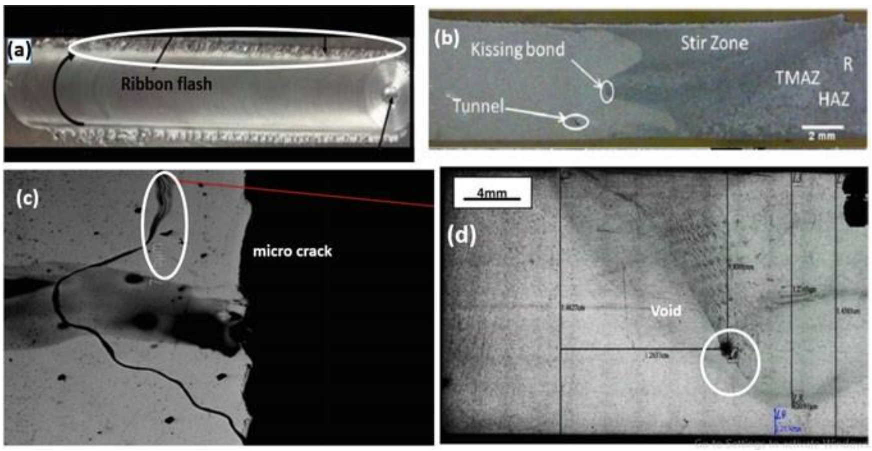

Figure 32 “Common defects in FSW (a) Ribbon Flash [165], (b) Kissing bond and tunnel defect, (c) Microcrack, (d) Void” [164]

Institutional Repository - Library & Information Centre - University of Thessaly
04/09/2026 08:51:35 EEST - 216.73.216.250

Kissing Bond

Kissing bonds form at the boundary between the workpiece and the pin offset, or toward the root-side where material bonding is inadequate. This defect arises from "insufficient stirring and low heat input, which reduce the flowability of plasticized material, leading to poor mechanical properties" (Figure 32(b)). Identifying kissing bonds is challenging and often requires non-destructive methods like ultrasound or detailed optical/SEM scanning after polishing and etching the sample. Proper combinations of welding and tool rotational speed, ensuring sufficient heat for bonding, can prevent this defect.

Tunnel Defect

Tunnel defects occur when input parameters are improperly balanced, often involving "low rotational speed combined with high welding speed". These conditions result in inadequate stirring of the "nugget zone, leading to the formation of tunnels along the weld" (Figure 32(b)). Adjusting the rotational and welding speeds appropriately can prevent tunnel defects [164].

Microcracks

Microcracks typically appear longitudinally to the weld, amongst the plunge and steady-state regions (Figure 32(c)). They often result from insufficient heat dissipation caused by low rotational speed or unexpected increases in welding speed, which disrupt material flow. Eliminating these defects requires "an optimal balance between tool rotation and welding speed" [164].

Void

Voids form due to inadequate material stirring, often caused by excessively high welding speeds. Increased welding speed also accelerates cooling, further impeding proper material stirring and resulting in void formation (Fig. 32d). Optimizing welding speed based on the thickness of the base material can significantly reduce voids [164].

Root Flaws

Root flaws originate in the lower region of the workpiece adjacent to the backing plate, manifesting as irregular planes in the welded zone, particularly on the advancing side. These flaws typically result from incorrect plunge depth or pin height, reducing ductility. Using a bobbin tool or properly setting plunge-depth and pin-height can minimize this defect [164].

Institutional Repository - Library & Information Centre - University of Thessaly
04/09/2026 08:51:35 EEST - 216.73.216.250

Surface Defects

Surface defects are formed as grooves, irregularities, or galling on the weld’s top or faying surface. These defects often result from an unsuitable set of process constraints, such as extreme or not enough heat input or irregular material stirring. Careful parameter selection can prevent these defects.

Oxide Entrapment

During FSW, under high-temperature conditions, the eutectic temperature of aluminum alloys (550°C) may be exceeded, causing localized melting and defect formation. Oxidation of freshly areas where the material is sheared and the subsequent contact of the exposed, flowing metal with the surrounding air at high temperatures can lead to oxide formation within the material, referred to as oxide entrapment [164].

Conclusion

Monitoring the thermal and mechanical properties of welded specimens is crucial. Properly governing welding temperature and speed can prevent parameter deviations and defect formation. The interplay between tool rotational speed and travel speed determines the peak temperatures achieved during FSW, which is key to minimizing weld defects.[164]

Institutional Repository - Library & Information Centre - University of Thessaly
04/09/2026 08:51:35 EEST - 216.73.216.250

Chapter 5. Applications of Stir Welding

5.1 Industrial applications

The initial product developed using an FSW device was A cooling apparatus featuring a honeycomb panel configuration, optimized for accelerated fish temperature reduction in onboard fishing containers. FSW machines are now commonly used across various industries, for instance the joining of large aluminum hollow panels, ship-constructions, the construction of offshore platforms, and the fabrication of high-speed ship-deck superstructures. In Norway, “Marine Aluminum manufactures pressed aluminum sections for applications in shipbuilding and railway rolling stock”.[164]

5.2 Aerospace Applications of FSW

United Launch Alliance has utilized FSW in the construction of inter-stage superstructure modules for its “Atlas V, Delta II, and Delta IV” rockets. Boeing followed suit, employing FSW technology for joining “shipment wall beams for the Boeing 747 cargo freighter and toenails for the Boeing C-17”. In the United States, the “longitudinal and circumferential welds in the propellant tanks of the Delta rocket” series were fabricated using FSW, as illustrated in Figure 33(b). Transitioning from conventional welding techniques to Friction Stir Welding in the production of space rocket propellant-tanks has resulted in significant cost savings. The Ariane 5 launch vehicle, designed for the “European Space Agency (ESA)” to lift heavy payloads, is also welded using FSW.

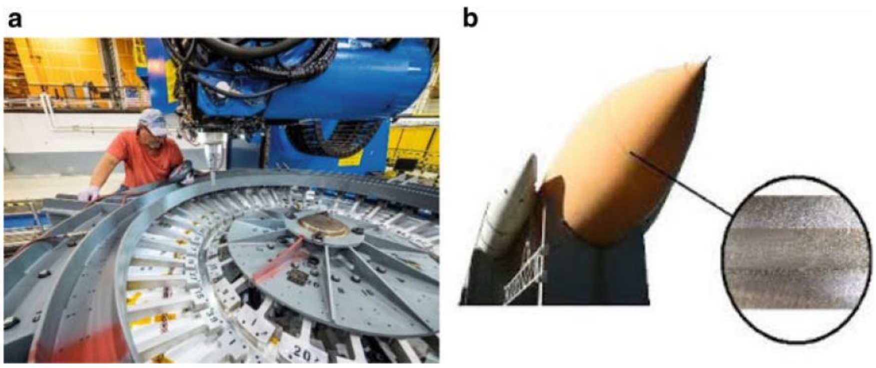

Figure 33 (a) “FS Weld of Orion EM-1 Crew Module”, (b) “FSW on fuel tank of Space-rocket” [164]

Institutional Repository - Library & Information Centre - University of Thessaly
04/09/2026 08:51:35 EEST - 216.73.216.250

Boeing has successfully applied FSW in the welding of aircraft superstructures, including lap-joining of 7075 aluminum sections. The technique is further employed for fabricating fighter plane deflectors. Boeing has undertaken numerous military projects involving components like “the base plate of the cargo section of the C-17 Globemaster III aircraft”. NASA has used FSW for the “outer propellant fuel tank of the Ares rocket”. Additionally, Germany-based “Airbus GmbH and Daimler/Chrysler Aerospace” have adopted FSW to produce airframe components such as “the fuselage, passenger cabins, wings, and vertical stabilizers”.[164] FSW is integral to “the final assembly of narrow-fuselage aircraft, particularly for the Airbus A3 series and the A380”. It is utilized for “lengthwise joints in the fuselage, outer links, and central wing containers using AA2xxx and AA7xxx aluminum alloys”.

Figure 34 “NASA’s Space Launch System (SLS) using FSW” [166]

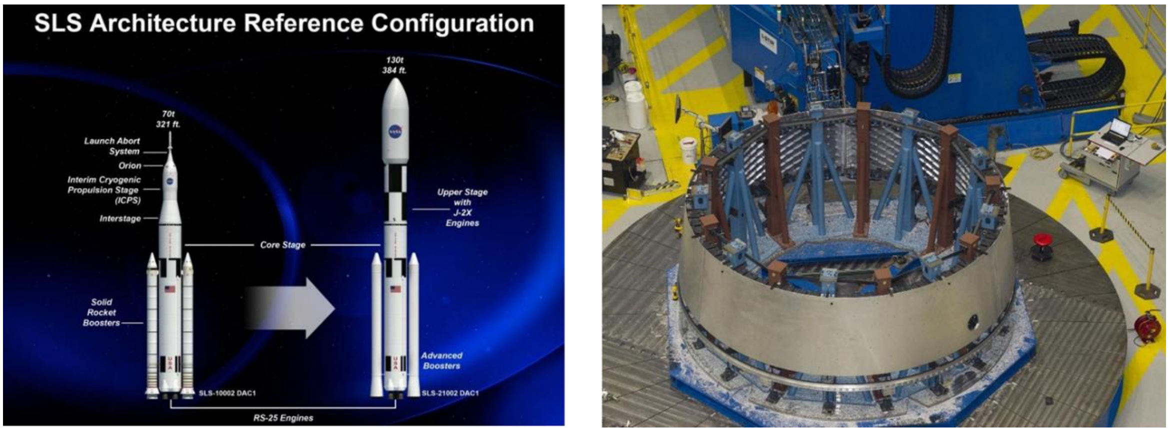

Figure 35 “The biggest FSW structure to construct the cryogenic tanks. (Michoud Assembly Facility (MAF))”[166]

Institutional Repository - Library & Information Centre - University of Thessaly
04/09/2026 08:51:35 EEST - 216.73.216.250

FSW also plays a critical role in manufacturing Airbus A400M panels and welding the "longitudinal and circumferential seams of Falcon 1 and Falcon 9 rocket fuel tanks at SpaceX" [98]. Fokker Space Company fabricated the "main cryogenic stage engine body of the Ariane-5 rocket, incorporating a nose section with 12 integral flat panels of AA7075 with stiffeners". Eclipse Aviation applied FSW in producing the Eclipse 500, a private-class five-seater airliner, using "rigid stringer panels made from AA2xxx (plating) and AA7xxx (stringers) aluminum alloys" [164].

The ZE41A-T5 magnesium alloy combined with AA 2024-T3 aluminum enhances strength and is commonly used in aerospace productions and defense applications for dissimilar FSW joints. Additionally, ZE41A-T5 Magnesium is an anti-corrosive alloy employed in "airplane gearbox and generator casings for military helicopters, which are frequently exposed to corrosive environments during operation" [164]. However, "the dissimilar joining of magnesium and aluminum alloys presents challenges due to differences in physical properties and the formation of intermetallic compounds such as Al12Mg17 and Al3Mg2 in the stir zone (SZ)". The Indian Space Research Organization (ISRO) has also implemented FSW techniques in constructing propellant tanks [167].

5.3 Automobile Applications of FSW

Friction Stir Welding (FSW) is widely utilized in the automotive sector for manufacturing spatial frames of car structures, fuel tanks, chassis components, bus body structures, and other transportation mediums. The Ford-GT utilizes FSW to effectively weld extruded bent sheets made of aluminum and fuel-tank housings. In the automotive industry, the technique is also used to produce "hood panels, suspension links, and driveshafts". FSW applications have extended beyond traditional materials like aluminum and magnesium. Notable automotive uses include "the rear seat frame of the 2001 Volvo V70, suspension components of the 2003 Lincoln Town Car L, hood and rear doors of the 2004 Mazda RX-8, space frame parts of the 2005 Ford GT and 2007 Audi R8, hood and trunk of the 2006 Mazda MX-5 Miata, rear hatch parts of the 2010 Toyota Plus, and front subframe parts of the 2013 Honda Accord" (Figure 36(a)) [168].

Institutional Repository - Library & Information Centre - University of Thessaly
04/09/2026 08:51:35 EEST - 216.73.216.250

In the automotive sector, the most frequently used aluminum alloy is AA7075, constituted of aluminum, zinc, magnesium, and copper. This alloy is the strongest among aluminum alloys and has strength comparable to steel while weighing only one-third as much. It is utilized for several automobile parts. Furthermore, AA 5454, known for its corrosion resistance, is used in suspension parts and wheel rims, while AA 5182, recognized for its excellent formability and resistance to stress corrosion cracking, is utilized in body panels and interiors. AA 5154 finds application in “wheels, drivetrain components, and underbody structures”. Additionally, AA 5022 is employed in making “bonnets, oil pans, floors, rear fenders, roofs, and doors” [164].

Figure 36 “(a)Dissimilar friction stir welding of cast aluminum and steel (engine cradles of the 2013 Honda Accord)” [168],

(b) “LR and BMW body panel from FSWed 6xxx series aluminum” [169]

In 1998, “TWI fabricated Friction Stir tailor-welded blanks for Land Rover and BMW body panels” [169]. Mg alloys are also significantly utilized in the automobile production, such as “in the engine brackets of the Chevrolet Corvette and the front-end of the Jaguar XJ351”. However, the significant cost of magnesium alloys limits their use in mass production. For instance, in a typical General Motors (GM) vehicle, the magnesium-to-aluminum weight consumption ratio is 4:123 [168].

Institutional Repository - Library & Information Centre - University of Thessaly
04/09/2026 08:51:35 EEST - 216.73.216.250

5.4 Other Applications of FSW (Nuclear, Shipbuilding, Electronics)

In shipbuilding, Friction Stir Welding techniques are utilized for joining ship-panels and outer-body structures. Honeycomb panels, which offer the additional benefit of high sound absorption, find application in ship cabin walls and railway carriages. Other applications span various industries, including the production of sailboat joints, refrigerators, helicopter landing platforms, oil-extraction platforms, ship masts, yacht supports, and railway transportation appliances. The Japanese Shinkansen express train utilized FSW-assembled finned panel floors and wagon-walls [164].

In marine industry, prefabricated panels produced via FSW can be found in “Freedom-class Littoral Combat Ships and Nichols Bros.’ Sea Fighter”. A specialized FSW machine was developed through a collaboration between the “University of Adelaide (Australia) and TWI” for welding curved-joints on the nose sections of cruise ships, utilizing 5 mm thick AA5083 sheets (Patent WO98/38084, Austria). Hydro Marine fabricated FSW roof panels, delivered to Alstom LHB (Germany), as depicted in Fig. 37 [169].

Figure 37 “Hydro Marine Aluminum manufactured a roof panel that was supplied to Alstom LHB. (Germany)” [169]

FSW has also been applied in electronics, such as “Siemen’s X-ray vacuum vessel”, and is capable of welding “3D-printed materials with a joint efficiency of 83.3%”. Within the

Institutional Repository - Library & Information Centre - University of Thessaly
04/09/2026 08:51:35 EEST - 216.73.216.250

nuclear sector, FSW serves as a crucial technique for joining components involved in nuclear waste containment. This is exemplified by its use in the production of 50mm thick copper containers, manufactured by SKB, designed for the secure storage of nuclear waste, as shown in Figure 38(a) [170].

Researchers have conducted extensive investigations into FSW for both similar and dissimilar metals. It has proven successful in automobile spare part production and aerospace applications, demonstrating significant potential in research and development. FSW has been employed to various materials, including "aluminum, copper, magnesium, titanium, and steel, as well as dissimilar combinations like aluminum-magnesium, magnesium-copper, and copper-aluminum".

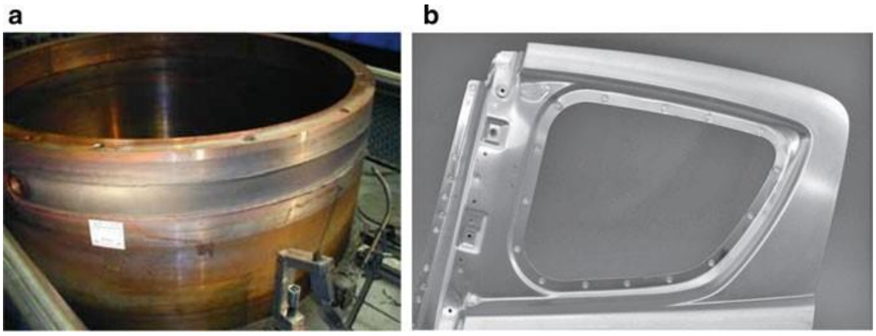

Figure 38 (a) "Nuclear waste encapsulation by SKB using a 50 mm thick copper container." [170], (b) "Exterior rear door panel. (Mazda RX-8)" [169]

Research areas include "material flow, temperature distribution, microstructural characterization, and the enhancement of weld mechanical properties. Tool wear during FSW has also been studied, as it is critical for tool design and predicting tool life within optimized process parameters". Furthermore, several FSW variants have been explored in the literature. Readers seeking a more comprehensive understanding should consult additional papers in these specialized areas.

Institutional Repository - Library & Information Centre - University of Thessaly
04/09/2026 08:51:35 EEST - 216.73.216.250

Chapter 6. Conclusion and Future Directions in Friction Stir Welding

Friction Stir Welding (FSW) stands out as a solid-state joining method renowned for its ability to effectively weld a diverse range of materials, including both similar and dissimilar types, across various geometrical arrangements. As “a solid-state process”, FSW get rid of common defects correlated with solidification, such as cracking, while providing benefits like enhanced mechanical strength due to finer microstructure and reduced energy consumption. This process finds applications across numerous industrial sectors, including aerospace, automotive, and electronics, underscoring its versatility and significance.

A critical aspect of achieving efficient FSW is the careful choice of input parameters, which govern heat generation and material flow. Key parameters include “rotational speed (RS), traverse speed (TS), plunge depth (PD), and tilt angle”. Among these, RS is often highlighted as the most influential. Optimization of these parameters plays a crucial role in achieving defect-free welds exhibiting excellent mechanical performance. Techniques such as “Taguchi methods, response surface methodology (RSM), factorial design (FD), and artificial intelligence (AI)-based approaches like machine learning (ML) and artificial neural networks (ANN)” have been utilized to identify optimal parameter combinations. “Hybrid and multi-objective optimization strategies” have also been explored, offering potential for further advancements in process efficiency.

FSW has driven innovations beyond traditional welding applications, inspiring the development of variants such as “friction stir processing, friction stir spot welding, and solid-state additive manufacturing”. These variants expand the capabilities of FSW, enabling greater flexibility in manufacturing. Despite these advancements, challenges remain, particularly tool wear when welding high-strength materials. Tool shaping and geometry is essential in defining weld quality. While specific designs are often proprietary, common configurations such as cylindrical threaded pins and concave shoulders are widely reported. Advanced designs, including MX Triflute™ and Flared-Triflute™, have also been developed to enhance performance.

The joint configurations in FSW typically include butt and lap joints, which require minimal surface preparation. The process is often likened to in situ extrusion, where material-flow and mixing primarily take place near the tool’s rotating shoulder. However, the

Institutional Repository - Library & Information Centre - University of Thessaly
04/09/2026 08:51:35 EEST - 216.73.216.250

complexities of material flow during FSW are not fully understood, presenting an area for further research. The process induces significant temperature rises, often reaching 400–500 °C in aluminum alloys, resulting in pronounced microstructural changes. These include the formation of “fine recrystallized grains, texture development, precipitate dissolution, and coarsening”. Three distinct microstructural zones are observed: “the nugget zone, characterized by intense deformation and fine equiaxed grains; the thermo-mechanically affected zone (TMAZ), featuring deformed and un-recrystallized grains; and the heat-affected zone (HAZ), marked by precipitate coarsening”. Also, residual-stresses in FSW are notably lower than in traditional fusion-welding processes.

Table 9 Key features, possibilities, and constraints of each Friction Stir Welding method. [171]

“Friction Stir Welding Technique	**Joint Efficiency**	**Surface Finish**	**Material Mixing Quality**	**Root Defect Formation**	**Internal Defects Formation**	**Implementation**
Conventional Tool	Satisfactory	Poor	Normal	Likely	Almost Always	Very Easy
Double-side Pass (Conventional tool)	Good	Poor	Normal	unlikely	Almost Always	Easy
Preheated Polymer	Good	Fair	Good	Reduced	Less likely	Difficult
Conventional Heated Tool	Good	Fair	Good	Reduced	Less likely	Easy
Stationary Shoulder	Very Good	Very Good	Good	Reduced	Less likely	Easy
Heated Stationary Shoulder	Excellent	Excellent	Very Good	Reduced	Less likely	Easy
i-FSW	Very Good	Fair	Good	Reduced	Less likely	Easy”

In terms of mechanical properties, FSW offers considerable advantages over fusion welding techniques. “Welded aluminum alloys can achieve up to 80% of the yield stress of the base material, with failure typically occurring in the HAZ”. For steel, overmatching behavior has been observed, with failures often occurring in the base material. Fatigue performance, despite being inferior than that of the base material, surpasses that of laser and MIG welds. Post-weld surface treatment to remove profile irregularities can elevate fatigue strength to levels equivalent to the base material. Additionally, the fracture-toughness of FSW joints is often superior or comparable to that of the base material. Corrosion resistance of FSW welds has yielded mixed results, with some studies highlighting improved resistance to pitting and

Institutional Repository - Library & Information Centre - University of Thessaly
04/09/2026 08:51:35 EEST - 216.73.216.250

stress corrosion cracking (SCC), while others indicate increased susceptibility to intergranular attack in high-strength aluminum alloys, particularly within the HAZ adjacent to the TMAZ.

Table 10 Summary of FSW Studies: Materials, Parameters, and Key Findings [172]

“Sr. No.	Author (Year)	Substrate Material	Parameters selected for study	Conclusion
1	*Elangovan K. , Balasubramanian V.* , (2008)	“AA2219 aluminium alloy “	“Tool pin profile and welding speed”	“square pin profiled tool produced defect free FSP region, irrespective of welding speeds”. - “the joints fabricated at a welding speed of 0.76mm/s showed superior tensile properties, irrespective of tool pin profiles”. - “the joint fabricated using square pin profiled tool at a welding speed 0.76mm/s exhibited maximum tensile strength, higher hardness and finer grains in the FSP region”.
2	Chen Thaiping, (2009)	“AA6061 aluminum alloy and SS400 lowcarbon steel”	“Lower transverse speed and rotation speed”	“-The lower transverse speed and rotation speed, which are the significant FSW process parameters, yield a higher C-notch Charpy impact value”.
3	Patil H. S. , Soman S. N. , (2010)	“AA6082-O aluminium”	“Welding speed and tool pin profiles”	- “The effect of tool pin profile and welding speed on the appearance of the weld is presented and no obvious defect was found”. - “It is found that the joint fabricated using taper screw thread pin exhibits superior tensile properties compared tri -flute pin profile, irrespective of welding speed”.
4	Arora A. & Mehta M. & De A. & DebRoy T. , (2009)	“L80 steel and AA7075 alloy”	“Load bearing capacity of tool pin”	“A three-dimensional heat transfer and visco-plastic model is used to compute the influence of pin length and diameter on traverse force during FSW. The total traverse force increases significantly with increase in pin length”
5	Reshad K., Seighalani, M.K. Givi Besharati, Nasiri A.M., and Bahemmat P. , (2009)	“Pure Titanium “	“Tool Material, Geometry, and Tilt Angle “	- “Using high-speed steel (HSS) tool for FSW of titanium will result in complete failure of the pin and severe wear of the shoulder nose because of heat generation from friction between the tool and the base metal. -Using brittle WC as a pin material for FSW of the Ti-CP and because of high wear and stress concentrations developing on the root of the pins threads Macro structural analysis of the welded joints shows that defects such as voids, lack of penetration, and cracks are more likely to occur.”
6	Kulekci Mustafa Kemal & Şik Aydin & Kaluç Erdinç, (2008)	“AA 5754 aluminium alloy plates “	“Tool rotation and pin diameter”	“Increasing tool rotation for a fixed tool pin diameter reduces fatigue strength of joints.” “Increasing tool pin diameter for a fixed tool rotation, decreases fatigue strength of joints.” “In FSW lap joints, an optimization between tool pin diameter, tool rotation and tool traverse speed is needed to obtain better fatigue strength.”
7	Arora A., Deb A. and DebRoy T.. (2011)	“AA6061 aluminum Alloys”	“Tool shoulder diameter”	“In order to determine the optimum tool geometry, the two components of the torque are used for various shoulder diameters. As the shoulder diameter increases, the sticking torque, MT, increases, reaches a maximum and then decreases. This behavior can be examined, which shows that two main factors affect the value of the sticking torque. First, the strength of the material is decreases with increasing temperature due to an increase in the shoulder diameter. Second, the area over which the torque is applied increases with shoulder diameter.”
8	Cao X., Jahazi M.. (2011)	“AZ31B-H24 magnesium alloy”	“Tool rotational speed and probe length”	“Tensile shear load initially increases with increasing tool rotational speed but decreases with further increase. Shear strength increases with increasing probe length and penetration depth in to the bottom sheet”.”

Institutional Repository - Library & Information Centre - University of Thessaly
04/09/2026 08:51:35 EEST - 216.73.216.250

FSW has successfully joined various metallic materials, including “aluminum, copper, titanium, steel, magnesium, and composites”. However, the process faces limitations when dealing with “high-melting-point or low-ductility” materials. Preheating has been shown to enhance weld quality and enable higher traverse speeds, particularly for materials like steel. Temperature monitoring and control are essential in FSW, with thermocouples frequently employed to measure thermal evolution. Additional sensors, such as load cells for force and torque measurements and acoustic sensors for frequency monitoring, contribute valuable data for optimizing process parameters. Data analysis using AI and ML algorithms has demonstrated potential for refining process efficiency and enabling real-time feedback systems.

Future Challenges

Future research on Friction Stir Welding (FSW) presents numerous opportunities for advancing the process, addressing its limitations, and expanding its industrial applications. A deeper understanding of the correlation among welding parameters and the flow of materials, particularly in magnesium alloys, remains a crucial area for exploration. This understanding will enable the creation of superior joints by mitigating improper material flow and optimizing the welding process. Additionally, more comprehensive studies are needed to unravel the mechanisms governing microstructural evolution within the stir zone, an area that remains insufficiently understood. Techniques such as “stop-action” analysis can provide valuable insights into this complex phenomenon.

From a microstructural and mechanical perspective, evaluating the corrosion resistance, wear resistance, fracture toughness, and fatigue-strength of FSW welds will be essential to broaden the range of practical applications. Further investigations into the “high-temperature plastic flow behavior and mechanical properties” of dissimilar materials, particularly hard alloys, can shed light on their performance during FSW. Analyzing the influences of peak temperatures on “microstructure and mechanical properties” using numerical and analytical methods will also contribute to refining the process for high-strength materials. Moreover, the role of “pre- and post-weld treatments” in enhancing the weld quality of steels warrants significant attention.

In the realm of simulation, modeling, and optimization, the development of advanced models incorporating tool-related constraints, like “temperature, torque, and shear stress”

Institutional Repository - Library & Information Centre - University of Thessaly
04/09/2026 08:51:35 EEST - 216.73.216.250

holds promise for reducing defect rates and improving joint quality. Expanding datasets to include a broader range of “materials, joint configurations, and process conditions” will enhance the reliability and applicability of these models. Cutting-edge Machine-Learning(ML) systems, including “ensemble models and deep learning architectures”, can further improve predictive models and enable a more nuanced understanding of parameter interactions. Incorporating real-time environmental factors, such as temperature and humidity, into predictive models will allow for more accurate representations of real-world conditions.

The integration of advanced technologies offers transformative potential for FSW. Real-time monitoring systems, utilizing sensors to track vibration, torque, and temperature, can be combined with “Internet of Things (IoT)” platforms to enable dynamic adjustments and predictive maintenance. “Artificial intelligence (AI) and machine learning (ML)” methodologies can revolutionize quality inspection, defect detection, and the prediction of tool wear and breakage. The deployment of digital twin technology will facilitate real-time process monitoring and establish consistent production capabilities across multiple FSW machines, while 5G technologies and cloud-based platforms can enhance process control and data sharing.

Tool geometry and wear remain critical challenges for FSW. Detailed investigations into the effects of tool profiles, such as bobbin tools, on weld quality and durability will enable the development of optimized designs. Additionally, ML-based systems for tool condition monitoring, particularly for predicting wear and breakage, will be instrumental in extending tool life and ensuring consistent weld quality.

Advancements in material and joint configuration capabilities will further expand the applications of FSW. Research into thick non-ferrous, ferrous, and composite materials, leveraging optimized temperature-based simulation techniques, will enable the welding of more complex structures. Studies on polymers, focusing on the influence of plunge depth, axial force, and heat generation, will offer new possibilities for FSW in emerging industries.

Economic considerations are another area ripe for investigation. Understanding the impact of welding conditions on process costs and evaluating the feasibility of commercial applications, especially for steels, will be crucial for broader industrial adoption. The integration of Industry 4.0 and 5.0 frameworks within FSW processes can further enhance operational efficiency, enabling smarter and more adaptive manufacturing systems.

Institutional Repository - Library & Information Centre - University of Thessaly
04/09/2026 08:51:35 EEST - 216.73.216.250

Ultimately, the ongoing refinement of multi-objective optimization techniques, incorporating real-time sensor data and AI-driven analysis, will be pivotal in balancing mechanical properties, cost, and efficiency. These advancements, combined with a deeper fundamental understanding of FSW, will drive its evolution, ensuring its relevance and adaptability to the needs of modern industries.

Institutional Repository - Library & Information Centre - University of Thessaly
04/09/2026 08:51:35 EEST - 216.73.216.250

References

[1] R.S. Mishra, Z.Y. Ma, Friction stir welding and processing, Center for Friction Stir Processing, Department of Materials Science and Engineering, University of Missouri, Rolla, MO 65409, USA; Institute of Metal Research, Chinese Academy of Sciences, Shenyang 110016, China.

[2] Padmanaban, G., Balasubramanian, V., An experimental investigation on friction stir welding of AZ31B magnesium alloy, Int. J. Adv. Manuf. Technol. 2010, 49, 111–121.

[3] Li, Y., Qin, F., Liu, C., Wu, Z., A Review: Effect of Friction Stir Welding on Microstructure and Mechanical Properties of Magnesium Alloys, School of Materials Science and Engineering, Taiyuan University of Science and Technology, Taiyuan 030024, China.

[4] Lee, W.B., Yeon, Y.M., Jung, S.B., Mechanical properties related to microstructural variation of 6061 Al alloy joints by friction stir welding, Mater. Trans. 2004, 45, 1700–1705.

[5] He, X., Gu, F., Ball, A., A review of numerical analysis of friction stir welding, Prog. Mater. Sci. 2014, 65, 1–66.

[6] Dialami, N., Chiumenti, M., Cervera, M., Agelet de Saracibar, C., Challenges in thermos-mechanical analysis of friction stir welding processes, Arch Comput. Methods Eng. 2017, 24, 189–225.

[7] Kıral, B.G., Tabanoğlu, M., Serindağ, H.T., Finite element modeling of friction stir welding in aluminum alloys joint, Math. Comput. Appl. 2013, 18, 122–131.

[8] Ulysse, P., Three-dimensional modeling of the friction stir-welding process, Int. J. Mach. Tools Manuf. 2002, 42, 1549–1557.

[9] Heurtier, P., Jones, M.J., Desrayaud, C., Driver, J.H., Montheillet, F., Allehaux, D., Mechanical and thermal modelling of friction stir welding, J. Mater. Process. Technol. 2006, 171, 348–357.

[10] Sato, Y.S., Kokawa, H., Distribution of tensile property and microstructure in friction stir weld of 6063 aluminum, Metall. Mater. Trans. A 2000, 32, 3023–3031.

[11] Mahoney, M.W., Rhodes, C.G., Rhodesoff, J.G., Bingel, W.H., Spurling, R.A., Properties of friction-stir-welded 7075 T651 aluminum, Metall. Mater. Trans. A 1997, 29, 1955–1964.

[12] Padhy, G.K., Wu, C.S., Gao, S., Friction stir based welding and processing technologies - processes, parameters, microstructures and applications: A review, MOE Key Lab for Liquid-Solid Structure Evolution and Materials Processing, Institute of Materials Joining, Shandong University, Jinan, 250061, China.

[13] J. Martin, Friction Stir Welding, The Welding Institute, UK, 2017 http://www.manufacturingchampions.in/Document/presentaion-9%202016%20Robotic%20FSW%20-%20Future%20Trends%20CII%20Conference%20of%20Welding.pdf.

[14] D. Li, X. Yang, L. Cui, F. He, X. Zhang, J. Mater. Process. Technol. 222 (2015) 391–398.

[15] L. Shi, C.S. Wu, H.J. Liu, Int. J. Mach. Tool Manuf. 91 (2015) 1–11.

[16] J.Q. Li, H.J. Liu, "Characteristics of the reverse dual-rotation friction stir welding conducted on 2219-T6 aluminum alloy," *Materials and Design*, vol. 45, pp. 148–154, 2013.

[17] W.Y. Li, T. Fu, L. Hutsch, J. Hilgert, F.F. Wang, J.F. Dos Santos, N. Huber, Mater. Des. 64 (2014) 714–720.

[18] M.K. Sued, D. Pons, J. Lavroff, E.H. Wong, Mater. Des. 54 (2014) 632–643

[19] W.M. Thomas, C.S. Wiesner, D.J. Marks, D.G. Staines, Sci. Technol. Weld. Join. 14 (2009) 247–253.

[20] H. Zhang, M. Wang, X. Zhang, G. Yang, Mater. Des. 65 (2015) 559–566.

[21] Q. Yang, S. Mironov, Y.S. Sato, K. Okamoto, Mater. Sci. Eng. A 527 (2010) 4389–4398.

Institutional Repository - Library & Information Centre - University of Thessaly
04/09/2026 08:51:35 EEST - 216.73.216.250

[22] P. Su, A. Gerlich, T.H. North, G.J. Bendzsak, Sci. Technol. Weld. Join. 11 (2013) 61–71.
[23] T.Y. Pan, SAE Technical Paper No. 2007-01-1702, 2007.
[24] Friction Stir Welding and Processing Mr. Sadaruddin Ansari Dep. of Mechanical Engineering, M.K.R Group of Institutions Chandaus, Aligarh, Uttar Pradesh, India
[25] R. S. Mishra, M. W. Mahoney, Y. Sato, Y. Hovanski and R. Verma, 2011. “Friction Stir Welding and Processing VI,”
[26] M. Aissani, S. Gachi and F. Boubenider, “Design and optimization of friction stir welding tool,” *Materials and Manufacturing Processes*, vol. 25, pp. 1199–1205, 2010.
[27] M. Azizieh, A.H. Kokabi, and P. Abachi, “Effect of rotational speed and probe profile on microstructure and hardness of AZ31/Al2O3 nanocomposites fabricated by friction stir processing,” *Materials & Design*, vol. 32, no. 4, pp. 2034-2041, 2011.
[28] J. Gandraa, R. Mirandaa, P. Vilac, A. Velhinho and J.P. Teixeira, “Functionally graded materials produced by friction stir processing,” *Journal of Materials Processing Technology*, vol. 211, no. 11, pp. 1659–1668, 2011.
[29] R.V. Marode, M. Awang, T.A. Lemma, S.R. Pedapati, A. Hassan, V.S.R. Janga et al., “Friction stir processing of AZ91 hybrid composites with exfoliated multi-layered graphene: A Taguchi Grey relational analysis,” *Journal of Alloys and Compounds*, vol. 972, p. 172703, 2024
[30] A. Hassan, M. Awang, S.R. Pedapati, K. Altaf, R.V. Marode and S.W. Ahmed, “Experimental investigation on tool pin profile for defect-free multi-layered laminates using friction stir additive manufacturing,” *Results in Engineering*, vol. 20, p. 101516, 2023.
[31] A. Hassan and S.R. Pedapati, “Exploration of possible defects originating in Al-5083 laminates synthesized through friction stir additive manufacturing technique,” *In International Conference on Renewable Energy and E-mobility*. Singapore: Springer Nature Singapore, pp.309-318, 2022
[32]ASM Handbook, “Properties and selection: Nonferrous alloys and special-purpose material,” ASM International, vol. 2, 1990.
[33] L. Fratini, F. Micari, G. Buffa and V.F. Ruisi, “A new fixture for FSW processes of titanium alloys,” *CIRP Annals - Manufacturing Technology*, vol. 59, pp. 271–274, 2010.
[34] H. Bisadi, A. Tavakoli, and M.T. Sangsaraki, “The influences of rotational and welding speeds on microstructures and mechanical properties of friction stir welded Al5083 and commercially pure copper sheets lap joints,” *Materials and Design*, vol. 43, pp. 80–88, 2013.
[35] A Review of Recent Improvements, Developments, Influential Parameters and Challenges in the Friction Stir Welding Process Sadiq Aziz Hussein, Ahmed Jasim Hashim, Salah Mahdi Khaleel, Mudhar A Al-Obaidi, Farhan Lafta Rashid
[36] N. Sharma, A.N. Siddiquee, Z.A. Khan and M.T. Mohammaed, “Material stirring during FSW of Al–Cu: Effect of pin profile,” *Materials and Manufacturing Processes*, vol. 33, Issue 7, pp. 786-794, 2018.
[37] J.Q. Li, and H.J. Liu, “Effects of tool rotation speed on microstructures and mechanical properties of AA2219-T6 welded by the external non-rotational shoulder assisted friction stir welding,” *Materials and Design*, vol. 43, pp. 299–306, 2013.
[38] N.S. Sundarama and N. Murugan, “Tensile behavior of dissimilar friction stir welded joints of aluminium alloys,” *Materials and Design*, vol. 31, no. 9, pp. 4184–4193, 2010.
[39] K. Elangovan and V. Balasubramanianb, “Influences of tool pin profile and tool shoulder diameter on the formation of friction stir processing zone in AA6061 aluminium alloy,” *Materials and Design*, vol. 29, pp. 362–373, 2008.
[40] K. Elangovan and V. Balasubramanianb, “Influences of tool pin profile and welding speed on the formation of friction stir processing zone in AA2219 aluminium alloy,” *Journal of Materials Processing Technology*, vol. 200, pp. 163–175, 2008.

Institutional Repository - Library & Information Centre - University of Thessaly
04/09/2026 08:51:35 EEST - 216.73.216.250

[41] A. Scialpi, L.A.C. De Filippis and P. Cavaliere, “Influence of shoulder geometry on microstructure and mechanical properties of friction stir welded 6082 aluminium alloy,” *Materials and Design*, vol. 28, pp. 1124–1129, 2007.
[42] A. Arora, A. De and T. DebRoy, “Toward optimum friction stir welding tool shoulder diameter,” *Scripta Materialia*, vol. 64, pp. 9–12, 2011.
[43] W.M. Thomas, E.D. Nicholas, S.D. Smith, in: S.K. Das, J.G. Kaufman, T.J. Lienert (Eds.), Aluminum 2001—Proceedings of the TMS 2001 Aluminum Automotive and Joining Sessions, TMS, 2001, p. 213.
[44] W.M. Thomas, K.I. Johnson, C.S. Wiesner, Adv. Eng. Mater. 5 (2003) 485.
[45] W.M. Thomas, R.E. Dolby, in: S.A. David, T. DebRoy, J.C. Lippold, H.B. Smartt, J.M. Vitek (Eds.), Proceedings of the Sixth International Conference on Trends inWelding Research, Pine Mountain, GA, ASM International, 2003, pp.203–211.
[46] Liu FC, Ma ZY (2008) Influence of tool dimension and welding parameters on microstructure and mechanical properties of friction-stir-welded 6061-T651 aluminum alloy. Miner Met Mater Soc ASM Int
[47] Mishra RS, Mahoney MW, Sato Y, Hovanski Y (2016) Friction stir welding and processing VIII. Frict Stir Weld Process VIII 50:1–300
[48] Rai R, Bhadeshia HKDH, Debroy T (2011) Review: friction stir welding tools. Sci Technol Weld Join 16(4):325–342
[49] Nandan R, Debroy T, Bhadeshia HKDH (2008) Recent advances in friction-stir welding—Process, weldment structure and properties. Prog Mater Sci 53:980–1023
[50] Prado HF, Murr RA, Shindo LE, Soto DJ (2001) Tool wear in the friction stir welding of aluminum alloy 6061+20% Al2O3: a preliminary study. Scr Mater 75–80
[51] A Review of Optimization and Measurement Techniques of the Friction Stir Welding (FSW) Process D.A.P. Prabhakar, Akash Korgal , Arun Kumar Shettigar , Mervin A. Herbert, Manjunath Patel Gowdru Chandrashekharappa , Danil Yurievich Pimenov and Khaled Giasin
[52] Yang, X.S. Optimization and metaheuristic algorithms in engineering. In *Metaheuristics in Water, Geotechnical and Transport Engineering*; Elsevier: Amsterdam, The Netherlands, 2013 pp. 1–23.
[53] Modi, V.K.; Desai, D.A. Review of Taguchi Method, Design of Experiment (DOE) & Analysis of Variance (ANOVA) For Quality Improvements through Optimization in Foundry. *J. Emerg. Technol. Innov. Res.* **2018**, *5*, 184–194.
[54] Jagdev, H.S.; Browne, J.; Keogh, J. Manufacturing Process Optimisation—A Survey of Techniques. In Proceedings of the Twenty-Eighth International: Matador Conference, Macmillan Education, Manchester, UK, 18–19 April 1990; pp. 205–215.
[55] Korgal, A.; Upadhyaya, S.; Anilkumar, T. Grain refinement of aluminium 4032 alloy with the impact of vibration using Taguchi technique and analysis of variance (ANOVA). *Mater. Today Proc.* **2022**, *54*, 507–512.
[56] Chauhan, A.; Kumar, S. Optimization of Friction Stir Welding Parameters for Similar Base Material Combinations. In *Advances in Engineering Materials: Select Proceedings of FLAME*; Springer: Berlin/Heidelberg, Germany, 2021; pp. 665–675.
[57] Krishna, G.G. Improving joint strength of the friction stir welding of dissimilar aluminium alloy by using coating technique. *Sadhan¯ a¯* **2022**, *47*, 7.
[58] Ismail, A.; Zulkipli, F.N.; Awang, M.; Ab Rahman, F.; Khalid, P.Z.M.; Baharudin, B.A. Optimum Welding Parameters for Friction Stir Welded AA6063 Pipe Butt Joint Using the Taguchi Method. *Trans. Marit. Sci.* **2021**, *10*, 404–413.
[59] Tutum, C.C.; Hattel, J.H. Optimisation of process parameters in friction stir welding based on residual stress analysis: A feasibility study. *Sci. Technol. Weld. Join.* **2010**, *15*, 369–377.
[60] Panwar, R.; Chandna, P. Parameter optimization of FSW aviation-grade AA8090 using Taguchi grey relational analysis. *Aircr. Eng. Aerosp. Technol.* **2023**, *95*, 715–724.

Institutional Repository - Library & Information Centre - University of Thessaly
04/09/2026 08:51:35 EEST - 216.73.216.250

[61] Seshu Kumar, G.S.V.; Kumar, A.; Rajesh, S.; Chekuri, R.B.R.; Ramakotaiah, K. An experimental study and parameter optimization of FSW for welding dissimilar 6061 and 7075 Al alloys. *Int. J. Interact. Des. Manuf.* **2023**, *17*, 215–223.
[62] Delir Nazarlou, R.; Arghavanian, R.; Omidbakhsh, F. The effect of pin shape on the corrosion behaviour of friction stir welded 1080 aluminium alloy. *Adv. Mater. Process.* **2023**, *9*, 507–518.
[63] El-Zathry, N.E.; Hassan, A.I.; El-Betar, A.A.; Sabry, I. Optimization of friction stir welding AA6082-T6 parameters using analysis of variance and grey relational analysis. *J. Phys. Conf. Ser.* **2022**, *2299*, 012015.
[64] Sefene, E.M.; Tsegaw, A.A. Temperature-based optimization of friction stir welding of AA 6061 using GRA synchronous with Taguchi method. *Int. J. Adv. Manuf. Technol.* **2022**, *119*, 1479–1490.
[65] Zhou, L.; Luo, L.Y.;Wang, R.; Zhang, J.B.; Huang, Y.X.; Song, X.G. Process parameter optimization in refill friction spot welding
of 6061 aluminum alloys using response surface methodology. J. Mater. Eng. Perform. **2018**, 27, 4050–4058.
[66] Patel, G.C.M.; Krishna, P.; Parappagoudar, M.B. Squeeze casting process modeling by a conventional statistical regression analysis approach. Appl. Math. Model. **2016**, 40, 6869–6888.
[67] Patel, G.C.M.; Shettigar, A.K.; Parappagoudar, M.B. A systematic approach to model and optimize wear behaviour of castings produced by squeeze casting process. J. Manuf. Process. **2018**, 32, 199–212.
[68] Mallieswaran, K.; Padmanabhan, R.; Balasubramanian, V. Friction stir welding parameters optimization for tailored welded blank sheets of AA1100 with AA6061 dissimilar alloy using response surface methodology. Adv. Mater. Process. **2018**, 4, 142–157.
[69] Vignesh, S.; Dinesh Babu, P.; Nalla Mohamed, M.; Martin Vinoth, S.; Surya, G.; Dinesh, S. Investigation on the process parameters of double-sided friction stir welded AA6082-T 6 joints with different tool pins using response surface methodology. In Advances in Manufacturing Processes: Select Proceedings of ICEMMM 2018; Springer: Singapore, 2019; pp. 309–319. ISBN 978-981-13-1723-1.
[70] Akhai, S.; Srivastava, P.; Sharma, V.; Bhatia, A. Investigating weld strength of AA8011-6062 alloys joined via friction-stir welding
using the RSM approach. J. Phys. Conf. Ser. **2021**, 1950, 012016.
[71] Zhang, C.Y.; Chen, Q.D.; Jean, M.D. Optimization of the welding properties of friction stir weld butt joints using the response surface method based on taguchi's design. Strength Mater. **2022**, 54, 267–280.
[72] Phanphet, S.; Sukprasert, N.; Wangmai, A.; Bangphan, S.; Bangphan, P. Application of factorial design to study the effect of moisture and rice of varieties on the production of Paddy Husker Machine. In Proceedings of theWorld Congress on Engineering,
London, UK, 4–6 July 2018; Volume 2.
[73] Medhi, T.; Hussain, S.A.I.; Roy, B.S.; Saha, S.C. An intelligent multi-objective framework for optimizing friction-stir welding process parameters. Appl. Soft Comput. **2021**, 104, 107190.
[74] Anand, R.; Sridhar, V.G. Microstructure and mechanical properties of interlock friction stir weld lap joint AA7475-T7 using fractional factorial design. Proc. Inst. Mech. Eng. Part C **2022**, 236, 318–329.
[75] Senapati, P.N.; Bhoi, R.K. Characterization of Friction-Stir Welded Joints of AA1100 by Factorial Design Based Hierarchical Regression Model. Ann. Chim. Sci. Mater. **2020**, 44, 271–280.
[76] Sahu, S.K.; Mishra, D.; Pal, K.; Pal, S.K. Multi-sensor-based strategies for accurate prediction of friction stir welding of polycarbonate sheets. Proc. Inst. Mech. Eng. Part C **2021**, 235, 3252–3272.

Institutional Repository - Library & Information Centre - University of Thessaly
04/09/2026 08:51:35 EEST - 216.73.216.250

[77] Bector, K.; Tripathi, A.; Pandey, D.; Butola, R.; Singari, R.M. A review on the fabrication of surface composites via friction stir processing and its modeling using ANN. In Advances in Manufacturing and Industrial Engineering: Select Proceedings of ICAPIE 2019 Springer: Berlin/Heidelberg, Germany, 2021; pp. 1–11.
[78] Eren, B.; Guvenc, M.A.; Mistikoglu, S. Artificial intelligence applications for friction stir welding: A review. Met. Mater. Int. **2021**, 27, 193–219.
[79] Patel, G.C.M.; Shettigar, A.K.; Krishna, P.; Parappagoudar, M.B. Back propagation genetic and recurrent neural network applications in modelling and analysis of squeeze casting process. Appl. Soft Comput. **2017**, 59, 418–437.
[80] Haykin, S. Neural Networks: A Comprehensive Foundation; Prentice Hall: Hoboken, NJ, USA, 1998.
[81] Patel, G.C.M.; Krishna, P.; Parappagoudar, M.B. An intelligent system for squeeze casting process—Soft computing-based approach. Int. J. Adv. Manuf. Technol. **2016**, 86, 3051–3065.
[82] Shojaeefard, M.H.; Akbari, M.; Asadi, P. Multi-objective optimization of friction stir welding parameters using FEM and neural network. Int. J. Precis. Eng. Manuf. **2014**, 15, 2351–2356.
[83] Shojaeefard, M.H.; Behnagh, R.A.; Akbari, M.; Givi, M.K.B.; Farhani, F. Modelling and Pareto optimization of mechanical properties of friction stir welded AA7075/AA5083 butt joints using neural network and particle swarm algorithm. Mater. Des. **2013**, 44, 190–198.
[84] Salhan, P.; Singh, R.; Jain, P.; Butola, R. Prediction of heat generation and microstructure of AA7075 friction stir welding using ANN: Effect of process parameters. Manuf. Lett. **2022**, 32, 5–9.
[85] Vangalapati, M.; Balaji, K.; Gopichand, A. ANN modeling and analysis of friction welded AA6061 aluminum alloy. Mater. Today Proc. **2019**, 18, 3357–3364.
[86] Senthilnathan, T.; Balachandar, K. Prediction of mechanical properties and optimization of process parameters in friction-stirwelded dissimilar aluminium alloys. World J. Eng. **2020**, 17, 519–526.
[87] Mukherjee, I.; Ray, P.K. A review of optimization techniques in metal cutting processes. Comput. Ind. Eng. **2006**, 50, 15–34.
[88] Okuyucu, H.; Kurt, A.; Arcaklioglu, E. Artificial neural network application to the friction stir welding of aluminum plates. Mater.Des. **2007**, 28, 78–84.
[89] Singh, R.; Kainthola, A.; Singh, T.N. Estimation of elastic constant of rocks using an ANFIS approach. Appl. Soft Comput. **2012**, 12,40–45.
[90] Monostori, L.; Márkus, A.; van Brussel, H.; Westkämpfer, E. Machine learning approaches to manufacturing. CIRP Ann. **1996**, 45,675–712.
[91] Chadha, U.; Selvaraj, S.K.; Gunreddy, N.; Sanjay Babu, S.; Mishra, S.; Padala, D.; Adefris, A. A survey of machine learning in friction stir welding, including unresolved issues and future research directions. Mater. Des. Process. Commun. **2022**, 2022, 2568347.
[92] Mishra, A.; Dutta, S.B. Detection of surface defects in friction stir welded joints by using a novel machine learning approach.Appl. Eng. Lett. **2020**, 5, 16–21.
[93] Rao, R.V.; Rai, D.P. Optimisation of welding processes using quasi-oppositional-based Jaya algorithm. J. Exp. Theor. Artif. Intell.**2017**, 29, 1099–1117.
[94] Rambabu, G.; Naik, D.B.; Rao, C.V.; Rao, K.S.; Reddy, G.M. Optimization of friction stir welding parameters for improved corrosion resistance of AA2219 aluminum alloy joints. Def. Technol. **2015**, 11, 330–337.
[95] Saeidi, M.; Manafi, B.; Besharati Givi, M.K.; Faraji, G. Mathematical modeling and optimization of friction stir welding process parameters in AA5083 and AA7075 aluminum alloy joints. Proc. Inst. Mech. Eng. Part B **2016**, 230, 1284–1294.
[96] Kumar, A.K.; Surya, M.S.; Venkataramaiah, P. Performance evaluation of machine learning based-classifiers in friction stir welding of Aa6061-T6 alloy. Int. J. Interact. Des. Manuf. **2023**, 17, 469–472.

Institutional Repository - Library & Information Centre - University of Thessaly
04/09/2026 08:51:35 EEST - 216.73.216.250

[97] Anandan, B.; Manikandan, M. Machine learning approach for predicting the peak temperature of dissimilar AA7050-AA2014A friction stir welding butt joint using various regression models. Mater. Lett. **2022**, 325, 132879.
[98] Aghbashlo, M.; Peng, W.; Tabatabaei, M.; Kalogirou, S.A.; Soltanian, S.; Hosseinzadeh-Bandbafha, H.; Lam, S.S. Machine learning technology in biodiesel research: A review. Prog. Energy Combust. Sci. **2021**, 85, 100904.
[99] Sahu, P.K.; Kumari, K.; Pal, S.; Pal, S.K. Hybrid fuzzy-grey-Taguchi based multi weld quality optimization of Al/Cu dissimilar friction stir welded joints. Adv. Manuf. **2016**, 4, 237–247.
[100] Pitchipoo, P.; Muthiah, A.; Jeyakumar, K.; Manikandan, A. Friction stir welding parameter optimization using novel multi objective dragonfly algorithm. Int. J. Light. Mater. Manuf. **2021**, 4, 460–467.
[101] Nadikudi, B.K.B. Parametric optimization of friction stir welding process parameters of dissimilar welded joints using grey relational analysis and desirability function approach. World J. Eng. **2022**, 20, 609–617.
[102] Van, A.L.; Nguyen, T.T. Optimization of friction stir welding operation using optimal taguchi-based ANFIS and genetic algorithm. Stroj. Vestn./J. Mech. Eng. **2022**, 68, 424–438.
[103] Anjinappa, C.S.; Alamri, S.; Afzal, A.; Razak Kaladgi, A.; Saleel, C.A.; Hasan, N.; Saleh, B. Response surface, neural network, and experimental approach to optimize process parameters and characterization of Al-Mg alloy by friction stir welding. Adv. Mech. Eng. **2022**, 14, 16878132221120460.
[104] Ambekar, M.; Kittur, J. Multiresponse optimization of friction stir welding process parameters by an integrated WPCA-ANN-PSO approach. Mater. Today Proc. **2020**, 27, 363–368.
[105] Wakchaure, K.N.; Thakur, A.G.; Gadakh, V.; Kumar, A. Multi-objective optimization of friction stir welding of aluminium alloy 6082-T6 Using hybrid Taguchi-Grey relation analysis-ANN method. Mater. Today Proc. **2018**, 5, 7150–7159.
[106] Al-Mahasneh, M.; Aljarrah, M.; Rababah, T.; Alu'datt, M. Application of hybrid neural fuzzy system (ANFIS) in food processing and technology. Food Eng. Rev. **2016**, 8, 351–366.
[107] Kandavalli, S.R.; Khan, A.M.; Iqbal, A.; Jamil, M.; Abbas, S.; Laghari, R.A.; Cheok, Q. Application of sophisticated sensors to advance the monitoring of machining processes: Analysis and holistic review. *Int. J. Adv. Manuf. Technol.* **2023**, *125*, 989–1014.
[108] Mishra, D.; Roy, R.B.; Dutta, S.; Pal, S.K.; Chakravarty, D. A review on sensor-based monitoring and control of friction stir welding process and a roadmap to Industry 4.0. *J. Manuf. Process.* **2018**, *36*, 373–397.
[109] Jaypuria, S.; Mahapatra, T.R.; Jaypuria, O. Metaheuristic tuned ANFIS model for input-output modeling of friction stir welding. *Mater. Today Proc.* **2019**, *18*, 3922–3930.
[110] Sahali, M.A.; Aini, A.; Bouzit, L.; Himed, L.; Benaissa, B. Experimental modeling and multi-objective optimization of friction stir welding parameters of AA 3004 aluminum alloy. *Int. J. Adv. Manuf. Technol.* **2023**, *124*, 1229–1244.
[111] Babalola, S.A.; Dutta, S.; Murmu, N.C.; Akinnuli, B.O. In-situ process reliability monitoring strategy for friction stir welding machine. *Mater. Today Proc.* **2022**, *66*, 3883–3889.
[112] Murthy, V.; Ullegaddi, K.; Mahesh, B.; Rajaprakash, B.M. Application of image processing and acoustic emission technique in monitoring of friction stir welding process. *Mater. Today Proc.* **2017**, *4*, 9186–9195.
[113] Balachandar, K.; Jegadeeshwaran, R.; Gandhikumar, D. Condition monitoring of FSW tool using vibration analysis–A machine learning approach. *Mater. Today Proc.* **2020**, *27*, 2970–2974.

Institutional Repository - Library & Information Centre - University of Thessaly
04/09/2026 08:51:35 EEST - 216.73.216.250

[114] Kumar, R.; Singh, K.; Pandey, S. Process forces and heat input as function of process parameters in AA5083 friction stir welds. Trans. Nonferrous Met. Soc. China 2012, 22, 288–298.
[115] Atharifar, H.; Lin, D.; Kovacevic, R. Numerical and experimental investigations on the loads carried by the tool during friction stir welding. J. Mater. Eng. Perform. 2009, 18, 339–350.
[116] Das, B.; Pal, S.; Bag, S. Design and development of force and torque measurement setup for real time monitoring of friction stir welding process. Measurement 2017, 103, 186–198.
[117] Gibson, B.T.; Lammlein, D.H.; Prater, T.J.; Longhurst, W.R.; Cox, C.D.; Ballun, M.C.; Strauss, A.M. Friction stir welding: Process, automation, and control. J. Manuf. Process. 2014, 16, 56–73.
[118] Zuluaga-Posada, M.; Hoyos, E.; Montoya, Y. Performance evaluation of a novel force measuring device for Friction Stir Welding (FSW) of aluminum alloys. DYNA 2019, 86, 150–155.
[119] Fleming, P.A.; Lammlein, D.H.; Wilkes, D.M.; Cook, G.E.; Strauss, A.M.; DeLapp, D.R.; Hartman, D.A. Misalignment detection and enabling of seam tracking for friction stir welding. Sci. Technol. Weld. Join. 2009, 14, 93–96.
[120] Das, B.; Pal, S.; Bag, S. Monitoring of friction stir welding process through signals acquired during the welding. In Proceedings of the AIMTDR 2014, Guwahati, India, 12–14 December 2014; pp. 12–14.
[121] Kumar, U.; Yadav, I.; Kumari, S.; Kumari, K.; Ranjan, N.; Kesharwani, R.K.; Pal, S.K. Defect identification in friction stir welding using discrete wavelet analysis. Adv. Eng. Softw. 2015, 85, 43–50.
[122] Arya, H.K.; Jaiswal, D. Parametric Study and Force Analysis of Friction Stir Welded Aa-6063 Joint. Int. J. Mech. Eng. 2022, 7, 756–768. Available online: https://kalaharijournals.com/ijme-vol7-issue-jan2022.php (accessed on 16 January 2023).
[123] Terra, C.S.; Silveira, J.L.L. Models for FSW forces using a square pin profile tool. J. Manuf. Process. 2021, 68, 1395–1404.
[124] Fehrenbacher, A.; Duffie, N.A.; Ferrier, N.J.; Pfefferkorn, F.E.; Zinn, M.R. Toward automation of friction stir welding through temperature measurement and closed-loop control. J. Manuf. Sci. Eng. 2011, 133, 051008.
[125] De Backer, J.; Bolmsjö, G.; Christiansson, A.K. Temperature control of robotic friction stir welding using the thermoelectric effect. Int. J. Adv. Manuf. Technol. 2014, 70, 375–383.
[126] Silva, A.C.F.; de Backer, J.; Bolmsjö, G. Temperature measurements during friction stir welding. Int. J. Adv. Manuf. Technol. 2017, 88, 2899–2908. Available online: https://link.springer.com/article/10.1007%2Fs00170-016-9007-4 (accessed on 12 February 2023).
[127] Threadgill, P.L.; Leonard, A.J.; Shercliff, H.R.; Withers, P.J. Friction stir welding of aluminium alloys. Int. Mater. Rev. 2009, 54, 49–93.
[128] Schmale, J.; Fehrenbacher, A.; Shrivastava, A.; Pfefferkorn, F.E. Calibration of dynamic tool–workpiece interface temperature measurement during friction stir welding. Measurement 2016, 88, 331–342.
[129] D'Errico; Calzavarini, R.; Settineri, L. Experiments on self-tuning regulation of cutting temperature in turning process. In Proceedings of the 1994 Proceedings of IEEE International Conference on Control and Applications, Glasgow, UK, 24–26 August 1994; pp. 1165–1169.
[130] de Backer, J.; Bolmsjö, G. Thermoelectric method for temperature measurement in friction stir welding. Sci. Technol. Weld. Join. 2013, 18, 558–565.
[131] Fehrenbacher, A.; Duffie, N.A.; Ferrier, N.J.; Pfefferkorn, F.E.; Zinn, M.R. Effects of tool—Workpiece interface temperature on weld quality and quality improvements through temperature control in friction stir welding. Int. J. Adv. Manuf. Technol. 2014, 71, 165–179.

Institutional Repository - Library & Information Centre - University of Thessaly
04/09/2026 08:51:35 EEST - 216.73.216.250

[132] Campanella, D.; Casavola, C.; Cazzato, A.; Fratini, L.; Moramarco, V.; Pappalettere, C. Residual Stress Measurement in Innovative Friction Stir Welding Processes. Key Eng. Mater. 2017, 754, 391–394.
[133] Brauer, H.; Otterbach, J.M.; Ziolkowski, M.; Toepfer, H.; Graetzel, M.; Bergmann, J.P. Friction stir weld inspection using the motion induced eddy current testing technique. AIP Conf. Proc. 2019, 2102, 080004.
[134] García Ruano, S.A.; Bertelli, F.; dos Santos, A.A., Jr. Evaluation of 7050 Aluminum Plates Joined by Friction Stir Welding Using Acoustoelastic. ASME Int. Mech. Eng. Congr. Expo. 2017, 58356, V002T02A089.
[135] Sevvel, P.; Babu, S.D.; Kumar, R.S. Peak Temperature Correlation and Temperature Distribution during Joining of AZ80A Mg Alloy by FSW-A Numerical and Experimental Investigation. Stroj. Vestn./J. Mech. Eng. 2020, 66, 395–407.
[136] da Silva, Y.C.; Oliveira Junior, F.J.; dos Santos, J.F.; Marcondes, F.; Silva, C. Numerical investigation of the influence of FSW parameters on the heat and mass transfer of austenitic stainless steels. Weld. World 2020, 64, 2019–2032.
[137] Subramaniam, S. Acoustic emission–based monitoring approach for friction stir welding of aluminum alloy AA6063-T6 with different tool pin profiles. Proc. Inst. Mech. Eng. Part B 2013, 227, 407–416.
[138] Soundararajan, V.; Atharifar, H.; Kovacevic, R. Monitoring and processing the acoustic emission signals from the friction-stirwelding process. Proc. Inst. Mech. Eng. Part B 2006, 220, 1673–1685.
[139] Chen, C.; Kovacevic, R.; Jandgric, D. Wavelet transform analysis of acoustic emission in monitoring friction stir welding of 6061 aluminum. Int. J. Mach. Tools Manuf. 2003, 43, 1383–1390.
[140] Park, S.H.C.; Sato, Y.S.; Kokawa, H. Effect of micro-texture on fracture location in friction stir weld of Mg alloy AZ61 during tensile test. *Scr. Mater.* **2003**, *49*, 161–166.
[141] Kouadri-Henni, A.; Barrallier, L. Mechanical properties, microstructure and crystallographic texture of magnesium AZ91-D alloy welded by friction stir welding (FSW). *Metall. Mater. Trans. A* **2014**, *45*, 4983–4996.
[142] Feng, A.H.; Ma, Z.Y. Microstructure evolution of cast Mg-Al-Zn during friction stir processing and subsequent aging. Acta Mater. 2009, 57, 4248–4260.
[143] Suhuddin, U.F.H.R.; Mironov, S.; Sato, Y.S.; Kokawa, H.; Lee, C.W. Grain structure evolution during friction-stir welding of AZ31 magnesium alloy. Acta Mater. 2009, 57, 5406–5418.
[144] Chen, J.; Fujii, H.; Sun, Y.F.; Morisada, Y.; Kondoh, K. Effect of grain size on the microstructure and mechanical properties of friction stir welded non-combustive magnesium alloys. Mater. Sci. Eng. A 2012, 549, 176–184.
[145] Sun, Y.F.; Fujii, H.S.; Takada, Y.; Tsuji, N.; Nakata, K.; Nogi, K. Effect of initial grain size on the joint properties of friction stir welded aluminum. Mater. Sci. Eng. A 2009, 527, 317–321.
[146] Kwan, C.; Wang, Z.R. Microstructure evolution upon annealing of accumulative roll bonding (ARB) 1100 Al sheet materials: Evolution of interface microstructures. J. Mater. Sci. 2008, 43, 5045–5051.
[147] Chang, C.I.; Lee, C.J.; Huang, J.C. Relationship between grain size and Zener-Holloman parameter during friction stir processing in AZ31 Mg alloys. Scr. Mater. 2004, 51, 509–514.
[148] Y.S. Sato, H. Kokawa, M. Enmoto, S. Jogan, Metall. Mater. Trans. A 30 (1999) 2429.
[149] A.P. Reynolds, Sci. Technol. Weld. Joining 5 (2000) 120.
[150] S. Benavides, Y. Li, L.E. Murr, D. Brown, J.C. McClure, Scripta Mater. 41 (1999) 809.
[151] J.Q. Su, T.W. Nelson, C.J. Sterling, J. Mater. Res. 18 (2003) 1757.
[152] Y.J. Kwon, I. Shigematsu, N. Saito, Mater. Trans. 44 (2003) 1343.
[153] Y.J. Kwon, I. Shigematsu, N. Saito, Scripta Mater. 49 (2003) 785.

Institutional Repository - Library & Information Centre - University of Thessaly
04/09/2026 08:51:35 EEST - 216.73.216.250

[154] Y. Li, L.E. Murr, J.C. McClure, Mater. Sci. Eng. A 271 (1999) 213
[155] J.Q. Su, T.W. Nelson, R.S. Mishra, M.W. Mahoney, Acta Mater. 51 (2003) 713.
[156] K.V. Jata, K.K. Sankaran, J.J. Ruschau, Metall. Mater. Trans. A 31 (2000) 2181.
[157] M. James, M. Mahoney, in: Proceedings of the First International Symposium on Friction Stir Welding, Thousand Oaks, CA, USA, June 14–16, 1999.
[158] C.D. Donne, E. Lima, J. Wegener, A. Pyzalla, T. Buslaps, in: Proceedings of the Third International Symposium on Friction Stir Welding, Kobe, Japan, September 27–28, 2001.
[159] M. Peel, A. Steuwer, M. Preuss, P.J. Withers, Acta Mater. 51 (2003) 4791.
[160] A.P. Reynolds, W. Tang, T. Gnaupel-Herold, H. Prask, Scripta Mater. 48 (2003) 1289.
[161] G. Biallas, R. Braun, C.D. Donne, G. Staniek, W.A. Kaysser, in: Proceedings of the First International Symposium on Friction Stir Welding, Thousand Oaks, CA, USA, June 14–16, 1999.
[162] G. Bussu, P.E. Irving, Int. J. Fatigue 25 (2003) 77.
[163] L. Magnusson, L. Kallman, in: Proceedings of the Second International Symposium on Friction Stir Welding, Gothenburg, Sweden, June 26–28, 2000.
[164] J. Paulo Davim, Atul Kumar Choudhary and Rahul Jain, Chapter 2 Fundamentals of Friction Stir Welding, Its Application, and Advancements of book Welding Technology 2022
[165] Baghdadi A, Sajuri Z, Kokabi AH (2018) Weldability and mechanical properties of dissimilarAl–MgSi to pure aluminium and Al–Mg using friction stir welding process. J Teknol Weld
[166] http://www.nasa.gov/exploration/systems/sls/
[167] Research areas in space by ISRO. AI, respond office capacity building program. ISRO HQ,Bengaluru
[168] Haghshenas M, Gerlich AP (2018) Joining of automotive sheet materials by friction-based welding methods: a review. Eng Sci Technol Int J 21(1):130–148
[169] Kallee SW. Industrial applications of friction stir welding. Woodhead Publishing Limited
[170] Ribton CN, Andrews RE (2001) Canister sealing for high level encapsulation TWI Ltd. In: International high-level radioactive waste management conference, Las Vegas, Nevada, USA, 29 Apr–3 May 2001
[171] Effect of Friction Stir Welding Techniques and Parameters on Polymers Joint Efficiency—A Critical Review, Miguel A. R. Pereira, Ana M. Amaro, Paulo N. B. Reis and Altino Loureiro
[172] Friction Stir Welding – Process and its Variables: A Review, Mandeep Singh Sidhu, Sukhpal Singh Chatha

Institutional Repository - Library & Information Centre - University of Thessaly
04/09/2026 08:51:35 EEST - 216.73.216.250